DAA/ AMES
A-FILE IN-02-CR

JOINT INSTITUTE FOR AERONAUTICS AND ACOUSTICS

90625

NCC2-326

National Aeronautics and
Space Administration
Ames Research Center

JIAA TR - 78

Stanford University

1958

CONTROL OF VORTICAL SEPARATION ON CONICAL BODIES

BY

Nikos J. Mourtos and Leonard Roberts

Stanford University
Department of Aeronautics and Astronautics
Stanford, CA 94305

JUNE 1987

(NASA-CR-181206) CONTROL OF VORTICAL SEPARATION ON CONICAL BODIES (Stanford Univ.) 195 p Avail: NTIS HC A09/MF A01 CSCL 01A

N87-27616

Unclas

G3/02 0090625

ABSTRACT

In a variety of aeronautical applications, the flow around conical bodies at incidence is of interest. Such applications include, but are not limited to, highly maneuverable aircraft with delta wings, the aerospace plane and nose portions of spike inlets.

For such conical bodies, starting at moderate angles of attack, the flow separates from the lee side, forming two vortices. Although the vortex lift contribution is highly desirable, as the angle of attack increases, the vortex system becomes asymmetric, and eventually the vortices breakdown. This causes problems with stability in all directions. Thus, some control of the separation process is necessary if the vortex lift is to be exploited at higher angles of attack.

The theoretical model which is used in this analysis has three parts. First, the "single line-vortex" model is used within the framework of "slender body theory", to compute the outer inviscid field for specified separation lines. Next, the three-dimensional boundary layer is represented by a momentum equation for the cross-flow, analogous to that for a plane boundary layer ; a von-Karman/Pohlhausen approximation is applied to solve this equation. The cross-flow separation for both laminar and turbulent layers is determined by matching the pressure at the upper and lower separation points. This iterative procedure yields a unique solution for the separation lines and consequently for the positions of the vortices and the vortex lift on the body.

In the last part, control of separation is achieved by blowing tangentially from a slot located along a cone generator. It is found that for very small blowing coefficients, the separation can be postponed or suppressed completely (i.e., separation is moved all the way to the leeward generator), in which case the results from R.T.Jones's theory are recovered.

ACKNOWLEDGEMENT

The work here presented has been supported by NASA Grant NCC 2–326.

NOMENCLATURE

English letter symbols :

a	characteristic width of the body
b	characteristic thickness of the body
b_j	half width of the wall jet
c	$= \sqrt{a^2 - b^2}$, geometric parameter of the ellipse
c_2	integration constant
C_f	friction coefficient defined by eq(A5.11)
C_{f0}	wall friction coefficient for zero pressure gradient defined by eq(10.20)
C_L	total lift coefficient defined by eq(3.5)
C_{LV}	vortex lift coefficient
C_p	pressure coefficient defined by eqs(3.2) and (10.21)
C_μ	blowing coefficient defined by eq(10.16)
E	exponential function used in boundary layer analysis
$F(x^*, y^*, z^*)$	function defined by eq(2.3)
$h_{1,2,3}$	metric (or Lame) coefficients defined in eqs(8.1)
H_2	boundary layer shape factor
$\imath$	$\sqrt{-1}$
$\Im()$	denotes the imaginary part of the complex quantity involved
k	$= \Gamma/2\pi$, vortex strength
	(also used as a constant)
K	spreading rate of the wall jet (constant)
K'	constant used in the wall jet analysis
K_η	second pressure gradient parameter defined by eq(A5.14)
l	characteristic dimension in the x - direction
L	lift force
M	Mach number
n	exponent in the boundary layer growth eq(8.13)
	(also exponent in the wall jet analysis)
N	normal force

p	static pressure
q	dynamic pressure
R	$= (a + b)/2$, local radius of the circular cone
$\Re()$	denotes the real part of the complex quantity involved
Re	Reynolds number
S	cross-sectional area of the cone
SC	separation criterion (function)
u	velocity component along the x or ξ - axes
U	dimensionless velocity along the x or ξ - axes
v	velocity component along the y or η - axes
V	dimensionless velocity along the η - axis
u_n	velocity normal to the line vortex
w	velocity component along z or ζ - axes
x, y, z	Cartesian coordinates fixed at the apex of the wing
x^*, y^*, z^*	dimensionless Cartesian coordinates
z	complex variable in the horizontal flat plate plane

Greek letter symbols :

α	angle of attack
γ	vortex sheet strength
Γ	circulation of the line vortex
δ	wing semi-apex angle in the (x, z) plane
	(also boundary layer thickness)
δ_y	displacement of the separation point
	from the leading edge along the y - axis
δ_z	displacement of the separation point
	from the leading edge along the z - axis
δ_1	displacement thickness in the direction of a cone generator
δ_2	displacement thickness in the circumferential direction
ϵ	eddy viscosity
ε	cone semi-apex angle in the (x, y) plane

ζ	complex variable in the vertical flat-plate plane
	(also coordinate in the direction normal to the surface)
η	coordinate along the circumference of the cross-section
θ	complex variable in the circle plane
	[also angular coordinate (windward point taken as zero)]
	(also boundary layer momentum thickness)
θ_{11}	momentum thickness in the longitudinal direction
θ_{22}	momentum thickness in the circumferential direction
$\theta_{12,21}$	momentum thicknesses due to the mutual effect
	of the longitudinal and circumferential flows
λ	dimensionless coordinate across the boundary layer
Λ_η	first pressure gradient parameter defined by eq(A5.6)
μ	molecular viscosity
ν	kinematic viscosity
ξ	coordinate along a cone generator
π	3.14159...
ϱ	fluid density
σ	complex variable in the ellipse plane
τ	wall shear stress
$\tau_{,0}$	wall shear stress with zero pressure gradient
φ	disturbance velocity potential
χ	complex potential
χ_s	complex potential due to a line source distribution
$\chi_{s1,s2}$	components of χ_s defined by eqs(6.3) and (6.4)
ψ	disturbance stream function

Subscripts :

BL	refers to the boundary layer
cf	refers to the cross-flow plane
e	refers to the non-viscous external flow
j	refers to the wall jet
L	refers to the laminar boundary layer

m	refers to the position in the jet profile where velocity is maximum
s	refers to the separation point
T	refers to the turbulent boundary layer
tr	refers to the transition point in the boundary layer
∞	refers to the undisturbed flow field
0	refers to the solution for leading edge separation
1	refers to the right vortex position

Superscripts :

$\bar{\sigma}$	complex conjugate of σ

Abbreviations :

BL	boundary layer
LE	leading edge
SPLS	separation point on the lower surface
SPUS	separation point on the upper surface

TABLE OF CONTENTS

LIST OF FIGURES

LIST OF TABLES

1. PROLOGUE

1.1 Motivation

In a variety of aeronautical as well as aerospace applications, the flow around bodies of general conical shape at high angle of attack needs to be studied. Such applications include, but are not limited to, highly maneuverable aircraft with delta wings such as the F–5F in fig(1.1), the aerospace plane and the nose portions of spike inlets.

The class of shapes of current interest may be generalized as conical bodies of various cross-sections. For example, the nose portion of the fuselage of the F–5F can be approximated by a circular cone, while the rear portion, being thinner and flatter, can be treated as a thin elliptical cone. The advantage of a semi-infinite cone considered here is the simple geometry and the assumption of conical flow, both of which simplify the analysis significantly.

For such conical bodies, even at small to moderate angles of attack, the flow separates from the lee side. From this separation, fluid with high vorticity is convected upwards, away from the body surface, so that the resulting flow pattern is quite different from that of attached flow in which the vorticity is only appreciable in the boundary layer.

In general, the flow pattern over a slender conical body goes through the following stages as the angle of attack increases :

(i) At zero angle of attack the flow is axisymmetric.

(ii) At very small angles of attack ($0° < \alpha < 6°$) the flow is attached everywhere.

(iii) At small angles of attack ($6° \leq \alpha \leq 20°$) the flow first separates and a symmetric, steady pair of vortices exists.

(iv) At moderate angles of attack ($20° \leq \alpha \leq 45°$) the symmetric vortex system yields to an asymmetric steady one (fig(1.1)), with two or more vortex cores.

(v) At large angles of attack ($45° \leq \alpha \leq 70°$) the asymmetric vortex system becomes unsteady and the vortices change locations randomly with time.

(vi) As $\alpha \to 90°$ the vortices become highly mixed and form a turbulent wake (end portions of vortices in fig(1.1)).

The present work is concerned with stage (iii) and only with the conical part of the vortices shown in fig(1.1). The numerical ranges for the angle of attack given in parentheses, although representative, are by no means absolute, since they have been determined from experiments with specific shapes, Reynolds numbers and other characteristics.

Figure(1.2) shows the vortex formation over the leading edges of a slender delta wing. For highly swept-back configurations, usually a shear layer separates from each of two cone generators, one on each side, which roll up into a pair of vortices. These primary vortices cause additional lift to be generated on the lee side surface. The steep pressure gradient between the minimum of pressure and the primary separation line causes a new flow separation, which usually takes the form of a small secondary vortex. The effect of these secondary vortices on the lift is usually small.

The contribution of vortex lift in the low range of incidence is highly desirable. As the angle of attack increases, however, and the vortex system becomes first asymmetric, then unstable and uncontrollable, a large dependance on vortex lift may cause serious problems with directional, rolling and longitudinal stability. Therefore, if the formation of the vortices could somehow be enhanced or suppressed as necessary, controlled flow could be extended to higher angles of attack.

The location and the strength of the vortices and, as a consequence, the vortex lift all depend on the location of the separation lines (as will be shown in later chapters). This leads to the idea of controlling the location of separation as a means of controlling the vortex lift.

1.2 Objective

The purpose of the present work is three-fold :

(i) First, to explore the influence of the position of separation on the vortex parameters (location, strength, lift). This is done through an inviscid analysis of the outer field for arbitrarily chosen separation lines.

(ii) Second, to determine uniquely the separation line locations through a boundary layer (viscous) analysis. Thus, the ambiguity introduced in the first step is removed.

(iii) Third, to control boundary layer separation by wall jet blowing. This also requires a viscous analysis and is based on the idea that a thin high-velocity layer of fluid ejected tangentially to the surface of the body reenergizes the boundary layer and makes it less susceptible to separation.

As was mentioned in the previous section, at high angles of attack (typical of highly maneuverable aircraft), the problem is not to get lift (since a large component of the thrust produced by the engines is vertical), but rather, to get rid of any asymmetries present in the vortex system. Thus, some reduction in vortex lift as a result of blowing is justified.

An alternate way to stabilize the vortices would be blowing from the apex along the axes of the vortices (brute force approach). However, as will be shown in later chapters, controlling the conditions which produce these vortices (i.e., boundary layer separation), is a more effective way to achieve our goal. This is indicated by the fact that very little tangential blowing produces very large changes in the vortex system.

1.3 Outline

In chapter 2 a summary of experimental and previous theoretical work is given, and a comparison is made of the various models currently in use for flows over conical bodies at incidence. The choice of the "single line-vortex" model as well as the use of "slender body theory" and the assumption of conical flow are also discussed. Finally, a conformal mapping sequence which allows simple transformations of various cross-section shapes is shown.

In chapter 3 an account is given of the Jones model (ref.13) for a flat delta wing at incidence with attached flow. This is the most basic of all the models and provides the linear lift dependence on α. In chapter 4 the Brown and Michael solution (ref.19) for the separated flow past a flat delta wing is discussed. The separation is assumed to take place along the sharp leading edges. This is the simplest model from which the vortical (non-linear with α) contribution to the lift can be determined. In chapter 5 the influence on the flow geometry and the lift as the separation lines are moved inwards towards the leeward generator is determined. For a sharp leading edge this results in a singularity along the leading edges. In chapter 6 the singularity is removed by considering rounded leading edges (elliptical cross-section). In chapter 7 the inviscid analysis is extented to cones of circular cross-sections and compared with the results of Bryson (ref.20), but for various locations of the separation lines.

In chapter 8 the three-dimensional boundary layer on the circular cone is solved by an extension of the Karman/Pohlhausen integral method to conical flow. In chapter 9 an iterative viscous/inviscid interaction scheme is introduced which allows the prediction of the separation lines on the cone. Comparison with observed separation lines from experiments is also made. In chapter 10 tangential blowing into the boundary layer is introduced as a means of controlling the position of the separation lines and ultimately the vortex lift. Finally in chapter 11 the limitations of the theory are discussed, the main conclusions are presented and suggestions for further research are given.

2. INTRODUCTION

2.1 Previous Theoretical Work

The fully attached flow past slender delta wings at incidence was first modelled by Jones (1946, ref.13), following earlier work with similar results by Munk (1924, ref.11) and Tsien (1938, ref.12). A little later Ward (1948, ref.14) completed the picture of the "slender body theory for attached flow" which was subsequently reviewed and extended by Adams and Sears (1953, ref.15).

The three-dimensional separated flow past inclined bodies is currently represented by three well-established inviscid models which are described below (fig(2.1)).

The first model is the "rolled-up core" established in 1957 by Mangler and Smith (ref.28). In this model, the inner turns of the rolled-up vortex sheet are represented by a single line-vortex, while a few turns on the outside of the spiral are represented explicitly in a numerical treatment (fig(2.1a)).

The second model is the "multiple line-vortex" established in 1967 by Sacks, Lundberg and Hanson (ref.22) and it is derived in the following manner. If on the vortex sheet that springs from the leading edge of the wing, lines are drawn along which the circulation is constant (constant jump in the velocity potential $\Delta\varphi$), these will also be streamlines of the mean flow. Each such line starts at a point on the leading edge and follows a helical path on the sheet, turning about the axis of the vortex as it proceeds downstream, thus dividing the sheet up into ribbons. The circulation about each ribbon is the same along the whole of its length and if it is allowed to condense into a line-vortex, a "multiple line-vortex" model is obtained (fig(2.1b)).

The third one is the "single line-vortex" model. It is the simplest available model and preceded those described above. It was finalized by Brown and Michael in 1954 (ref.19) following earlier work by Legendre (ref.16), Adams (ref.17) and Edwards (ref.18). In this model, explicit representation of the outer turns of the spiral sheet is omitted, so that the cut, which in the first model connects the end of the vortex sheet with the concentrated vortex, now extends from the line-vortex to its associated separation line on the body (fig(2.1c)). A more detailed comparison of the three models is undertaken in the next section.

2.2 A Comparison between the Three Models of Vortex Separation

The arguments in this section follow those in refs.30 and 32 which should be consulted if a more detailed discussion is desired.

The main advantage of the "rolled-up core" model of Mangler and Smith is, of course, its greater realism in describing separation. Thus, it is not surprising that it gives the closest approximation to the real flow in the infinite Reynolds number limit. Using the panel-method terminology, the "rolled-up core" model constitutes a higher order method than for example the "multiple line-vortex" model of Sacks et al, which means that it gives greater accuracy for a similar number of elements and has therefore the ability to predict a smooth behaviour of the flow. Thus, when many turns of a rolled-up configuration need to be represented, the "rolled-up core" model is the best one to use.

Of course, there is a price for all these advantages, i.e., a greater programming effort. The computing time is also greater for the same number of elements than that required by the "multiple line-vortex" model. Also, the absence of any representation of secondary separation, may become important in some applications.

The main advantage of the "multiple line-vortex" model is its flexibility, which makes it possible to use one program to calculate very different vortex structures with only minimal changes. The approximation of the real flow in the infinite Reynolds number limit is also very good, and it is superior to the one given by the "single line-vortex" model but inferior to the one of the "rolled-up core" model.

Unfortunately there are also complexities associated with the use of the "multiple line-vortex" model. More computational storage space is required compared with the "rolled-up core" model, and a large number of elements is essential for accuracy. In addition, if many turns of a "rolled-up" configuration need to be represented, the calculation will be disrupted by vortices from adjacent turns pairing-off and rotating one around the other. Also, since the integration of ordinary differential equations, which is required in the streamwise direction in order to find the shapes of the line-vortices, may be an unstable process, the shapes sometimes become chaotic. When they do not become chaotic the shapes turn out to be helices with their pitch becoming smaller as the streamline gets closer to the axis of the vortex. It follows that a line-vortex starting near the apex of a delta wing should follow a helix of very small pitch, and such a helix requires very many elements to describe it with any realism. As more vortices are introduced to increase the accuracy of the solution, the closer to the apex the first one starts, thus making the problem worse.

The main advantage of the "single line-vortex" model is its simplicity. This feature makes it especially attractive for initial investigations, and its use usually reveals the underlying structure of families of solutions of the more realistic models. Simplicity is also an important advantage when it becomes necessary to iterate the inviscid solution with a boundary layer solution in order to determine the separation lines.

A disadvantage which arises with the use of the "single line-vortex" model is the inability to find solutions for very small relative incidences (α/ε). For example, for the symmetric flow past a circular cone Bryson (ref.20) found no solutions with the vortex close to the separation line when $(\alpha/\varepsilon) < 1.5 \csc \theta_s$, whereas solutions have been found with the "rolled-up core" model. In addition, since the vortex system is represented only globally in this model, the position of the vortices suffers in accuracy especially for asymmetric configurations.

For the present work, the main purpose is to obtain a fast estimate of the velocity and pressure fields around the body which, when combined with a boundary layer analysis including the effects of blowing, will enable us to predict the separation lines. The "single line-vortex" model seems adequate for this purpose and will serve to demonstrate an approach that may be subsequently applied to the more elaborate models.

2.3 Previous Experimental Work

The experimental observations of separated flows on conical bodies, although limited, offer some very useful guidelines for the solutions which follow in the next chapters.

Jorgensen (1957, ref.34) was the first to test cones with elliptical cross-section. He pointed out that there are distinct aerodynamic advantages to the use of elliptical cones, namely, that with their major axis horizontal, they develop greater lift and have higher lift-to-drag ratios than circular cones of the same fineness ratio and volume. However, his "lift coefficient versus angle of attack curves" are all linear, probably because the range of incidences tested was not high enough, so the vortex system either had not formed yet or was still too weak to affect the lift significantly.

Rainbird, Crabbe and Jurewicz (1963, ref.35) experimented with circular cones in a water tunnel, while Schindel and Chamberlain (ref.39), and Friberg (refs.36,37) at M.I.T. tested circular and elliptic, two-dimensional and three-dimensional bodies. One of the interesting points of their results is the discovery of a secondary vortex system, similar to that shown in fig(1.2), above certain angles of attack. The observed positions of the separation lines from their experiments will be used for comparison with the predictions of the present theory in chapter 9.

Finally, Wood and Roberts (ref.64) at Stanford University showed that it is possible to control the vortex system by blowing tangentially from the leading edge of a slender wing, towards the leeward generator. Their work provides much of the motivation for the present analysis.

2.4 Slender Body Theory

From the mathematical point of view, "slender body theory" begins with the Prandtl-Glauert equation

$$(1 - M_\infty^2)\frac{\partial^2\varphi}{\partial x^2} + \frac{\partial^2\varphi}{\partial y^2} + \frac{\partial^2\varphi}{\partial z^2} = 0 \tag{2.1}$$

which is valid for supersonic as well as subsonic Mach numbers. Equation(2.1) may be further approximated for slender elongated wings or bodies. It follows that, since the geometrical properties of the body or wing vary only slowly in the x - direction, the derivative $\partial^2\varphi/\partial x^2$ must also be small. This argument can be made more rigorous (ref.15) by introducing dimensionless coordinates

$$x = lx^* \tag{2.2a}$$

$$y = ay^* \tag{2.2b}$$

$$z = az^* \tag{2.2c}$$

where l is a characteristic length and a is a characteristic width of the body. If a function F is defined such that

$$\varphi(x,y,z) = u_\infty l F(x^*,y^*,z^*) \tag{2.3}$$

then eq(2.1) becomes

$$(1-M_\infty^2)\left(\frac{a^2}{l^2}\right)\frac{\partial^2 F}{\partial x^{*2}} + \frac{\partial^2 F}{\partial y^{*2}} + \frac{\partial^2 F}{\partial z^{*2}} = 0 \tag{2.4}$$

so that for sufficiently small values of the parameter $(1-M_\infty^2)(a^2/l^2)$ the first term can be neglected. One thus obtains the Laplace equation for the cross-flow

$$\frac{\partial^2 \varphi}{\partial y^2} + \frac{\partial^2 \varphi}{\partial z^2} = 0 \tag{2.5}$$

However, the interpretation of slenderness is quite different for the various speed regimes. For $M_\infty > 1$ "slender" means that the wing lies well within the Mach cone from the apex. That was the reason why Ward (ref.14) limited his theory to pointed bodies and wings. Relatively blunt bodies and wings may qualify as "slender" at low supersonic speeds, whereas at hypersonic speeds eq(2.1) is not valid and the theory fails entirely for most practical shapes. For $M_\infty < 1$, on the other hand, the word "slender" becomes less restrictive, although we must keep in mind that eq(2.1) is not valid in the transonic regime. Since leading edge separation is essentially confined to highly swept wings, the application of "slender body theory" seems appropriate.

2.5 Remarks on the Assumption of "Conical Flow"

The term "conical flow" implies that there is a point in the flow field, called the vertex of the flow, such that all physical quantities are constant along rays drawn from the vertex. The simplest example is the inviscid supersonic flow past a circular cone at zero incidence, with an attached shock.

Strictly speaking, the flow over a conical body must be supersonic everywhere for the "conical flow" model to apply, since for subsonic flow the boundary conditions at infinity cannot be satisfied by a conical flow field. Nonetheless it has been observed that the subsonic flow past a slender conical body is approximately conical in a region downstream of the apex and well upstream of the trailing edge. This is due to the fact that at relative incidences (α/ε) sufficient to cause separation, the circumferential pressure gradients are much larger than the axial pressure gradient caused by thickness and base effects. For a more thorough discussion on the subject of "conical flow" ref.7 should be consulted.

The assumption of conical flow is facilitated in this model by two other assumptions. First, that the cone is of infinite length, thus avoiding the trailing edge region where the conicality assumption would break down. Second, the use of "slender body theory" which does not distinguish between subsonic and supersonic regimes since the first term in the Prandtl-Glauert equation is neglected, and there is no "upstream influence".

2.6 Conformal Mapping in the Cross-Plane

Figure(2.2) shows the various relations which transform the cross-section of the cone from a flat plate (Brown and Michael solution), to an ellipse (Schindel solution) and finally to a circle (Bryson solution). The flat plate is most easily solved when transformed so that the vortex system is symmetrical with respect to a vertical plate. For the ellipse, the easiest way is by a transformation to a circle and application of the circle theorem, which allows one immediately to write the complex potential in terms of the vortex system and its image.

3. A FLAT DELTA WING WITH ATTACHED FLOW

3.1 The Flow Model

This chapter presents the Jones solution for a flat delta wing, since this will be the departing as well as the destination point for the solutions which follow in the next chapters. It is the departing point since it excludes separation, and it is also the destination point of a separated configuration as the vortex system is being suppressed by shifting the separation line from the leading edge inwards, toward the leeward generator of the wing. Although only the flat delta wing is mentioned here, the lift coefficient based on the projected wing area is exactly the same regardless of cross-section, within the framework of "slender body theory without separation". The configuration of the model is shown in fig(3.1). The flow pattern in any cross-plane is the familiar two-dimensional flow caused by a flat plate normal to a free stream with velocity $u_\infty\alpha$ (fig(3.2)). However, the scale of the flow field increases continually along the x - axis, and this fact gives rise to the three-dimensionality of the problem. The potential function for the flow at the wing is given by

$$\varphi = \pm u_\infty \alpha \sqrt{a^2 - y^2} \tag{3.1}$$

where the positive sign is for the upper surface and the negative sign is for the lower surface. From eq(3.1) it may be seen that the gradient of the potential (i.e., the velocity), is singular at the leading edges ($y = \pm a$).

3.2 Pressure Distribution

The pressure coefficient is defined as

$$C_p \equiv \frac{p - p_\infty}{q_\infty} \tag{3.2}$$

where q_∞ is the free stream dynamic pressure. Following the analysis in ref.13, the pressure distribution in a cross-section at a distance x from the apex may be expressed as a function of the relative incidence α/ε

$$\frac{C_p}{\varepsilon^2} = \left(1 - \frac{y^2}{a^2 - y^2}\right)\left(\frac{\alpha}{\varepsilon}\right)^2 \mp 2\frac{a}{\sqrt{a^2 - y^2}}\left(\frac{\alpha}{\varepsilon}\right) \tag{3.3}$$

whereas the difference in pressure between the upper and lower surfaces is

$$\frac{\Delta C_p}{\varepsilon^2} = 4\frac{a}{\sqrt{a^2 - y^2}}\left(\frac{\alpha}{\varepsilon}\right) \tag{3.4}$$

The pressure distribution from eq(3.3) has been plotted in fig(3.3). The singularity at the leading edge is the result of an infinite suction there, as the flow tries to make a 180° turn from the lower to the upper surface. In a realistic description of the flow such a singularity cannot exist, and it is necessary to introduce a vortex sheet at the leading edge which feeds a vortex whose strength is such that the singularity is removed. In other words, a leading edge Kutta condition must be satisfied. This more realistic description of the flow was first provided by Brown and Michael (ref.19) and is shown in the following chapter.

3.3 Lift

The lift coefficient is based on the projected area of the body ($2a \cdot x/2$), and is given by

$$C_L \equiv \frac{L}{q_\infty a x} \tag{3.5}$$

The Jones solution yields the classical result from "slender body theory"

$$\frac{C_L}{\varepsilon^2} = 2\pi \frac{\alpha}{\varepsilon} \tag{3.6}$$

which shows that the lift grows linearly with angle of attack (fig(3.4)). The fact that the lift (i.e. the area between the two curves in fig(3.3)) is finite despite an infinite pressure peak at the leading edge should not be surprising, since the singularity is of the $1/\sqrt{y}$ type, and becomes an infinite slope when integrated over y.

Equation(3.6) verifies what is already known from experiments, i.e., that C_L/ε^2 is a function of α/ε, and suggests that a similar relationship should be sought for the more complex separated flow. Equation(3.6) will also be derived as a particular case from the more general flow configuration in chapter 4.

Experiments show that the linear dependence of lift on the angle of attack is a fairly good approximation for small angles of incidence. As the angle of attack increases, however, the lift departs rapidly from the Jones value. In the next four chapters, an effort is made to capture this departure. It is done by acknowledging the fact that the flow separates at some angle of attack, and the Jones model is no longer a realistic representation of the flow field.

4. A FLAT DELTA WING WITH LEADING EDGE SEPARATION

4.1 The flow model

This chapter discusses the Brown and Michael solution for the separated flow past a flat delta wing. The configuration of the model is shown in fig(4.1). The flow is assumed to separate along the two leading edges and to give rise to a pair of line-vortices. Since the strength of these vortices must grow in the x - direction for a conical flow field, they must be fed with vorticity from the leading edge. Otherwise Kelvin's theorem would be violated. The connection between the leading edges and the vortices is achieved with plane vortex sheets emanating from the leading edges. This is the simplest possible way to model separation.

A solution is now sought to satisfy eq(2.5) subject to the appropriate boundary conditions (section(4.2)). This is easily done by introducing the complex potential for the flow

$$\chi = \varphi + \imath\psi \tag{4.1}$$

Note that although eq(2.5) is two-dimensional, the three-dimensional character of the problem will still enter through the boundary conditions. After using the transformation on the lower half of fig(2.2), the complex potential may be written as

$$\chi(\zeta) = -\imath u_\infty \alpha \zeta - \imath k \ln \frac{\zeta - \zeta_1}{\zeta + \bar{\zeta}_1} \tag{4.2}$$

where $k = \Gamma/2\pi$ is the vortex strength. Transforming eq(4.2) back to the physical plane gives

$$\chi(z) = -\imath u_\infty \alpha \sqrt{z^2 - a^2} - \imath k \ln \frac{\sqrt{z^2 - a^2} - \sqrt{z_1^2 - a^2}}{\sqrt{z^2 - a^2} + \sqrt{\bar{z}_1^2 - a^2}} \tag{4.3}$$

where z_1 is the location of the right vortex, and $\bar{z}_1$ is the complex conjugate of z_1. The first term represents uniform flow past the plate (for small α) while the second term represents a vortex pair in the leeward side.

4.2 Boundary Conditions

The conditions that the solutions of eq(2.5) must satisfy are the following :

(i) Tangency condition on the wing. This is automatically satisfied by choice of the complex potential.

(ii) Separation condition on the wing. The separation line has to be specified since the present inviscid model is unable to predict it. In this chapter, the separation condition is simply the Kutta condition that the flow leave the plate tangentially at the leading edge and is most easily obtained in the ζ - plane, where this condition requires the presence of a stagnation point at the origin. When transformed back to the physical plane it reads

$$\frac{u_\infty \alpha}{k} = \frac{1}{\sqrt{z_1^2 - a^2}} + \frac{1}{\sqrt{\bar{z}_1^2 - a^2}} \tag{4.4}$$

(iii) The disturbances must vanish at infinity. This condition is also satisfied automatically by the complex potential.

(iv) The fluid pressure must be continuous everywhere. This condition, however, cannot be met with the present model. The reason is that straight vortex sheets cannot be aligned with the flow. This difficulty could of course be circumvented by assuming curved vortex sheets, which would form part of a three-dimensional stream surface. The solution then would provide both the shape and the strength of the sheet (refs.28–33). However, the problem is greatly simplified by assuming straight feeding sheets and past experience has shown that such a model does capture the main features of the flow. The last condition needs therefore to be replaced by the following :

(iv)′ The vortex system (feeding sheet and concentrated vortex) must be force-free since only the wing and not the fluid can sustain forces. This requires that the force on the sheet be cancelled by an equal magnitude and opposite direction force on the vortex. The force on the vortex arises from its inclination to the local velocity vector, which in turn, derives partly from the free stream component u_∞ along the x - axis and partly from the cross-flow velocity at its location. Thus, the force per unit length of the vortex may be written as

$$-\imath \varrho u_n \Gamma = -\imath \varrho u_n \gamma \frac{a}{\varepsilon} \tag{4.5}$$

where

$$\gamma = \frac{d\Gamma}{dx} = const \tag{4.6}$$

is the vortex sheet strength and

$$u_n = -u_\infty \varepsilon \frac{z_1}{a} + (v + \imath w)_1 \tag{4.7}$$

The force on the feeding sheet arises from the growth in Γ along the length of the vortex. The vector force per unit length of each filament representing the vorticity lying between x and $x + dx$ is

$$\imath \varrho u_\infty \gamma (z_1 - a) \tag{4.8}$$

Setting the vector sum of the two forces equal to zero according to the previous discussion and taking the complex conjugate of the resulting expression yields a condition for the induced velocity at the vortex location

$$(v - \imath w)_1 = \varepsilon u_\infty \left(\frac{2\bar{z}_1}{a} - 1 \right) \tag{4.9}$$

This velocity may also be calculated by differentiating the complex potential in the physical plane (eq(4.3)) after the effect of the right vortex has been subtracted

$$(v - \imath w)_1 = \frac{d\chi}{dz} + \frac{\imath k}{z - z_1} \tag{4.10}$$

Equating the right sides of eqs(4.9) and (4.10) yields the second relation between the two unknowns

$$\imath k \left[\frac{z_1}{z_1^2 - a^2 + \sqrt{(z_1^2 - a^2)(\bar{z}_1^2 - a^2)}} - \frac{z_1}{\sqrt{(z_1^2 - a^2)(\bar{z}_1^2 - a^2)}} - \frac{z_1}{z_1^2 - a^2} + \frac{1}{2} \frac{a^2}{z_1(z_1^2 - a^2)} \right]$$

$$= \varepsilon u_\infty \left(\frac{2\bar{z}_1}{a} - 1 \right) \tag{4.11}$$

Equations(4.4) and (4.11) must be solved to determine the unknown quantities k and z_1.

4.3 Vortex Position and Strength

Solving the system of eqs(4.4) and (4.11) numerically by the Newton-Raphson technique (refs.65,66) yields the position and the strength of the vortex as a function of the relative incidence. The vortex location is shown in fig(4.2). As may be seen, the vortex moves away from the surface and closer to the center-line of the wing for increasing α/ε.

Figure(4.3) shows that the vortex strength grows almost linearly with the relative incidence, the only departure from linearity occurring when the vortex system first appears, i.e., at very low angles of attack.

4.4 Pressure Distribution

The first-order expression for the pressure coefficient is given by (ref.19)

$$C_p = \alpha^2 - 2\frac{u}{u_\infty} - \frac{v^2 + w^2}{u_\infty^2} \tag{4.12}$$

and its three-dimensional character is revealed by the inclusion of u which is $\partial\varphi/\partial x$. The first term on the right is necessary when the coordinates are fixed on the wing and are tilted through the angle of attack, as is the case in the present analysis. Obviously, there is no contribution to the lift from this term, since it is exactly the same for both surfaces.

The velocities may be computed by differentiating the complex potential

$$u = \Re\left\{\frac{d\chi}{dx}\right\} = \Re\left\{\frac{d\chi}{da}\frac{da}{dx}\right\} = \varepsilon\Re\left\{\frac{d\chi}{da}\right\} \tag{4.13}$$

$$v = \Re\left\{\frac{d\chi}{dz}\right\} = \Re\left\{\frac{d\chi}{d\zeta}\frac{d\zeta}{dz}\right\} \tag{4.14}$$

$$w = -\Im\left\{\frac{d\chi}{dz}\right\} = -\Im\left\{\frac{d\chi}{d\zeta}\frac{d\zeta}{dz}\right\} \tag{4.15}$$

where of course for this case of a flat wing $w = 0$ at the surface.

Figure(4.4) shows the pressure distribution on the surface of the flat cross-section for $\alpha/\varepsilon = 1.0$, as compared with the corresponding pressure distribution in attached flow. The singularity which appeared in the Jones solution has now been removed, since the flow no longer has to negotiate the sharp turn at the leading edge, but there is a pressure jump there due to the vortex sheet, equal to $\varrho u_\infty \Gamma/x$. This pressure jump is necessary to generate the force on the vortex sheet which balances the force on the vortex.

The very low pressure region on the upper surface is the vortex signature, and its position corresponds approximately to the lateral location of the vortex. The peak suction is an indication of the vortex strength, while the width of the suction is inversely proportional to the distance of the vortex from the surface.

The difference between the solid lines and the dotted lines in fig(4.4) is, of course, the vortex lift.

4.5 Lift

The normal force is most easily computed by calculating the change in downward momentum through an infinite plane perpendicular to the longitudinal axis x of the wing at the trailing edge (Trefftz plane). Thus

$$N = -\varrho u_\infty \int\int \left(\frac{\partial \varphi}{\partial z} - u_\infty \alpha\right) dz dy \tag{4.16}$$

Note that $\partial\varphi/\partial z$ is the velocity component in a plane perpendicular to the wing surface, and therefore it contains the upwash contribution of the free stream. Integrating with respect to z produces a contour integral of the velocity potential

$$N = -\varrho u_\infty \int_c \varphi dy \tag{4.17}$$

The contour is shown in fig(4.5) and includes the cuts connecting the separation points with the centers of the vortices. The vortices may be included in the body without affecting the normal force, since the forces on them cancel those on their feeding sheets. In terms of the complex potential

$$N = -\varrho u_\infty \Re \left\{ \int_c \chi dz + \int_c \psi dz \right\} \tag{4.18}$$

Note that the z in the first integral is the complex variable in the physical plane while z in the second integral is the real variable in the direction normal to the wing surface. Since $\psi = 0$ on the body and is single-valued on the vortices and the feeding sheets, the second integral vanishes. Furthermore, the function $\chi(z)$ is analytic in the field external to the contour ; hence, the integral is independent of the path provided that it encloses the original contour. The simplest way to integrate eq(4.18) is by transforming it to the ζ - plane (fig(4.5b))

$$N = -\varrho u_\infty \Re \left\{ \int_c \chi(\zeta) \frac{dz}{d\zeta} d\zeta \right\} \tag{4.19}$$

The integral of the logarithm can be evaluated by deforming the contour into a large circle whose radius $\rightarrow \infty$. Since there are no singularities between the original contour and the large circle the integrals are equal. The remaining integration is done along the vertical line between the branch points and yields

$$N = \pi \varrho a^2 u_\infty^2 \alpha + \varrho u_\infty \Gamma (\zeta_1 + \bar{\zeta}_1) \tag{4.20}$$

Transforming back to the z - plane gives

$$N = \pi \varrho a^2 u_\infty^2 \alpha + \varrho u_\infty \Gamma \left(\sqrt{z_1^2 - a^2} + \sqrt{\bar{z}_1^2 - a^2} \right) \tag{4.21}$$

or in dimensionless form

$$\frac{C_L}{\varepsilon^2} = 2\pi \frac{\alpha}{\varepsilon} + \frac{2\Gamma}{a u_\infty} \frac{\sqrt{z_1^2 - a^2} + \sqrt{\bar{z}_1^2 - a^2}}{a} \frac{\alpha}{\varepsilon} \tag{4.22}$$

Equation(4.22) contains C_L because for small angles of attack the normal force can be taken equal to the lift. This is in agreement with the well known result that for a lightly loaded wing (small perturbation flow) the induced drag is a second-order quantity. The first term, being identical to the right side of eq(3.6), is the linear contribution from "slender body theory", while the second term is the non-linear vortex lift. Figure(4.6) shows both components, as well as the total lift, as functions of the relative incidence. It may be seen, that the vortex lift is initially very small, but as the relative incidence increases it soon becomes the dominant term in the total lift. At $\alpha/\varepsilon = 1.0$ it has approximatelly the same magnitude as the Jones lift while at $\alpha/\varepsilon = 2.0$ it is approximatelly twice as large as the Jones lift.

Brown and Michael have also carried out a second order approximation to eq(4.22). The analytical expression for this result is given by

$$\frac{C_L}{\varepsilon^2} = 2\pi\frac{\alpha}{\varepsilon} + 4.987\left(\frac{\alpha}{\varepsilon}\right)^{\frac{5}{3}} + 1.322\left(\frac{\alpha}{\varepsilon}\right)^{\frac{2}{3}} \tag{4.23}$$

This result is very similar to the expression derived by Smith (ref.29) using his "rolled-up core" model for thin slender wings in conical flow

$$\frac{C_L}{\varepsilon^2} = 2\pi\frac{\alpha}{\varepsilon} + 4.9\left(\frac{\alpha}{\varepsilon}\right)^{1.7} \tag{4.24}$$

Thus, it was verified that C_L/ε^2 is a function of the relative incidence α/ε even for the case of vortical separation.

5. A FLAT DELTA WING WITH DISPLACED SEPARATION

5.1 The Flow Model

The effect of vortex separation on the lift of a slender delta wing was examined in the previous chapter. The next step is to explore the effect of the location of the separation lines on the formation of the vortex system and consequently on the vortex lift. The easiest way to perform this task is through an inviscid analysis, in which the separation lines are selected arbitrarily . The flat delta wing offers once more the simplest geometry.

The flow configuration is shown in fig(5.1) and is identical to the one used in the previous chapter, except that the separation lines have now been displaced a distance δ_y, still along generators but closer to the leeward generator of the wing.

The complex potential is still given by eqs(4.2) and (4.3), respectively, for the transformed and physical plane.

5.2 Boundary Conditions

The requirement for separation from a point $a - \delta_y$ in the physical plane translates into

$$\left.\frac{d\chi}{d\zeta}\right]_{\zeta_s} = 0 \tag{5.1}$$

where

$$\zeta_s = \pm \imath \sqrt{\delta_y(\delta_y - 2a)} \tag{5.2}$$

is the corresponding stagnation point in the transformed plane. The positive sign is used for separation from the upper surface while the negative sign is used for separation from the lower surface. Substituting eqs(4.2) and (5.2) into eq(5.1) and transforming the resulting expression back into the physical plane yields

$$\frac{u_\infty \alpha}{k} = \frac{1}{\sqrt{z_1^2 - a^2 - \imath\sqrt{\delta_y(\delta_y - 2a)}}} + \frac{1}{\sqrt{\bar{z}_1^2 - a^2 + \imath\sqrt{\delta_y(\delta_y - 2a)}}} \tag{5.3}$$

where the signs in front of the square roots correspond to the flow separating from the upper surface (i.e., the positive sign is used in eq(5.2)).

The procedure for balancing the forces on the vortex system is the same as that described in section (4.2). The force on the concentrated vortex is still expressed by eq(4.5) while the force on the vortex sheet is now

$$-\imath \varrho u_\infty \gamma(z_1 - a + \delta_y) \tag{5.4}$$

Setting again the vector sum of the two forces equal to zero and taking the complex conjugate gives an expression for the induced velocity at the location of the vortex

$$(v - \imath w)_1 = \varepsilon u_\infty \left(\frac{2\bar{z}_1}{a} - 1 + \frac{\delta_y}{a} \right) \tag{5.5}$$

Equating the right sides of eqs(4.10) and (5.5) now yields

$$
\imath k \left[\frac{z_1}{z_1^2 - a^2 + \sqrt{(z_1^2 - a^2)(\bar{z}_1^2 - a^2)}} - \frac{z_1}{\sqrt{(z_1^2 - a^2)(\bar{z}_1^2 - a^2)} + \imath\sqrt{\delta_y(\delta_y - 2a)(z_1^2 - a^2)}} \right.
$$

$$
\left. - \frac{z_1}{z_1^2 - a^2 - \imath\sqrt{\delta_y(\delta_y - 2a)}} + \frac{1}{2}\frac{a^2}{z_1(z_1^2 - a^2)} \right] = \varepsilon u_\infty \left(\frac{2\bar{z}_1}{a} - 1 + \frac{\delta_y}{a} \right) \qquad (5.6)
$$

The numerical solution of eqs(5.3) and (5.6) gives k and z_1 in terms of α/ε and δ_y/a.

5.3 Uniqueness of the Solution

An interesting result which occurred when the separation lines were forced away from the leading edges of the wing, was the appearance of two more families of solutions. They are discussed in some detail in section (6.3) ; here only the one which seems to agree with physical observations regarding the locus of the vortex positions for increasing relative incidence will be considered further.

5.4 Existence of the Solution

Another interesting aspect of the model with displaced separation lines is the difficulty in finding solutions for small α/ε. The farther away the separation line is moved on the lower surface, the higher the minimum value of α/ε for which vortex solutions first appear. This may be justified physically from observations of the actual flow over a flat delta wing. Since this flow separates at the leading edges, it is normal to expect some difficulty in the formation of the vortex system when the separation line is forced away from its natural position. Also, since in this model no account of the viscosity has been taken so far, it must be concluded that it is the kinematics of the flow field which prevent the formation of the vortices at low angles of attack.

The situation is quite different when the separation line is moved on the upper surface however. Then, there is no difficulty in finding solutions. The $(\alpha/\varepsilon)_{min}$ remains zero as it was for the Brown and Michael solution. This may be explained by the fact, that although the separation line again shifts away from its natural position, it now moves towards the attached flow solution (i.e., the Jones solution which was discussed in chapter 3).

5.5 Vortex Position and Strength

Figure(5.2) shows the vortex location for various positions of the separation line. For a given separation line (i.e., constant δ_y/a) the change in vortex location for increasing relative incidence resembles in general the Brown and Michael result, which corresponds to leading edge separation, except that it is displaced inward and toward the surface as the separation line moves inward. For a given angle of attack (i.e. constant α/ε), on the other hand, the vortex is displaced toward the leeward generator of the wing. As the separation line approaches the center-line of the wing (i.e., $(\delta_y/a) \to 1$), both curves collapse into the center of the cross-section, and the Jones solution is recovered. An interesting point illustrated in fig(5.2) is the sensitivity of the vortex position to very small displacements of the separation line. For $\alpha/\varepsilon = 3$, for example, it is seen that by displacing the separation only 1% causes a 10% shift of the y - vortex coordinate.

From the numerical solution, the coordinates of the vortex were related to the Brown and Michael solution through the curve-fit approximate expressions given below

$$y_1 \simeq y_{10}\left(1 - \sqrt{\frac{\delta_y}{a}}\right) \tag{5.7}$$

$$z_1 \simeq z_{10} \left(1 - \sqrt{\frac{\delta_y}{a}} \right)^{0.5} \tag{5.8}$$

The growth of the vortex strength with relative incidence is, as expected, similar to the Brown and Michael case (fig(5.3)), and it is very sensitive to small displacements of the separation line ; for $\alpha/\varepsilon = 3$, a 5% displacement of the separation reduces the vortex strength by approximately 25%.

An approximate expression for the decay of vortex strength with distance of separation from the leading edge is given by (fig(5.6))

$$k \simeq k_0 \left(1 - \sqrt{\frac{\delta_y}{a}} \right)^{1.2} \tag{5.9}$$

where the Jones solution ($k = 0$) is recovered for $(\delta_y/a) = 1$.

5.6 Pressure Distribution

The analysis and formulation of section (4.4) are also valid in this case. Although δ_y does not show explicitly in the equations, it affects the solution for the vortex position and strength – as was discussed in the previous section – and as a result, the pressure and force on the wing.

The pressure distribution for $(\delta_y/a) = 0.05$ is shown in fig(5.4). It is very similar to the pressure distribution for the Brown and Michael solution but the singularity at the leading edge has been reintroduced.

5.7 Lift

The vortex lift coefficient (fig(5.5)) is also related to that for the Brown and Michael solution by means of a similar approximate formula (fig(5.6))

$$C_{LV} \simeq C_{LV0}\left(1-\sqrt{\frac{\delta_y}{a}}\right)^3 \tag{5.10}$$

Both figs(5.5) and (5.6) clearly show the diminishing of the vortex lift contribution for increasing distance of the separation line from the leading edge, recovering the Jones lift in the limit as $(\delta_y/a) \to 1$. From a comparison of the exponents in eqs(5.9) and (5.10) as well as the two curves in fig(5.6), however, it may be seen that the vortex lift decays much faster than the strength of the vortex. This is so because the vortex lift is affected both by the strength and the position of the vortex. As the separation line moves inwards, the vortex gets closer to the wing surface so that the area that can benefit from the increased circulation also diminishes. In other words, the decay of the vortex lift is the result both of a diminishing vortex strength and of a diminishing area of lower pressure on the upper surface of the wing.

One may argue that the practical value of this solution (i.e., a flat delta wing with displaced separation lines) is minimal because of the leading edge singularity ; however, it represents the limiting case for a delta wing of finite thickness with very small leading edge radius.

6. A DELTA WING WITH ELLIPTICAL CROSS-SECTION

6.1 The Flow Model

There are two reasons that make rounded leading edges desirable. The first one is to get rid of the singularity which reappeared at the leading edge of the flat delta wing when the separation line was displaced ; a rounded leading edge eliminates the requirement of infinite acceleration and the resulting infinite velocity and pressure, although some suction will still exist. The second one is the necessity for a rounded edge in order to control separation by blowing.

From the analytical point of view, the elliptical cross-section is the most convenient one to consider, since it may be easily related to both the flat plate as well as the circle by means of the Joukowski transformation (fig(2.2)). The flow configuration is shown in fig(6.1), the only new element from the previous one being the thickness.

It is now easier to write the complex potential in the circle-plane (fig(2.2)), since the circle theorem allows one to write directly the contributions of the vortex system and its image

$$\chi_{cf}(\theta) = -\imath u_\infty \alpha \left(\theta - \frac{R^2}{\theta}\right) - \imath k \ln\left(\frac{(\theta-\theta_1)}{(\theta+\bar{\theta}_1)}\frac{(\theta\theta_1 + R^2)}{(\theta\bar{\theta}_1 - R^2)}\right) \tag{6.1}$$

The first term on the right side represents uniform flow past the circle (the angle of attack has been assumed small), and the second term represents a vortex pair on the leeward side together with its image inside the circle.

To this result we need to add the complex potential for an expanding ellipse of constant axis ratio, in order to satisfy the tangency condition on the surface of the cone

$$\chi_s = \chi_{s1} + \chi_{s2} \tag{6.2}$$

where

$$\chi_{s1} = u_\infty b\varepsilon \ln \frac{\sigma + \sqrt{\sigma^2 - c^2}}{2} \tag{6.3}$$

and

$$\chi_{s2} = -u_\infty \varepsilon \delta \left\{ x \left[\ln 2\sqrt{x(1-x)} - 1 \right] + \frac{1}{2} \right\} \tag{6.4}$$

The derivation of χ_{s1} and χ_{s2} is given in appendix 1. χ_s represents a source distribution on the horizontal plane of symmetry of the cone, directly related to the thickness. The total complex potential in the physical plane is of course

$$\chi = \chi_{cf} + \chi_s \tag{6.5}$$

The velocity field is computed in the same manner as in section 4.4, except that now the evaluation of the derivative $d\chi/da$ is more involved (see appendix 3).

6.2 Boundary Conditions

The position of the separation point in the physical plane can be represented by $\sigma_s(a-\delta_y,\delta_z)$ (fig(6.2)). Under the Joukowski transformation σ_s goes into a point θ_s in the θ - plane, given by

$$\theta_s = \frac{1}{2}\left[a-\delta_y+\imath\delta_z+\sqrt{(a-\delta_y)^2+2\delta_z(a-\delta_y)\imath-\delta_z^2-c^2}\right] \tag{6.6}$$

Here δ_y and δ_z are related by

$$\frac{(a-\delta_y)^2}{a^2}+\frac{\delta_z^2}{b^2}=1 \tag{6.7}$$

since σ_s is a point of the elliptical cross-section. Requiring the presence of a stagnation point at σ_s is equivalent to

$$\left.\frac{d\chi_{cf}}{d\theta}\right]_{\theta_s}=0 \tag{6.8}$$

or, from eq(6.1)

$$\frac{u_\infty\alpha}{k}=\left[\frac{\bar{\theta}_1^2+2\theta_s\bar{\theta}_1-R^2}{(\theta_s+\bar{\theta}_1)(\theta_s\bar{\theta}_1-R^2)}-\frac{R^2+2\theta_s\theta_1-\theta_1^2}{(\theta_s-\theta_1)(\theta_s\theta_1+R^2)}\right]\frac{\theta_s^2}{\theta_s^2+R^2} \tag{6.9}$$

From the force balance, referring to fig(6.2), we may derive, in a similar manner to that described in chapters 4 and 5, an expression for the induced velocity at the vortex location

$$[v - \imath w]_1 = u_\infty \varepsilon \left(\frac{2\bar{\sigma}_1}{a} + \frac{\delta_y + \imath \delta_z}{a} - 1 \right) \tag{6.10}$$

As before, this result can be combined with eq(4.10) – written in the σ - plane – to give the second equation needed to solve for the unknowns k and σ_1

$$- \imath u_\infty \alpha \left(1 + \frac{\sigma_1}{\sqrt{\sigma_1^2 - c^2}} \right) \left[\frac{1}{2} + \frac{2R^2}{(\sigma_1 + \sqrt{\sigma_1^2 - c^2})^2} \right]$$

$$+ u_\infty \frac{b\varepsilon}{\sqrt{\sigma_1^2 - c^2}} + \frac{\imath k c^2}{2(\sigma_1^2 - c^2)(\sigma_1 + \sqrt{\sigma_1^2 - c^2})} - \imath k \left(1 + \frac{\sigma_1}{\sqrt{\sigma_1^2 - c^2}} \right)$$

$$\left[\frac{\sigma_1 + \sqrt{\sigma_1^2 - c^2}}{(\sigma_1 + \sqrt{\sigma_1^2 - c^2})^2 + 4R^2} - \frac{\bar{\sigma}_1 + \sqrt{\bar{\sigma}_1^2 - c^2}}{(\sigma_1 + \sqrt{\sigma_1^2 - c^2})(\bar{\sigma}_1 + \sqrt{\bar{\sigma}_1^2 - c^2}) - 4R^2} \right.$$

$$\left. - \frac{1}{\sigma_1 + \bar{\sigma}_1 + \sqrt{\sigma_1^2 - c^2} + \sqrt{\bar{\sigma}_1^2 - c^2}} \right] = \varepsilon u_\infty \left(\frac{2\bar{\sigma}_1}{a} + \frac{\delta_y + \imath \delta_z}{a} - 1 \right) \tag{6.11}$$

The numerical solution of eqs(6.9) and (6.11) gives k and σ_1 in terms of α/ε and θ_s.

6.3 Uniqueness of the solution

Given the thickness of the wing and the position of the separation point, three solutions for the locus of the vortex positions for increasing α/ε were found again (fig(6.3)) :

In the first solution, the vortex moves farther form the wing surface and becomes stronger as the angle of attack increases. This is the only solution which agrees with experimental observations.

In the second solution, which appears in fig(6.3) as an extension of the first one, the vortex moves closer to the wing and its strength increases as the angle of attack increases.

In the third solution, the vortex is under the wing and again moves farther away and becomes stronger as the angle of attack increases.

The second solution dissappears when the separation point is exactly at the leading edge. It should be noted that all three families of solutions exist also for the limiting cases of the flat delta wing (see section (5.2)), as well as for the circular cone.

Although it might be interesting to investigate the question of stability for the second and third solutions, they are regarded as unrealistic and will not be considered further in the present analysis.

6.4 Existence of the Solution

As is shown in fig(6.3) there is a minimum value of the parameter α/ε below which no solution exists. This is in agreement with experimental observations (refs.34–39), although the theoretical $(\alpha/\varepsilon)_{min}$ may sometimes be larger than its corresponding value from experiments. The discrepancy between the experimental and theoretical values in this case results from the inability to satisfy the force balance for the vortex system due to the oversimplified representation of the vortex sheet.

In fig(6.5), the vortex solution boundaries are shown as functions of thickness and separation location. One sees that $(\alpha/\varepsilon)_{min}$ becomes smaller as the thickness of the wing diminishes. In the limiting case of a flat delta wing separation begins immediately for any $\alpha > 0$ (provided that the separation is fixed at the leading edge). This is also in agreement with experimental observations (refs.34–39).

6.5 Vortex Position and Strength

Approximate scaling laws similar to the ones shown in section (5.5), were also derived for an elliptical cross-section 10% thick

$$y_1 \simeq y_{10}\left(1-\sqrt{\frac{\delta_y}{a}}\right) = y_{10}\left(1-\frac{\eta}{a}\right) \tag{6.12}$$

$$z_1 \simeq z_{10} \tag{6.13}$$

$$k \simeq k_0\left(1-\sqrt{\frac{\delta_y}{a}}\right)^{1.05} = k_0\left(1-\frac{\eta}{a}\right)^{1.05} \tag{6.14}$$

Here η is the distance from the leading edge to the separation point along the surface, and the reference values are the ones corresponding to the flow separating from the leading edge. By comparison with those for the flat cross-section (see table(6.1)) it may be concluded that there is (almost) no variation in the vertical distance of the vortex from the wing surface as the wing acquires thickness, whereas the horizontal distance of the vortex from the center-line varies in the same manner as for the flat cross-section. As for the vortex strength, it appears to decay more slowly for the thick cross-section. Its growth with α/ε is shown in fig(6.4) for a cross-section 5% thick and it is almost identical to the one for the flat cross-section with the same location of separation.

6.6 Pressure Distribution

Equation(4.12) may once more be used to compute the pressure coefficient, except that w is no longer zero at the surface for the case of the elliptical cross-section.

The pressure distribution for an elliptical cone 20% thick, is shown in fig(6.6). Note that the infinite suction singularity at the leading edge has been removed, but there is still some suction there. Comparing fig(6.6) with fig(5.4), one sees that the vortex suction is now larger (more negative peak). This is an indication of increasing vortex lift with thickness.

6.7 Lift

The normal force may be calculated in the same manner as for the flat delta wing. Equations(4.16) through (4.19) are still valid with the appropriate change of complex variable (z into σ). The source term may be omitted from the complex potential since it is axisymmetric and therefore does not produce any downward momentum. The integration is performed again in the ζ - plane (fig(6.7)), as described in section (4.5), and the result in the present instance reads

$$N = \varrho u_\infty \Gamma(\zeta_1 + \bar{\zeta}_1) + 2\varrho u_\infty^2 \pi\alpha \left(R^2 + \frac{c^2}{4}\right) - \varrho u_\infty^2 \pi\alpha \left(R - \frac{c^2}{4R}\right)\left(R + \frac{c^2}{4R}\right) \tag{6.15}$$

Transforming back to the σ - plane

$$N = \pi\varrho u_\infty^2 a^2 \alpha + \varrho u_\infty \Gamma \Re\left\{\left(1 + \frac{a+b}{a-b}\right)\sqrt{\sigma_1^2 - c^2} + \left(1 - \frac{a+b}{a-b}\right)\sigma_1\right\} \tag{6.16}$$

or, in the usual dimensionless form

$$\frac{C_L}{\varepsilon^2} = 2\pi\frac{\alpha}{\varepsilon} + \frac{2\Gamma}{u_\infty a^2 \alpha}\Re\left\{\left(1 + \frac{a+b}{a-b}\right)\sqrt{\sigma_1^2 - c^2} + \left(1 - \frac{a+b}{a-b}\right)\sigma_1\right\}\frac{\alpha}{\varepsilon} \tag{6.17}$$

Figure(6.8) collects lift curves for all the configurations considered thus far. The discussion in section (5.7) regarding the various curves for different δ_y is valid for elliptical cross-sections as well. A comparison with the flat delta wing (see also table 6.1) clearly shows that the general trend is to achieve higher C_L for given α/ε as thickness is added on the wing.

The approximate scaling law showing the variation of vortex lift with δ_y is again similar to the one for the flat cross-section

$$C_{LV} \simeq C_{LVo}\left(1 - \sqrt{\frac{\delta_y}{a}}\right)^{2.6} = C_{LVo}\left(1 - \frac{\eta}{a}\right)^{2.6} \tag{6.18}$$

As was the case with the vortex strength, thickness causes the vortex lift to decay more slowly with shifting of the separation point toward the leeward generator.

7. A CIRCULAR CONE

7.1 The Flow Model

The circular cross-section may be looked at as one of the limiting cases of the elliptical cross-section, as $b \to a$, the other one being the flat plate ($b \to 0$, chapters 3, 4, 5). The flow configuration is shown in fig(7.1), and was first treated by Bryson (ref.20). The complex potential is given again by eq(6.5) except that the source term is now different

$$\chi_{s1} = u_\infty R\varepsilon \ln \theta \tag{7.1}$$

The difference is that the ellipse semi-minor axis has been replaced by the circle radius, and the plane source distribution has been replaced by a linearly growing source distribution along the axis of the cone. The logarithmic part could have been taken care of directly by the conformal transformation (see fig(2.2)). The transformation, however, would not change b into R. Thus, it is worth noting, that conformal mapping, although it comes very helpful in handling the cross-flow, cannot fully take into account three-dimensional effects such as the expansion of the body.

7.2 Vortex Position and Strength

The conditions and approach for the solution follow from the case of the elliptical cross-section with $b = 1.0$ and therefore they will not be repeated here. The only change that may be worth including in the computer programs is to replace the position of the separation point as given by $(a - \delta_y, \delta_z)$ for the case of the ellipse, by a separation angle

θ_s (the angle between the windward generator and the separation line).

As was seen from fig(6.5) the minimum value of α/ε for which a vortex solution first appears when the separation point is fixed at the leading edge ($\theta_s = 90°$) is 6.22. Because this value is unrealistically high for practical applications, a separation angle close to the one observed in most experiments with circular cones ($\theta_s = 145°$) was taken as a reference. For such angle, no simple formulae could be derived to relate the vortex coordinates, strength and lift for small excursions from this separation location as was done for the flat plate and the elliptical cross-section. It may be stated however, that again the vortex moves closer to the surface of the cone and becomes weaker as the separation point shifts towards the leeward generator.

Figure(7.2) shows the domain of vortex solutions. The lower boundary of this domain is a function of both the location of separation and the relative incidence. It is worth noting that for small separation angles (θ_s) vortex solutions cease to exist before the vortex reaches the surface of the cone. The upper boundary of the domain is the equivalent Foppl curve (i.e., the locus of the limiting vortex positions for high angles of attack, ref.20) for the case of a circular cone.

7.3 Pressure Distribution

The pressure distribution for a circular cone is shown in fig(7.3) for $\alpha/\varepsilon = 2.0$ this time, since the separation would have to be moved quite close to the leeward generator in order to get solution for $\alpha/\varepsilon = 1.0$ as in the previous cases. The same features may once more be identified (suction due to the vortex, and jump due to the vortex sheet). It is also worth noting that the Jones pressure distribution, shown in fig(7.3) with dotted line, is almost identical to the one for vortex separation, up to an angle of almost 100° from the windward point. The main difference, however, between the two cases is that the

Jones pressure distribution has only one adverse gradient while the pressure distribution for vortical separation has two adverse gradients since the two flows (starting respectively at the windward and leeward points) move toward each other.

7.4 Lift

From section (6.7) we may also get the lift coefficient for the limiting case of $b = a$

$$\frac{C_L}{\varepsilon^2} = 2\pi\frac{\alpha}{\varepsilon} + \frac{4\Gamma y_1}{u_\infty a^2 \alpha}\frac{\alpha}{\varepsilon} \tag{7.2}$$

The above expression is plotted in fig(7.4). The lift curves do not go through zero as in the previous cases because of the absence of vortex solutions for small α/ε. Thus it is implied that at the point where they start they are connected with the Jones lift curve by a vertical straight line. This means that the vortex strength does not develop gradually from zero as in the flat cross-section case, but rather, it jumps into a certain starting value for the first α/ε for which solutions are found.

7.5 Summary of Inviscid Results

From the inviscid analysis in chapters 3 through 7 the following conclusions may be drawn :

(i) The lift on conical bodies at incidence has two components ; the Jones lift and the vortex lift. The Jones lift is calculated assuming attached flow everywhere on the wing surface and grows linearly with angle of attack. The vortex lift is computed (in the present analysis) with the "single line-vortex" model and grows non-linearly with angle of attack.

The fact that the two lift components are decoupled suggests that blowing is a practical solution for changing the lift on the body without changing its attitude.

(ii) As the separation lines are moved from the leading edges toward the center-line of the wing, vortex lift is suppressed and in the limit, as the separation lines coincide with the center-line, the Jones solution is recovered. This suggests that displacing the separation is indeed a viable mechanism for controlling vortex position and vortex lift.

(iii) The vortex lift increases with increasing thickness of the wing (assuming always the same position of the separation lines). This advantage however cannot be realized at small angles of attack due to increased difficulty in finding solutions.

So far, the separation lines have been chosen arbitrarily. In reality however, the position of separation must be determined through a viscous analysis. In other words, the velocity and pressure fields computed for the outer inviscid field, are introduced into the boundary layer equations ; integration of these equations yields two locations where the boundary layer leaves the surface, one on each side of the hypothetical separation line which was arbitrarily chosen for the inviscid analysis. This procedure is undertaken in the next chapter for the circular cone.

8. THE BOUNDARY LAYER ON A CIRCULAR CONE AT INCIDENCE

8.1 Introduction

The main purpose of the viscous analysis is to predict the line(s) on the surface of the cone along which the boundary layer will separate.

In general, the boundary layer on a cone goes through the following stages as the angle of attack increases (ref.52) :

(i) At $\alpha = 0$ it is similar to that on a semi-infinite flat plate or airfoil section and it may be studied by plane-flow methods.

(ii) At small α it thickens at the top of the cone and thins at the bottom due to the circumferential flow induced by the angle of attack.

(iii) At $\alpha/\varepsilon \simeq 0.5$ an adverse circumferential pressure gradient first appears at the top of the cone.

(iv) At some higher α, a separation bubble appears embedded at the base of the boundary layer growing in extent as α increases.

(v) At $\alpha/\varepsilon \simeq 1.0$ the boundary layer is no longer thin and the vortex bubble already existing at the top is in the process of coalescence into a symmetric pair of strong steady vortices.

(vi) At $\alpha/\varepsilon \gg 1$ (i.e. a slender cone at very large incidence) the circumferential flow becomes similar to the plane flow about a cylinder and a von-Karman vortex street is shed at the top of the cone.

In the present analysis we are concerned with stage (v).

8.2 The Three-Dimensional Boundary Layer

Here are discussed briefly the properties that distinguish three-dimensional boundary layers from two-dimensional ones.

(i) Secondary flow.

In three-dimensional flow there are always pressure gradients at an angle to the main flow direction, providing a centrifugal force which distorts the outer flow streamlines. In the case of a cone at incidence for example, there is a circumferential pressure gradient while the main flow direction is almost longitudinal. Since the pressure is constant across a thin boundary layer, particles following a streamline within the layer are subject to the same circumferential pressure gradient as are those following the outer streamline. However, the boundary layer particles have lower inertia and tend to take a course conforming more closely to the direction of the circumferential pressure gradient as is shown in fig(8.1).

(ii) Streamline divergence.

The normal growth of a two-dimensional boundary layer is due to diffusion of vorticity (fig(8.2a)). In a three-dimensional boundary layer over a surface curved transversely to the direction of the flow (fig(8.2b)) it is necessary for the flow to spread itself over a progressively wider extent of surface as it grows. This spreading results in a thinner layer, than in the corresponding two-dimensional case. If the same velocity gradient is sustained between the surface and the outer flow in the two cases, the boundary layer on a cone will be thinner by $1/\sqrt{3}$ than on a flat plate, resulting in a skin friction greater by $\sqrt{3}$ (ref.46), provided that equal lengths for the growth of the boundary layers are considered in the two cases. Stated differently, the cone boundary layer is similar to that on a flat plate with Reynolds number three times as great.

(iii) Separation.

In plane flow separation occurs when a reverse-flow velocity profile appears, or equivalently when $\tau = 0$. In three-dimensional flow such a criterion fails to establish the separation lines because there is no way to decide which component of the shear stress is the important one to consider. However, it may be observed that at a separation line the wall stream surface bifurcates, and at a line of reattachment (if such occurs) the two stream surfaces join again at the wall. Thus, at the base of the boundary layer, there is embedded a distinct bubble that does not exchange fluid with the rest of the flow. It is therefore possible to generalize the definition of a separation region in three-dimensions as a bubble of fluid embedded in the boundary layer between the solid boundary and a stream surface meeting the body in a closed curve and containing a sheet pattern of vorticity.

Of course, the kind of separation which is of interest for the present problem occurs when the embedded vortex sheet coalesces to form strong concentrated vortices. The mechanism of coalescence is described in ref.45. The vortex sheet is represented by a series of individual vortices as in fig(8.3), while the effect of the wall is represented by the image vortices below the wall. If the fluid above the wall imposes no additional constraint (i.e. boundary layer of locally infinite thickness), each vortex would move more to the left toward the separation point under the influence of the induced field of its image. Vortices initially near the separation point tend to remain fixed, however, because the layer is supposed to remain thin. Therefore, each vortex moving upstream tends to overtake the vortex ahead of it, and coalescence into a single strong vortex ensues.

8.3 The Boundary Layer Equations on a Circular Cone

The three-dimensional boundary layer equations are given in appendix 4, written in a general system of orthogonal curvilinear coordinates. For a circular cone a coordinate system like the one described in section (A4.3) is obviously convenient. The geodesic coordinates are taken to be the cone generators while the geodesic parallels are the circles swept by the meridional angle, so the corresponding metric coefficient is the local radius of the cone (fig(8.4)). This gives

$$h_1 = 1 \tag{8.1a}$$

$$h_2 = R(\xi) = \xi \sin \varepsilon \simeq \xi\varepsilon \tag{8.1b}$$

$$h_3 = 1 \tag{8.1c}$$

The last equality in eq(8.1b) is validated by the assumption that the cone is slender. For the aforementioned coordinate system on a circular cone at an angle of attack, eqs(A4.3)–(A4.6) reduce to

continuity

$$u + \xi\frac{\partial u}{\partial \xi} + \frac{1}{\varepsilon}\frac{\partial v}{\partial \eta} + \xi\frac{\partial w}{\partial \zeta} = 0 \tag{8.2}$$

momentum in ξ - direction

$$u\frac{\partial u}{\partial \xi} + \frac{v}{\varepsilon\xi}\frac{\partial u}{\partial \eta} + w\frac{\partial u}{\partial \zeta} - \frac{v^2}{\xi} = \frac{1}{\varrho}\frac{\partial \tau_\xi}{\partial \zeta} \tag{8.3}$$

momentum in η - direction

$$u\frac{\partial v}{\partial \xi} + \frac{v}{\varepsilon\xi}\frac{\partial v}{\partial \eta} + w\frac{\partial v}{\partial \zeta} + \frac{uv}{\xi} = -\frac{1}{\varrho\varepsilon\xi}\frac{\partial p}{\partial \eta} + \frac{1}{\varrho}\frac{\partial \tau_\eta}{\partial \zeta} \tag{8.4}$$

momentum in ζ - direction

$$\frac{\partial p}{\partial \zeta} = 0 \tag{8.5}$$

Furthermore, eqs(A4.7) and (A4.8) become

$$\frac{\partial u_e}{\partial \eta} = \varepsilon v_e \tag{8.6}$$

$$-\frac{1}{\varrho}\frac{\partial p}{\partial \eta} = v_e\left(\frac{\partial v_e}{\partial \eta} + \varepsilon u_e\right) \tag{8.7}$$

Integrating eq(8.4) across the boundary layer (i.e. from $\zeta = 0$ on the body surface to $\zeta \to \infty$ outside the boundary layer), one obtains

$$\int_0^\infty \left(u\frac{\partial v}{\partial \xi} + \frac{v}{\varepsilon\xi}\frac{\partial v}{\partial \eta} + w\frac{\partial v}{\partial \zeta} + \frac{uv}{\xi} + \frac{1}{\varrho\varepsilon\xi}\frac{\partial p}{\partial \eta}\right) d\zeta = -\frac{\tau_\eta}{\varrho} \tag{8.8}$$

The normal velocity component w, can be replaced by

$$w = -\frac{1}{\xi}\int_0^\zeta \left(u + \xi\frac{\partial u}{\partial \xi} + \frac{1}{\varepsilon}\frac{\partial v}{\partial \eta}\right) d\zeta \tag{8.9}$$

from the continuity eq(8.2). When this substitution is made and integration is carried out, eq(8.8) becomes

$$\frac{\partial}{\partial \xi}\int_0^\infty u(v_e - v)d\zeta + \frac{1}{\varepsilon\xi}\frac{\partial}{\partial \eta}\int_0^\infty v(v_e - v)d\zeta + \frac{1}{\varepsilon\xi}\frac{\partial v_e}{\partial \eta}\int_0^\infty (v_e - v)d\zeta$$

$$+\frac{2}{\xi}\int_0^\infty u(v_e - v)d\zeta + \frac{v_e}{\xi}\int_0^\infty (u_e - u)d\zeta = \frac{\tau_\eta}{\varrho} \tag{8.10}$$

The displacement and momentum thicknesses δ and θ respectively are defined as follows

$$\delta_1 \equiv \int_0^\infty \frac{u_e - u}{u_e}d\zeta \tag{8.11a}$$

$$\delta_2 \equiv \int_0^\infty \frac{v_e - v}{v_e}d\zeta \tag{8.11b}$$

$$\theta_{11} \equiv \int_0^\infty \frac{u(u_e - u)}{u_e^2}d\zeta \tag{8.11c}$$

$$\theta_{22} \equiv \int_0^\infty \frac{v(v_e - v)}{v_e^2}d\zeta \tag{8.11d}$$

$$\theta_{12} \equiv \int_0^\infty \frac{v(u - u_e)}{u_e v_e}d\zeta \tag{8.11e}$$

$$\theta_{21} \equiv \int_0^\infty \frac{u(v_e - v)}{u_e v_e} d\zeta \tag{8.11f}$$

Incorporating the above definitions into eq(8.10) gives the integral form of the boundary layer equation for the cross-flow

$$v_e^2 \frac{\partial \theta_{22}}{\partial \eta} + v_e \frac{\partial v_e}{\partial \eta}(\delta_2 + 2\theta_{22}) + \varepsilon u_e v_e(\delta_1 + 2\theta_{22})$$
$$+ \varepsilon u_e v_e[(n+2)\theta_{21} - 2\theta_{22}] = \frac{\tau_\eta R}{\varrho} \tag{8.12}$$

Here n is the exponent in the boundary layer growth expression

$$\delta = k_{BL} \xi^n \tag{8.13}$$

Equation(8.12) may also be written as

$$v_e^2 \frac{\partial \theta_{22}}{\partial \eta} + \left(v_e \frac{\partial v_e}{\partial \eta} + \varepsilon u_e v_e \right)(\delta_2 + 2\theta_{22})$$
$$+ \varepsilon u_e v_e[\delta_1 - \delta_2 + (n+2)\theta_{21} - 2\theta_{22}] = \frac{\tau_\eta R}{\varrho} \tag{8.14}$$

This equation is similar to the corresponding momentum equation for a two-dimensional boundary layer, the primary difference being the presence of the last term on the left side which contains the momentum thicknesses due to the interaction of the longitudinal and circumferential flows.

So far no assumptions have been made regarding the state of the boundary layer. Therefore, the above derivations are valid for both laminar and turbulent boundary layers, on condition that in the latter case u and v denote the time averages of the respective velocity components. The primary difference, however, between the two cases (i.e. laminar and turbulent) will be the rate of growth of the boundary layer (eq(8.13)). In the laminar case $n = 0.5$ while in the turbulent case $n = 0.8$ (refs.40 and 41).

The last term in eq(8.14) was evaluated numerically for several cases (α, ε) and several locations (η). Its maximum contribution to the total value of the shear stress on the right side, occured when $\Lambda_\eta = 0$ (eq(A5.6)), and was approximately 13% for the laminar layer and 21% for the turbulent one. At separation $(\Lambda_\eta = -12)$, its contribution was only 0.6% and 0.9% respectively for the two cases. Thus, it seems reasonable to neglect this term ; when this is done, eq(8.14) becomes

$$v_e^2 \frac{\partial \theta_{22}}{\partial \eta} + v_e(\delta_2 + 2\theta_{22}) \left(\frac{\partial v_e}{\partial \eta} + \varepsilon u_e \right) = \frac{\tau_\eta R}{\varrho} \tag{8.15}$$

This result is exactly analogous to the corresponding equation for the two-dimensional boundary layer. Thus, the Karman/Pohlhausen method can be applied. The solution follows immediatelly from the two-dimensional case, and the procedure is shown in appendix 4. Table(8.1) illustrates the analogy between the various quantities involved in the two cases.

8.4 Laminar Boundary Layer

The separation criterion for the two-dimensional laminar boundary layer was established analytically by Pohlhausen and may be written in the equivalent conical terms as

$$\left(\frac{\theta_{22}}{\tau_{\eta,0}}\right)\left(\frac{dp}{d\eta}\right) \simeq 0.7 \tag{8.16}$$

Following the analysis in appendix 5, the above expression leads to eq(A5.32), which is repeated here

$$SC_L \equiv E_L^{-1} V^{-6} \left(\frac{dV}{d\eta} + \varepsilon U\right) \int_0^{\eta_s} E_L V^5 d\eta = -0.334 \tag{8.17}$$

U and V are the dimensionless external velocities

$$U \equiv \frac{u_e}{u_\infty} \tag{8.18a}$$

$$V \equiv \frac{v_e}{u_\infty} \tag{8.18b}$$

whereas E_L is defined by

$$E_L \equiv exp\left[6\varepsilon \int_0^{\eta} \frac{U}{V} d\eta\right] \tag{8.19}$$

For sufficiently slender bodies and small angles of attack, as has already been assumed in the inviscid solution,

$$u_e \simeq u_\infty \Rightarrow U \simeq 1.0 \tag{8.20}$$

so eqs(8.17) and (8.19) reduce to

$$SC_L = E_L^{-1} V^{-6} \left(\frac{dV}{d\eta} + \varepsilon \right) \int_0^{\eta_s} E_L V^5 d\eta = -0.334 \tag{8.17a}$$

$$E_L = exp \left[6\varepsilon \int_0^{\eta} \frac{d\eta}{V} \right] \tag{8.19a}$$

Thus, if the outer field is known, eqs(8.19a) and (8.17a) can be integrated. Starting from the reattachment point ($\eta = 180°$ for the usual range of angles of attack) the function SC_L is computed until the point is reached for which $SC_L = -0.334$. This will identify the upper separation point η_{su}. The integration is then carried out from the windward point ($\eta = 0°$) until the separation criterion is satisfied again at some location. This will identify the lower separation point η_{sl}. The two points at which the boundary layer leaves the surface will, of course, enclose the point at which the vortex sheet emanates in the inviscid outer solution.

8.5 Turbulent Boundary Layer

The separation criterion for two-dimensional turbulent boundary layer was determined experimentally by Nikuradse, and may be written in conical terms as

$$\left(\frac{\theta_{22}}{\tau_{\eta,0}} \right) \left(\frac{dp}{d\eta} \right) \simeq 4.7 \tag{8.21}$$

This result may be tranformed in a similar manner as for the laminar boundary layer (appendix 4)

$$SC_T \equiv \frac{1}{E_T V^5}\left(\frac{dV}{d\eta} + \varepsilon U\right)\left[\int_{\eta_{tr}}^{\eta_s} E_T V^4 d\eta + c_2\right] = -3.75 \tag{8.22}$$

where E_T is now defined by

$$E_T = exp\left[5.25\varepsilon \int_{\eta_{tr}}^{\eta} \frac{U}{V} d\eta\right] \tag{8.23}$$

If one assumes as in the laminar case that $U \simeq 1$, eqs(8.22) and (8.23) reduce to

$$SC_T = \frac{1}{E_T V^5}\left(\frac{dV}{d\eta} + \varepsilon\right)\left[\int_{\eta_{tr}}^{\eta_s} E_T V^4 d\eta + c_2\right] = -3.75 \tag{8.22a}$$

$$E_T = exp\left[5.25\varepsilon \int_{\eta_{tr}}^{\eta} \frac{d\eta}{V}\right] \tag{8.23a}$$

The integration of the turbulent boundary layer equations is carried out in the same way as for the laminar boundary layer, assuming that the boundary layer is turbulent from its start. For a given cone (ε) and angle of attack (α) the upper separation point is almost the same as for the laminar case, since the boundary layer which develops from the upper reattachment point has very little space to travel. The lower separation point, on the other hand, will occur at a larger distance η_{sl} since the turbulent boundary layer can progress farther into an adverse pressure gradient before separating, due to its increased momentum near the surface.

9. DETERMINATION OF THE SEPARATION LINES ON THE CIRCULAR CONE

9.1 Viscous/Inviscid Interaction

The boundary layer analysis in the previous chapter was made possible by assuming that the term containing the momentum thicknesses due to the interaction of the longitudinal and circumferential flows was negligible compared with the rest of the terms in the momentum equation. Thus, for both the laminar and the turbulent case eq(8.14) was reduced to eq(8.15) which is similar to the momentum equation for the two-dimensional boundary layer (table(8.1)).

On the other hand, the derivation of eq(8.14) in the first place, was made possible by the use of the simplified coordinate system described in section(8.3), which led to the simple expressions for the metric coefficients of eqs(8.1).

Unfortunately for an elliptical cone only one of these coefficients is unity, while the other two, when expressed in terms of the local coordinates, contain hyperbolic and trigonometric functions which lead to more complicated form for the boundary layer equations. For this reason, the viscous analysis is restricted to circular cones only.

The boundary layer separation in the cross-plane is sketched in fig(9.1). The matching of the viscous and inviscid flow fields is illustrated in fig(9.2), and is described below :

Velocity distributions as functions of the angle θ around the circular cross-section of the cone calculated (for $a = b = R = 1$) using the "single line-vortex" model are introduced into eqs(8.17a) and (8.19a) for the laminar case and into eqs(8.22a) and (8.23a) for the turbulent case. The integrations are carried out numerically by the Romberg method (refs.65,66). First, the starting point is taken at the upper reattachment point ($\theta = 180°$

if α is large enough) and procceding clockwise (for the right side of the cone) the point where the top boundary layer leaves the surface is identified. Similarly, starting at $\theta = 0°$ and proceeding counterclockwise (for the right side of the cone again), the point where the boundary layer leaves the surface is identified when $SC_L = -0.334$ or $SC_T = -3.75$ depending on the state of the boundary layer.

For a given cone geometry and angle of attack, the only acceptable solution (in terms of the assumed separation angle) is the one which yields the same pressures at both points where the boundary layer leaves the surface. This assumption is justified by the fact that the two streamlines which separate from the surface form a bubble (fig(9.1)) inside which there is no flow and therefore the pressure must be uniform.

9.2 Converged Solutions for Laminar and Turbulent Boundary Layers

Fig(9.3) shows the converged solutions for a cone with $\varepsilon = 5°$ at $\alpha = 30°$, for laminar and turbulent boundary layers. It may be seen, that the main difference between the two cases is the location of the lower separation. As was expected, when the boundary layer is turbulent, separation is delayed until a larger angle. The locations of the upper and inviscid separations as well as the vortex positions are almost identical for the two cases.

9.3 Comparison with Experiments

Friberg (ref.37) performed several experiments with circular cones in which the external flow was subsonic and the boundary layer was laminar. He was able to fit his observed separation lines reasonably well by the formula

$$\theta_s = 90 + (73 - \sqrt{51.4\alpha - 450})(0.76 + 0.024\varepsilon) \tag{9.1}$$

$$\text{for} \qquad 10 \leq \alpha \leq 30 \qquad \text{and} \qquad 5 \leq \varepsilon \leq 20$$

Jorgensen (ref.34), on the other hand, with his experiments in which the external flow was supersonic and the boundary layer turbulent, revealed a separation angle of 147°, which is also the angle that Bryson (ref.20) uses in his model.

In fig(9.4) the experimental results from both references are shown together with predictions of the present theory. The flat part which is common to all the curves in the low range of angles of attack represents attached flow (no vortex solutions exist in this range). At $\alpha \simeq 5°$ which corresponds to $\alpha/\varepsilon \simeq 1$ separation first takes place and all the separation angles change rapidly as α increases. Finally, at $\alpha \simeq 15°$ which corresponds to $\alpha/\varepsilon \simeq 3$, each separation angle reaches a limiting value which remains constant as α increases.

The agreement of the theoretical predictions with experimentally determined points is excellent. Most points seem to fall on the lower separation curve for the turbulent boundary layer.

Another feature shown by Friberg's experiments is that, although there is clearly a trend of the separation lines to move windward as α increases, surprisingly, there are exceptions such as the last point ($\alpha = 30°$) for the $\varepsilon = 5°$ cone in fig(9.4).

Lastly, it must be noted that Friberg's experiments showed a separation angle which is a function of both α and ε and not only of their ratio α/ε, while the present theory shows that the separation angle is almost a unique function of α/ε.

9.4 Pressure Distribution

The modified pressure distributions for $\alpha/\varepsilon = 2$ are shown in figs(9.5a) and (9.5b) respectively for the laminar and turbulent boundary layers. The flat portion of these curves represents the separation bubble where the pressure is required to be uniform. Although the initial inviscid pressure distributions are almost identical since the inviscid separation is almost the same ($\theta_s = 157°$ and $\theta_s = 159°$) for the two cases, the modified curves which result from the inclusion of the boundary layer show two characteristic differences. First, the separation bubble is larger for the laminar case (see also fig(9.3)), and second, the vortex suction is more pronounced for the turbulent case.

10. CONTROL OF SEPARATION BY BLOWING

10.1 Introduction

So far it has been shown that the boundary layer on a circular cone at incidence, as it develops from the windward stagnation line towards the leeward generator, will sooner (when it is laminar) or later (when it is turbulent) separate due to the adverse pressure gradient which encounters. It is possible, however, to postpone this separation, by replacing the natural boundary layer with a turbulent wall jet. The increased (due to the jet) momentum near the surface reenergizes the boundary layer, thus allowing the viscous flow to remain attached for a larger arc.

The mechanism of delaying the boundary layer separation through blowing is sketched in fig(10.1). The wall jet changes the location of separation, and this in turn changes all the vortex parameters (position, strength and lift). In other words, blowing changes the entire (inviscid) outer flow field by changing the conditions which generate this field.

Although the behavior of a wall jet flowing around a curved surface has been the subject of study for almost two centuries, the idea of using a thin, high velocity, tangential jet of fluid to control the location of separation on wings with rounded edges is relatively new. Wood and Roberts (ref.64) have recently examined the practicality of such a scheme by performing a wind tunnel experiment in which a wall jet was used, as a cross-flow plane device, to control the separation and hence the positions of the associated vortices on a conical delta wing.

The analysis in this chapter follows after Roberts (ref.63). Although in our case there is an external flow, the jet velocity is assumed to be much higher than the velocity of the outer field (i.e. $v_j \gg v_e$). Therefore the jet will be treated as issuing into quiescent surroundings. In addition, since the thickness of the boundary layer and the width of the jet are small compared to the local radius of the cone (i.e., $\delta/R, b_j/R \ll 1$) curvature effects will also be neglected.

10.2 The Flow Model

The profile of the wall jet is shown in fig(10.2). The jet consists of two parts ; an inner flow adjacent to the wall having a highly non-linear velocity profile characteristic of a turbulent wall flow, and an outer flow having a velocity profile typical of a free turbulent plane jet. The jet emerges from a point source into the fluid and spreads, increasing its width and decreasing its velocity due to turbulent diffusion in the jet and friction at the surface. At a distance η downstream of the jet exit the velocity v_j can be expressed as

$$v_j = v_m(\eta) f\left(\frac{\zeta}{b_j}\right) \tag{10.1}$$

where v_m is the maximum velocity, occuring at $\zeta = \zeta_m(\eta)$, and $b_j = b_j(\eta)$ is the half width of the jet (at which point $v_j = v_m/2$). The velocity profile in the outer flow ($\zeta > \zeta_m$) is assumed to take the form

$$v_j = v_m sech^2\left[\frac{k_j(\zeta - \zeta_m)}{(1 - \zeta_m)}\right] \qquad \text{for} \qquad \zeta > \zeta_m \tag{10.2}$$

This velocity profile is suggested by the classical free jet solution by Tollmien, modified to give $v_j = v_m$ at $\zeta = \zeta_m$. The constant k_j is determined such that $v_j = v_m/2$ at $\zeta = b_j$. Thus

$$k_j = tanh^{-1}\left(\frac{1}{\sqrt{2}}\right) = 0.8814 \tag{10.3}$$

The velocity profile for the inner flow is assumed to depend on the variable $(\zeta/\zeta_m)^{1/n}$ (where $n = 7$), as suggested by turbulent wall flow, and is chosen to give a maximum value $v_j = v_m$ at $\zeta = \zeta_m$. Thus

$$v_j = v_m\left[2\left(\frac{\zeta}{\zeta_m}\right)^{\frac{1}{n}} - \left(\frac{\zeta}{\zeta_m}\right)^{\frac{2}{n}}\right] \tag{10.4}$$

The value of ζ_m is determined by matching the second derivative of the velocity profiles given by eqs(10.2) and (10.4). The result is written

$$\zeta_m = b_j(1 + k_j n)^{-1} \tag{10.5}$$

10.3 The Wall Jet Equations

In addition to the approximations mentioned in section (10.1) (i.e. that $v_j \gg v_e$ and $b_j/R \ll 1$), the assumption is also made that the contribution of the shear stress at the wall and the contribution of the wall layer momentum ($\zeta < \zeta_m$) to the overall momentum balance are small. Under these assumptions we have :

continuity equation

$$\frac{\partial v}{\partial \eta} + \frac{\partial w}{\partial \zeta} = 0 \tag{10.6}$$

momentum equation

$$v\frac{\partial v}{\partial \eta} + w\frac{\partial v}{\partial \zeta} = -\frac{\partial}{\partial \eta}\left(\frac{p}{\varrho}\right) + \frac{\partial}{\partial \zeta}\left(\frac{\tau_\eta}{\varrho}\right) \tag{10.7}$$

The pressure is imposed by the external flow, so that

$$\frac{\partial p}{\partial \zeta} = 0 \tag{10.9}$$

The shear stress is determined from

$$\frac{\tau_\eta}{\varrho} = \epsilon\frac{\partial v}{\partial \zeta} \tag{10.9}$$

Using eqs(10.6) and (10.7) the integral form of the momentum equation is written

$$\frac{d}{d\eta}\int_0^\infty (v^2 + p)d\zeta = -\frac{\tau_\eta}{\varrho} \tag{10.10}$$

Neglecting the pressure term and substituting the velocity profiles from eqs(10.2) and (10.4) gives

$$\frac{1}{v_m^2}\frac{d}{d\eta}(b_j v_m^2) = -\frac{3}{4}k_j C_f \tag{10.11}$$

In eq(10.10) the contribution to the integral for the region $0 < \zeta < \zeta_m$ has been ignored since this is $O(\zeta_m/b_j)$, i.e., $O(1/n)$ where n is large, particularly for large Reynolds number flows.

Equation(10.11) indicates that the momentum in the wall jet is reduced by the action of wall friction. However, for our purposes, the jet will travel only a very short distance before separating, so it is reasonable to assume that its momentum will remain constant.

$$b_j v_m^2 = const \tag{10.12}$$

Having neglected curvature effects, eq(17) in ref.63 shows that the spreading rate of the jet will be constant, equal to that for a wall jet along a plane surface, i.e.,

$$b_j = K\eta \tag{10.13}$$

where

$$K = 0.073 \tag{10.14}$$

is an experimentally determined constant. It follows from eq(10.12) that the velocity of the jet is reduced as $1/\sqrt{\eta}$, i.e.,

$$v_m = \sqrt{\frac{C_\mu R v_e^2}{K\eta}} \tag{10.15}$$

where the blowing coefficient is defined as the ratio of the jet momentum to that of the external flield, just outside the boundary layer

$$C_\mu \equiv \frac{b_j v_m^2}{R v_e^2} \tag{10.16}$$

10.4 Wall Jet Separation

The only pressure gradient to which the jet is subject, after neglecting curvature effects, is the one due to the external flow. An approximate relationship for the influence of pressure gradient on wall shear stress for wall jets is

$$\tau_\eta = \tau_{\eta,0} - K'\zeta_m \left(\frac{dp}{d\eta}\right) \tag{10.17}$$

where $\tau_{\eta,0}$ is the shear stress at the wall with zero pressure gradient. From experiments by Bradshaw and Gee (ref.55) it is known that

$$K' \simeq \frac{1}{4} \tag{10.18}$$

Thus separation (where $\tau_\eta = 0$) occurs when the following condition is satisfied

$$\left(\frac{\zeta_m}{\tau_{\eta,0}}\right)\left(\frac{dp}{d\eta}\right) \simeq 4 \tag{10.19}$$

Table(10.1) compares the separation criteria for the boundary layer and the wall jet. The right side is approximately the same for both cases. The wall jet, however, has greater momentum near the wall. As a result, its characteristic dimension (distance of maximum velocity from the wall) is smaller than the corresponding characteristic dimension of the boundary layer (momentum thickness). In addition, higher velocities near the wall imply larger velocity gradients which result in greater shear stress at the wall. Thus, the first factor on the left side of the separation criterion is much smaller for the wall jet than for the boundary layer. As a consequence, the pressure gradient at separation is much larger for the wall jet and enables it to go farther against an adverse pressure gradient.

Using the following definitions

$$C_{f0} \equiv \frac{\tau_{\eta,0}}{\frac{1}{2}\varrho v_m^2} \tag{10.20}$$

$$C_p \equiv \frac{p - p_\infty}{\frac{1}{2}\varrho u_\infty^2(1+\alpha^2)} \tag{10.21}$$

$$\eta = \Delta\theta_s R \tag{10.22}$$

$$Re_m \equiv \frac{v_m \zeta_m}{\nu} \tag{10.23}$$

together with eqs(8.18b),(10.5),(10.13) and the experimental result (ref.63)

$$C_{f0} = 0.0315 Re_m^{-0.182} \simeq 0.004 \tag{10.24}$$

which is valid for $Re \simeq O(10^4)$, the separation condition eq(10.19) transforms into

$$\Delta\theta_s^2 = \frac{21.527}{(1+\alpha^2)} \left[\frac{V^2}{(\partial C_p/\partial\eta)}\right]_s C_\mu \tag{10.25}$$

Equation(10.25) is plotted in fig(10.4). It is seen, that the blowing intensity required for a given displacement of the lower separation point depends only on the state of the boundary layer (i.e. whether it is laminar or turbulent), and is almost independent of the cone geometry and angle of attack, as is indicated by the almost horizontal curves.

10.5 Converged Solutions before and after Blowing

Figures(10.3a) and (10.3b) show the converged solutions for a cone with $\varepsilon = 5°$ at $\alpha = 30°$ for the two states of the boundary layer (laminar and turbulent) before and after blowing. The main observation, which reveals the beauty of the idea of blowing as a means of controlling separation, is that very small blowing intensities are required to move the separation points from their natural locations, as predicted by the viscous/inviscid scheme in chapter 9, to points very close to the leeward generator. For both states of the boundary layer, blowing causes the separation to occur at a larger angle from the windward stagnation line, thus moving the vortices closer to the surface of the body toward the leeward generator. Smaller blowing intensity is required for the turbulent boundary layer for the same final configuration. This is explained by the fact that the separation for the turbulent boundary layer occurs naturally at a larger angle, and therefore the required $\Delta\theta_s$ is smaller.

10.6 Pressure Distribution

The modified pressure distributions for the configurations shown in fig(10.3) are plotted in fig(10.5). It is seen, that blowing has the following effects :

(i) It pushes the vortices (and as a result the vortex suction) closer to the leeward generator, thus closing the flow field. In the limit, as separation is suppressed completely, the results from the Jones theory are recovered.

(ii) It reduces the size of the separation bubble. This is shown by the diminishing of the flat portion of the curves which represents the distance between the upper and lower separation points.

(iii) It weakens the vortices (as is shown from the diminishing vortex suction) by pushing them closer to the surface. In effect, this reduces the vortex lift contribution, which is equivalent to reducing the angle of attack. Thus, it is seen that blowing allows control of the lift on a highly maneuverable aircraft without changing its attitude.

10.7 Lift

The relation between the lift and blowing coefficients is shown in fig(10.6). The fact that the curves drop more sharply as the relative incidence increases indicates that for a given body (ε) blowing becomes more effective as angle of attack increases.

The limit of all the curves is of course the Jones lift. Although it may seem impossible to eliminate separation completely, from fig(10.6) one may pick off each curve the point where the lift is within 5% of the Jones value. For all practical purposes, the vortex lift can then be neglected.

As a reminder, it is repeated that at the high angles of attack to which some of the highly maneuverable aircraft operate, the main problem is to eliminate any asymmetries of the vortex system, vortex breakdown, or both. Thus, the desire to sacrifice some of the vortex lift in order to achieve this goal is not surprising. As Wood (ref.64) has pointed out, however, there is an exception to the rule that blowing reduces the vortex lift. This occurs when, for a given configuration, blowing stabilizes the vortex system which otherwise would have broken down.

11. EPILOGUE

11.1 Discussion

It is well known from previous studies that the "single line-vortex" model has the following disadvantages when used to represent the inviscid outer field about bodies at high angle of attack :

(i) The position of the vortices is not very accurate. This should be expected, since the vortices are represented only globally in this model. To clarify this point a little further, we should remind ourselves that, in reality, the vorticity which is shed from the surface of conical bodies at incidence is distributed and not concentrated as the "single line-vortex" assumes. More complicated models which take this fact into account (see for example Smith ref.29) give vortex core locations which agree much better with experimental observations. The predicted vortex locations are even worse when asymmetric vortex solutions are sought. Nevertheless, as Smith has pointed out (ref.8) the crude vortex locations given by the "single line-vortex" model are very useful as initial guesses for the more complex numerical "rolled-up core" model.

(ii) The vortex lift is overestimated. This again is the result of a very strong suction generated on the upper surface of the body under the locations of the vortices. For delta wings, however, the non-linear lift is not a large part of the total unless the aspect ratio is very small, hence the error in the total lift is not too serious. The "rolled-up core" model also shows some suction, but the pressure peaks are much lower thus giving better agreement with experiments.

(iii) Vortex solutions cannot be found below a minimum value of the relative incidence, which depends on the thickness of the wing and the location of separation. Experimental observations (refs.34–39), partially verify this result, since at small angles of attack the body radius, as it grows in the longitudinal direction, prevents the departure of free vortices. When the angle of attack becomes sufficiently high, the vorticity in the boundary layer accumulates along generators on the upper surface of the body. The vortices generally do not separate from the body until some higher angle of attack is reached. However, the "rolled-up core" model gives solutions for much lower values of the relative incidence. The present work shows that, as long as the separation occurs on the upper surface, the minimum values of the relative incidence below which solutions do not exist for the "single line-vortex" model are reasonable and agree well with experiments (see Bryson ref.20). Trouble occurs when solutions are sought for which the separation takes place on the lower surface of the body. First, the straight feeding sheet has to pierce through the wing in this case, and this is physically impossible. Second, as the angle of attack decreases the vortex approaches the separation point and inevitably comes around the leading edge in which case the feeding sheet assumes an almost horizontal position. When this happens, the force balance between the vortex and its sheet is no longer possible, and as a result no solutions can be found.

(iv) The pressure distribution is poorly predicted by this theory, principally because the vorticity in the feeding sheets is neglected. On the body surface, the pressure jumps at the point where the vortex sheet emanates. This is also physically impossible. In reality the vortex sheet adjusts its position and shape so that it coincides with a three-dimensional stream surface. Since the normal velocity across such a surface is zero, the force on the vortex sheet is zero as well. In this model, however, the pressure jump is necessary to create the force on the vortex sheet which balances the force on the vortex.

Regarding the boundary layer solution for conical bodies the following may be said : the agreement of the predicted separation points with experiments is very good. Although this might have been expected when the terms dropped out of the cross-flow momentum equation were found to be small, there was still the question of how an unrealistic pressure jump resulting from the "single line-vortex" model would affect the boundary layer solution. Fortunately, because the lower boundary layer separates well before the point where the vortex sheet emanates (for the inviscid solution), the calculation of the boundary layer takes place in a region which is not affected much by the pressure jump across the vortex sheet.

11.2 Conclusions

(i) The "single line-vortex" model is limited in its accuracy but is adequate for the initial investigation of vortex flow control by tangential blowing.

(ii) Displacement of the vortex separation has been shown to influence the location and strength of the vortices for both flat plate and elliptical cross-section conical bodies.

(iii) The three-dimensional boundary layer over a circular cone has been analyzed. A method analogous to the Karman/Pohlhausen technique has been used to solve the cross-flow momentum equation, and the predicted separation lines agree well with experiments.

(iv) Blowing tangentially from slots located symmetrically along cone generators near the point of cross-flow separation is an effective way to control vortex location and strength. For sufficiently large blowing the dependence on vortex lift can be drastically reduced, and the effects of flow asymmetries may be made negligible.

11.3 Recommendations for Further Research

Additional work using an improved model should be undertaken in the following areas of the present model :

(i) Inviscid outer field : A better representation of the vortex sheets is desirable in order to get more accurate vortex positions and eliminate the pressure jump on the surface of the body. In addition, inclusion of the secondary vortices which were mentioned in section(1.1) may indirectly affect the main vortex parameters by influencing the locations of separation due to their close proximity on the surface.

(ii) Boundary layer : Two improvements are desirable in the boundary layer model. The first is an extension to non-circular cross-sections, and the second involves asymmetrical vortex configurations. The first may be accomplished by approximating the metric coefficients for very thin elliptical cross-sections. For the second a two-parameter integral method is necessary in order to match the pressure at the edges of each separation bubble (right and left) simultaneously.

(iii) Wall Jet : If blowing around leading edges with very small radius of curvature is desired (thin elliptical cross-section), then curvature effects must be included as is done in ref.63. Control of asymmetrical vortex shedding could also be analyzed in a similar manner provided that an appropriate boundary layer model is devised (see discussion in item (ii) above).

REFERENCES

A. GENERAL

1. H.Werle : "Flow Visualization Techniques for the Study of High Incidence Aerodynamics" AGARD LS–121, No.3, March 1982.
2. D.Hummel : "On the Vortex Formation over a Slender Delta Wing at Large Angles of Incidence" AGARD CP–247, No.15, 1978.
3. G.E.Erickson, W.P.Gilbert : "Experimental Investigation of Forebody and Wing Leading Edge Vortex Interactions at High Angles of Attack" AGARD CP–342, No.11, April 1983.
4. J.N.Nielsen : "Missile Aerodynamics" McGraw-Hill book company inc., New York, 1960.
5. H.Ashley, M.Landahl : "Aerodynamics of Wings and Bodies" Addison-Wesley publishing company inc., Reading, Massachusetts, 1965.
6. H.W.Liepmann, A.Roshko : "Elements of Gasdynamics" John Wiley and Sons, New York, 1957.
7. J.H.B.Smith : "Remarks on the Structure of Conical Flow" Progress in Aeronautical Science, Vol.12, Pergamon press, 1972.
8. J.H.B.Smith : "A Review of Separation in Steady Three-Dimensional Flow" AGARD CP–168.
9. L.H.Schindel : "Separated Flow about Lifting Bodies" MIT TR–80, September 1963.
10. N.Rott : "Vortices" 3rd annual W.R.Sears Distinguished Lecture, Cornell University, April 30, 1987.

B. SLENDER BODY THEORY WITHOUT SEPARATION

11. Max M.Munk : "The Aerodynamic Forces on Airship Hulls" NACA report No.184, 1924.
12. H.S.Tsien : "Supersonic Flow over an Inclined Body of Revolution" Journal of the Aeronautical Sciences, Vol.5, 1938.
13. R.T.Jones : "Properties of Low Aspect Ratio Pointed Wings at Speeds below and above the Speed of Sound" NACA report No.835, 1946, also NACA TN–1032, 1946.
14. G.N.Ward : "Supersonic Flow past Slender Pointed Bodies" Quarterly Journal of Mechanics and Applied Mathematics, Vol.1, part 1, March 1948.

15. Mac C.Adams, W.R.Sears : "Slender Body Theory–Review and Extension" Journal of the Aeronautical Sciences, February 1953.

C. "SINGLE LINE-VORTEX" MODEL

16. R.Legendre : "Ecoulement au Voisinage de la Pointe Avant d'une Aile Forte Fleche Aux Incidences Moyennes" La Recherche Aeronautique (ONERA) No.30,31 1952 and No.31,35 1953.

17. Mac C.Adams : "Leading Edge Separation from Delta Wings at Supersonic Speeds" Journal of Aeronautical Sciences, Vol.20, 1953.

18. R.H.Edwards : "Leading Edge Separation from Delta Wings" Journal of Aeronautical Sciences, Vol.21, 1954.

19. C.E.Brown, W.H.Michael : "On Slender Delta Wings with Leading Edge Separation", Journal of Aeronautical Sciences, Vol.21, 1954, also NACA TN–3430, 1955.

20. A.E.Bryson : "Symmetric Vortex Separation on Circular Cylinders and Cones", Journal of Applied Mechanics, December 1959.

21. L.H.Schindel : "Effect of Vortex Separation on Lifting Bodies of Elliptic Cross-Section" MIT TR–118, September 1965.

D. "MULTIPLE LINE-VORTEX" MODEL

22. A.H.Sacks, R.E.Lundberg, C.W.Hanson : "A Theoretical Investigation of the Aerodynamics of Slender Wing-Body Combinations Exhibiting Leading Edge Separation" NASA CR–719, 1967.

23. S.B.Angelucci : " A Multi-Vortex Method for Axisymmetric Bodies at Angle of Attack" Journal of Aircraft, Vol.8, No.12, December 1971.

24. A.J.Peace : "A Multi-Vortex Model of Leading Edge Vortex Flow" International Journal of Numerical Methods in Fluids, 1983.

25. C.Rehbach : "Etude Numerique de Nappes Tourbillonnaires Issues d'une Ligne de Dicollement pres du Bord d'Attaque" La Recherche Aeronatique No.6, 1973.

26. O.A.Kandil, E.H.Atta, A.H.Nayfeh : "Three-Dimensional Steady and Unsteady Asymmetric Flow past Wings of Arbitrary Planforms" NASA CR–145235, 1977.

27. D.Finkleman : "Non-Linear Vortex Interaction on Wing-Canard Configurations" Journal of Aircraft, Vol.9, 1972.

E. "ROLLED-UP CORE" MODEL

28. K.W.Mangler, J.H.B.Smith : "A Theory of the Flow past a Slender Delta Wing with Leading Edge Separation" RAE, Report Aero 2593, 1957.
29. J.H.B.Smith : "Improved Calculations of Leading Edge Separation from Slender, Thin, Delta Wings" Proc.Roy.Soc.A., Vol.306, 1968.
30. J.H.B.Smith : "Inviscid Fluid Models Based on Rolled-Up Vortex Sheets for Three-Dimensional Separation at High Reynolds Number" AGARD LS–94, No.9.
31. S.P.Fiddes : "A Theory of the Separated Flow past a Slender Elliptic Cone at Incidence" AGARD CP–291, No.30, 1980.
32. J.H.B.Smith : "Theoretical Modeling of Three-Dimensional Vortex Flows in Aerodynamics" AGARD CP–342, No.17, 1983, also Aeronautical Journal, April 1984.
33. J.E.Barsby : "Separated Flow past a Slender Delta Wing at Incidence" Aeronautical Quarterly, Vol.XXIV, 1973.

F. EXPERIMENTAL INVESTIGATIONS OF SEPARATION

34. L.H.Jorgensen : "Elliptic Cones Alone and with Wings at Supersonic Speeds" NACA TN–4045, October 1957.
35. W.J.Rainbird, R.S.Crabbe, L.S.Jurewicz : "A Water-Tunnel Investigation of the Flow Separation about Circular Cones at Incidence" NRC of Canada Aero Rep. LR–385, September 1963.
36. E.G.Friberg : "Measurement of Vortex Separation, part I : Two-Dimensional Circular and Elliptic Bodies" MIT TR–114, August 1965.
37. E.G.Friberg : "Measurement of Vortex Separation, part II : Three-Dimensional Circular and Elliptic Bodies" MIT TR–115, August 1965.
38. W.J.Rainbird, R.S.Crabbe, D.J.Peake, R.F.Meyer : "Some Examples of Separation in Three-Dimensional Flows" Canadian Aeronautics and Space Journal, December 1966.
39. L.H.Schindel, T.E.Chamberlain : "Vortex Separation on Slender Bodies of Elliptic Cross-Section" MIT TR–138, August 1967.

G. BOUNDARY LAYER

40. H.Schlichting : "Boundary Layer Theory" Mc Graw Hill book company inc., San Francisco, 1979.
41. F.M.White : "Viscous Fluid Flow" Mc Graw Hill book company inc., San Francisco, 1974.

42. B.Thwaites : "Approximate Calculations of the Laminar Boundary Layer" The Aeronautical Quarterly, Vol.1, November 1949.

43. F.K.Moore : "Laminar Boundary Layer on Circular Cone in Supersonic Flow at Small Angle of Attack" NACA TN–2521, October 1951.

44. F.K.Moore : "Laminar Boundary Layer on Cone in Supersonic Flow at Large Angle of Attack" NACA Rep. 1132, 1953.

45. F.K.Moore : "Three-Dimensional Laminar Boundary Layer Flow" Journal of the Aeronautical Sciences, August 1953.

46. F.K.Moore : "Three-Dimensional Boundary Layer Theory" Advances in Applied Mechanics, Vol.4, Academic Press, New York, 1956.

47. J.C.Cooke, M.G.Hall : "Boundary Layers in Three Dimensions" Progress in Aeronautical Sciences, Vol.2, Pergamon Press, 1962.

48. A.Mager : "Three-Dimensional Laminar Boundary Layers" from "High Speed Aerodynamics and Jet Propulsion", Vol.4 : "Theory of Laminar Flows" edited by F.K.Moore, Princeton University Press, 1964.

49. J.C.Cooke : "The Laminar Boundary Layer on an Inclined Cone" ARC R&M No.3530, August 1965.

50. J.C.Cooke : "Supersonic Laminar Boundary Layers on Cones" ARC CP No.1063, November 1966.

51. H.A.Dwyer : "Solution of a Three-Dimensional Boundary Layer Flow with Separation" AIAA Journal, Vol.6, No.7, July 1968.

52. W.Geissler : "Three-Dimensional Laminar Boundary Layer over a Body of Revolution at Incidence and with Separation" AIAA Journal, Vol.12, No.12, December 1974.

53. R.S.Crabbe : "Flow Separation about Elliptic Cones at Incidence" AIAA paper No. A65–29841.

H. WALL JETS

54. M.B.Glauert : "The Wall Jet" Journal of Fluid Mechanics, Vol.1, August 1956.

55. P.Bradshaw, M.T.Gee : "Turbulent Wall Jets with and without an External Stream" ARC R&M No.3252, also ARC No.22008, June 1960.

56. I.S.Gartshore, B.G.Newman : "The Turbulent Wall Jet in an Arbitrary Pressure Gradient" Aeronautical Quarterly, Vol.XX, part 1, February 1969.

57. B.R.Ramaprian : "Turbulent Wall Jets in Conical Diffusers" AIAA Journal, Vol.11, No.12, November 1972.

58. B.R.Ramaprian : "Turbulence Measurements in an Equilibrium Axisymmetric Wall Jet" Journal of Fluid Mechanics, Vol.71, part 2, September 1974.

59. R.N.Sharma, S.V.Patankar : "Numerical Computations of Wall Jet Flows" International Journal of Heat and Mass Transfer, Vol.25, No.11, November 1978.

60. R.N.Sharma "Experimental Investigation of Conical Wall Jets" AIAA Journal, Vol.19, No.1, September 1979.

61. B.E.Launder, W.Rodi : "The Turbulent Wall Jet" Progress in Aerospace Sciences, Vol.19, 1981.

62. B.E.Launder, W.Rodi : "The Turbulent Wall Jet – Measurements and Modeling" Annual Review of Fluid Mechanics, Vol.15, 1983.

63. L.Roberts : "A Theory for Turbulent Curved Wall Jets" AIAA paper No. 87–0004, January 1987.

64. N.J.Wood, L.Roberts : "The Control of Vortical Lift on Delta Wings by Tangential Leading Edge Blowing" AIAA paper No. 87–0158, January 1987.

I. NUMERICAL METHODS

65. J.H.Ferziger : "Numerical Methods for Engineering Application" John Wiley and Sons inc., New York, 1981.

66. G.Dahlquist, A.Bjorck, N.Anderson : "Numerical Methods" Prendice-Hall inc., New Jersey, 1974.

FIGURES

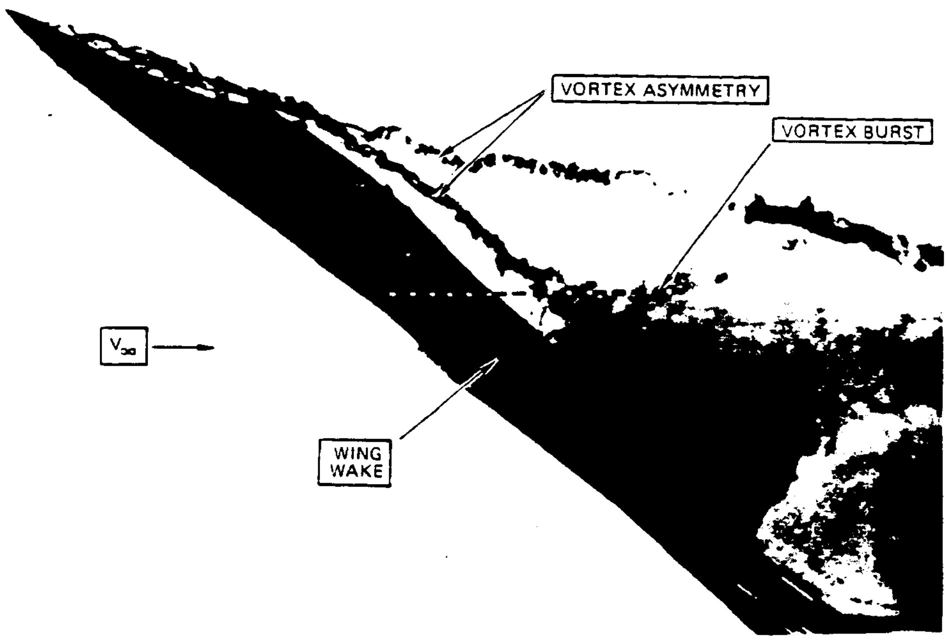

Figure 1.1 Model of F–5F at $\alpha = 40°$, in Northrop water tunnel. The vortex system is asymmetric, and the lower vortex has burst at some point over the wing. [G.E.Erickson, W.P.Gilbert : "Experimental Investigation of Forebody and Wing Leading Edge Vortex Interactions at High Angles of Attack" AGARD CP–342, No.11, July 1983]

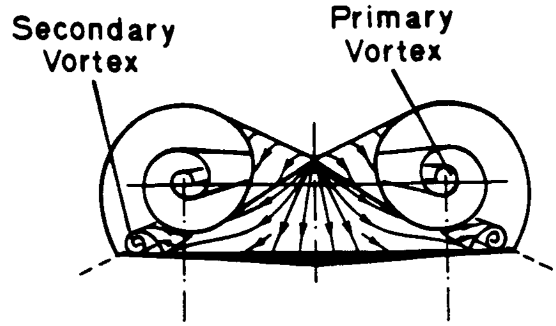

Figure 1.2 Vortex formation over a slender delta wing at incidence.

a. "Rolled-up core" model.

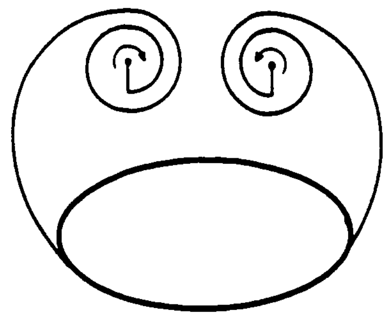

b. "Multiple line-vortex" model.

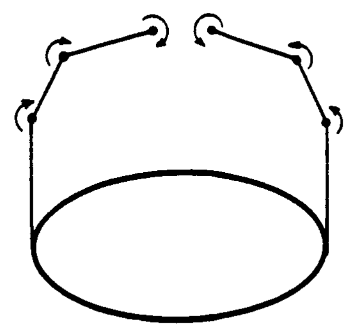

c. "Single line-vortex" model.

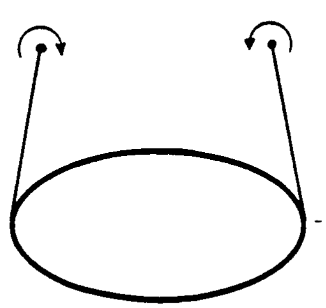

Figure 2.1 Three models representing vortex separation in the cross-plane of a conical body.

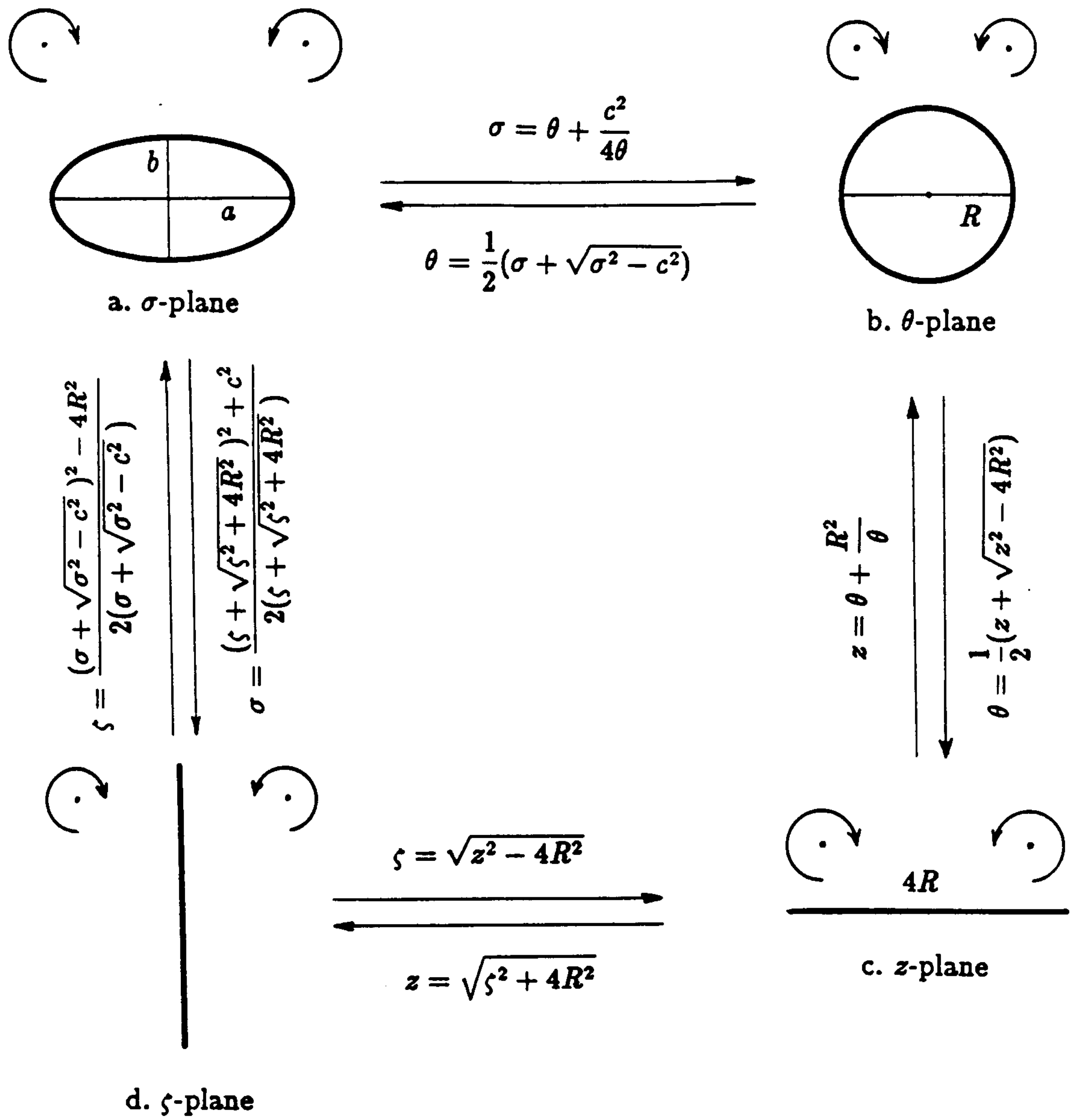

Figure 2.2 Conformal mapping in the cross-plane.

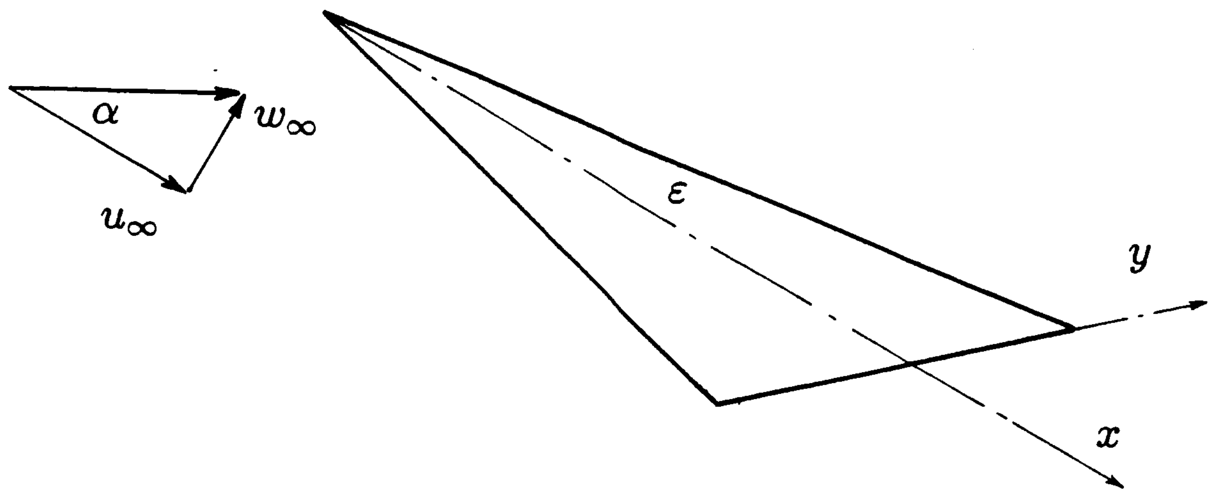

Figure 3.1 A flat delta wing at incidence.

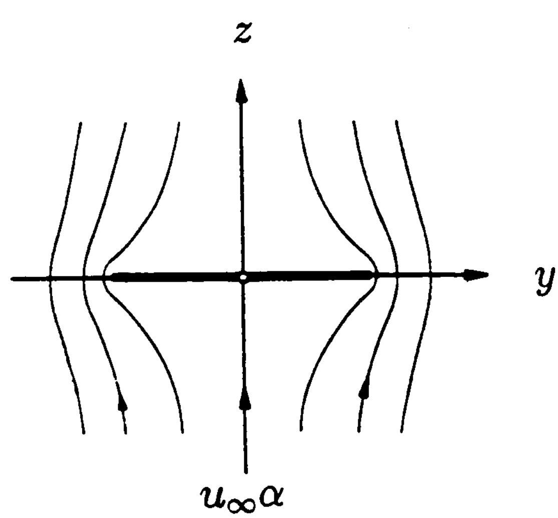

Figure 3.2 Schematic of the streamlines in the cross-plane of a flat delta wing at incidence with attached flow.

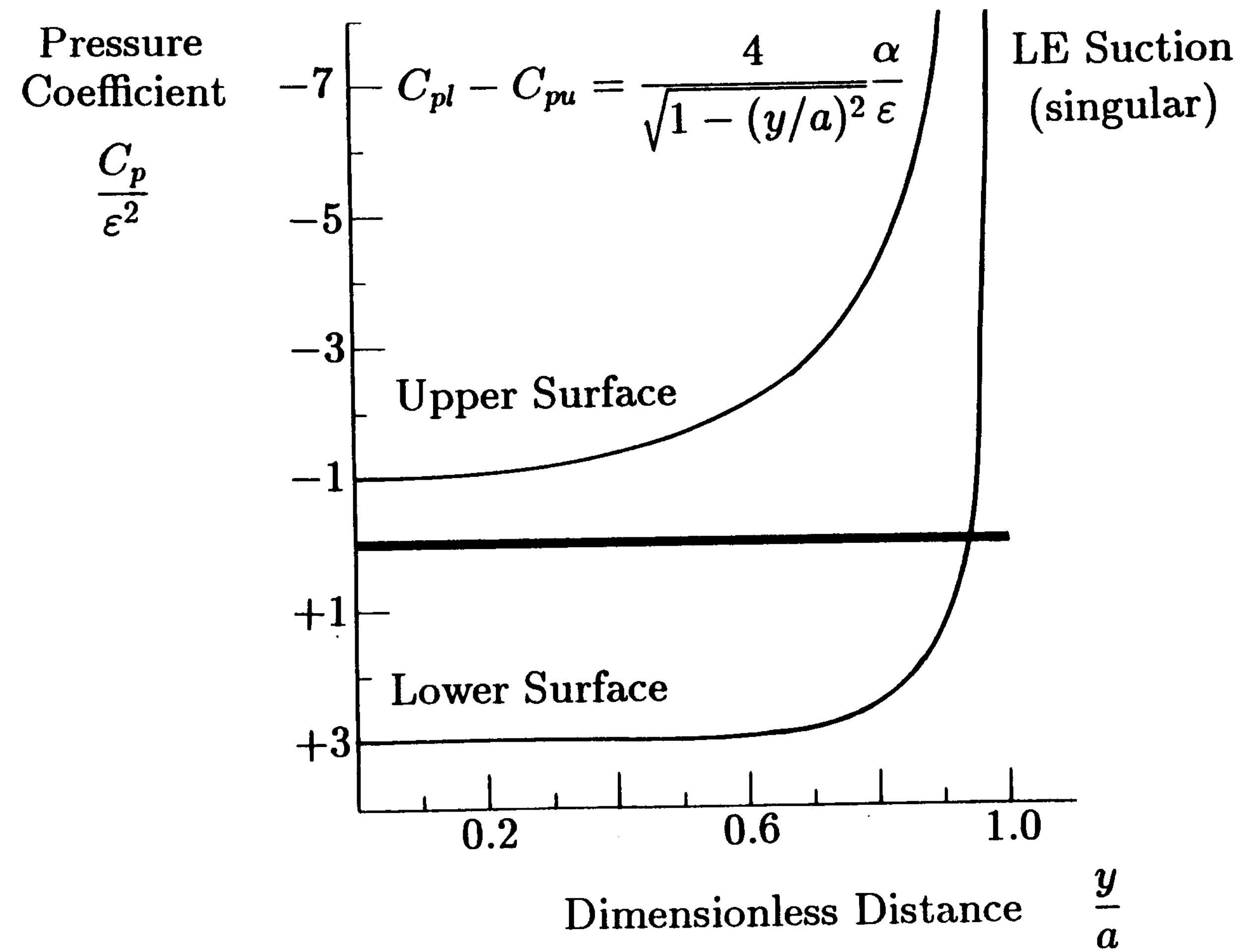

Figure 3.3 Pressure distribution on a flat delta wing with attached flow for $\alpha/\varepsilon = 1$.

C-2

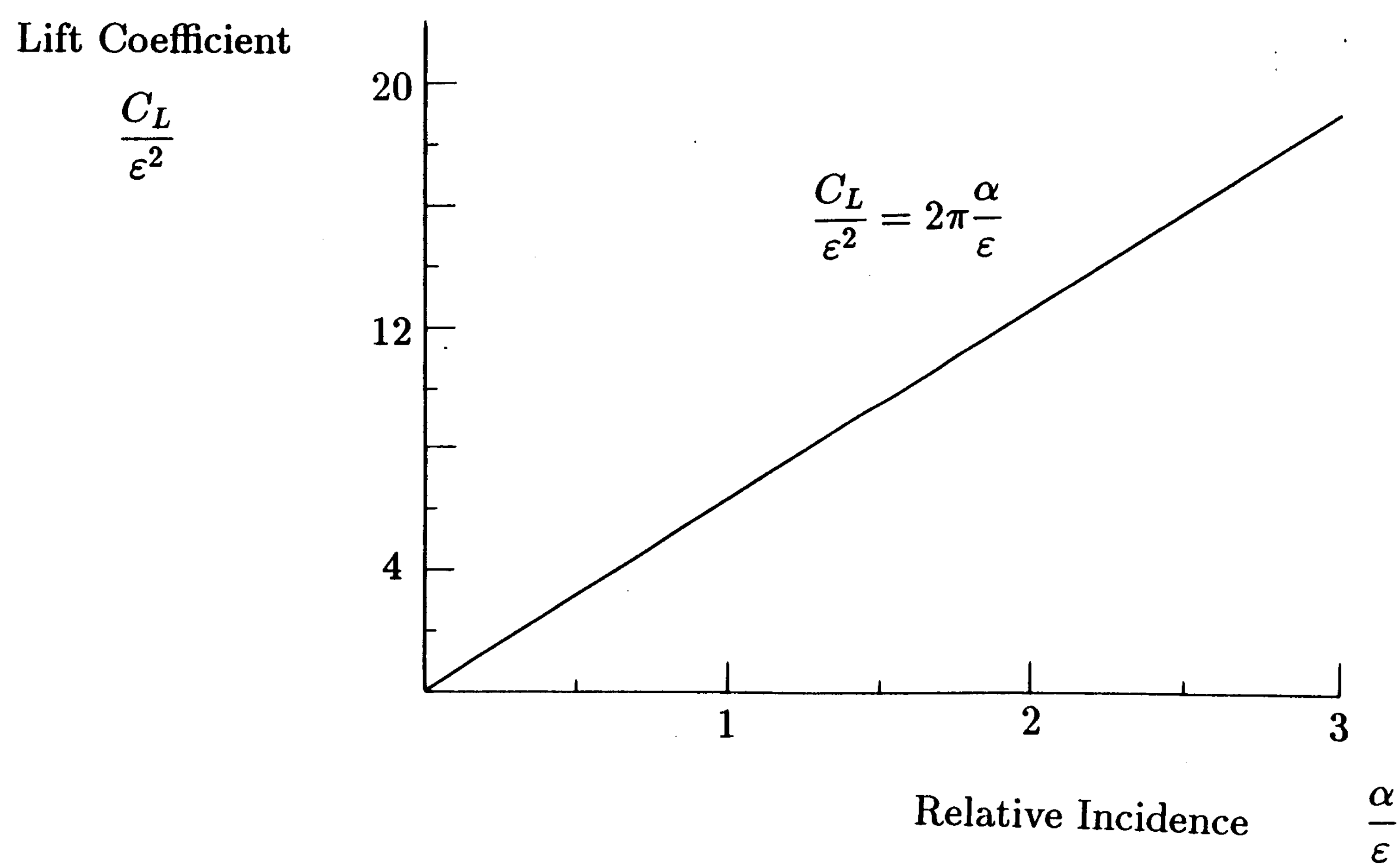

Figure 3.4 Lift vs. relative incidence for a flat delta wing with attached flow.

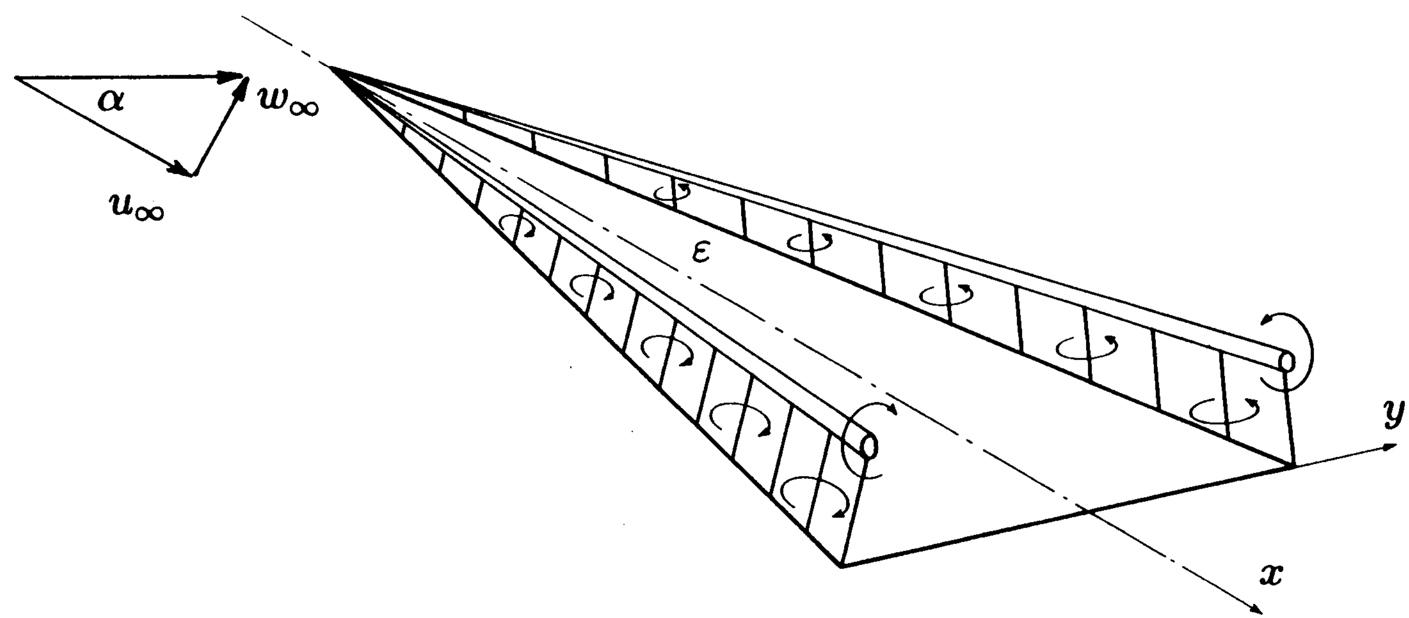

Figure 4.1 "Single-line vortex" model
on a flat delta wing with leading-edge separation.

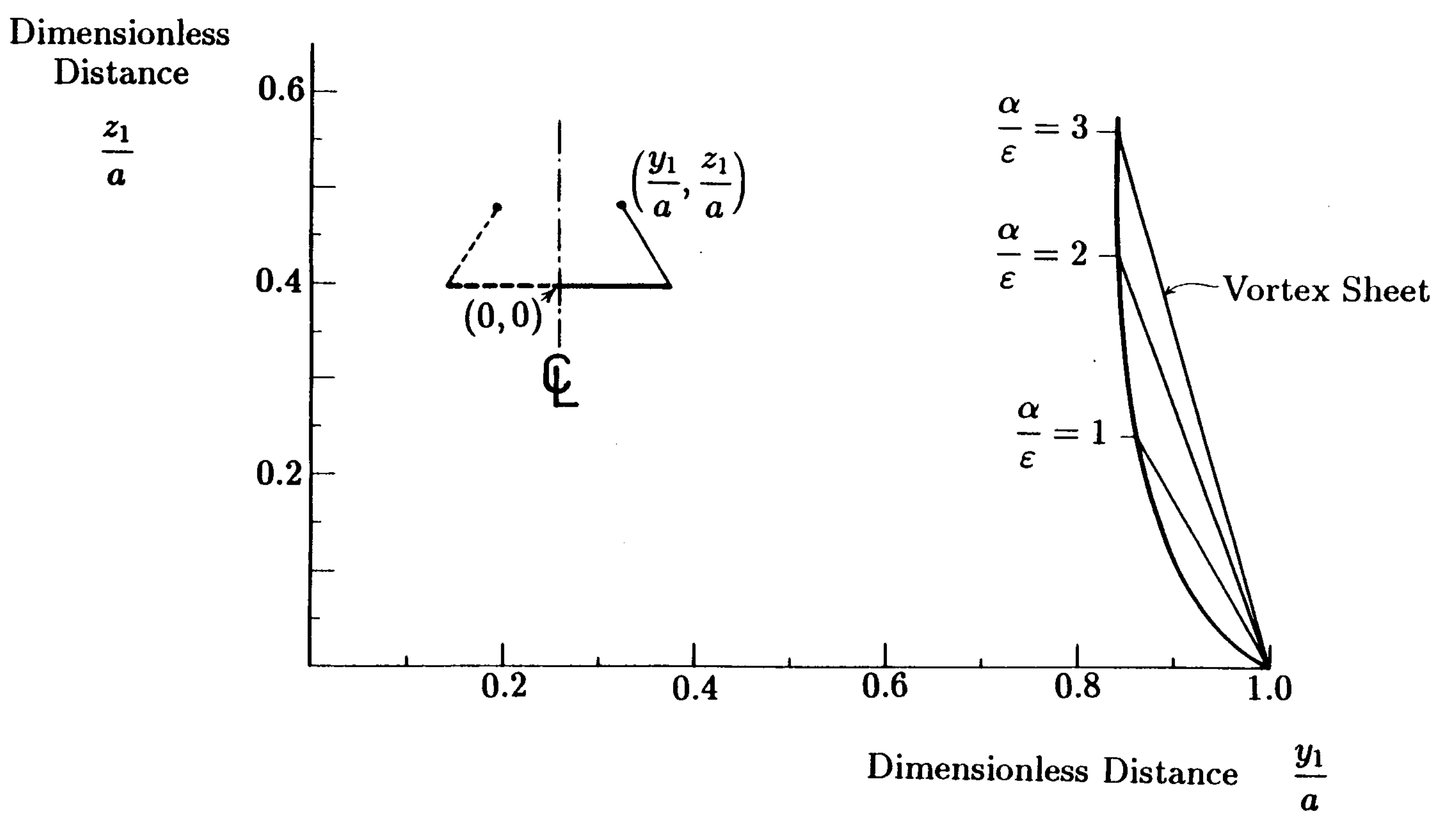

Figure 4.2 Locus of vortex positions for a flat delta wing with leading-edge separation.

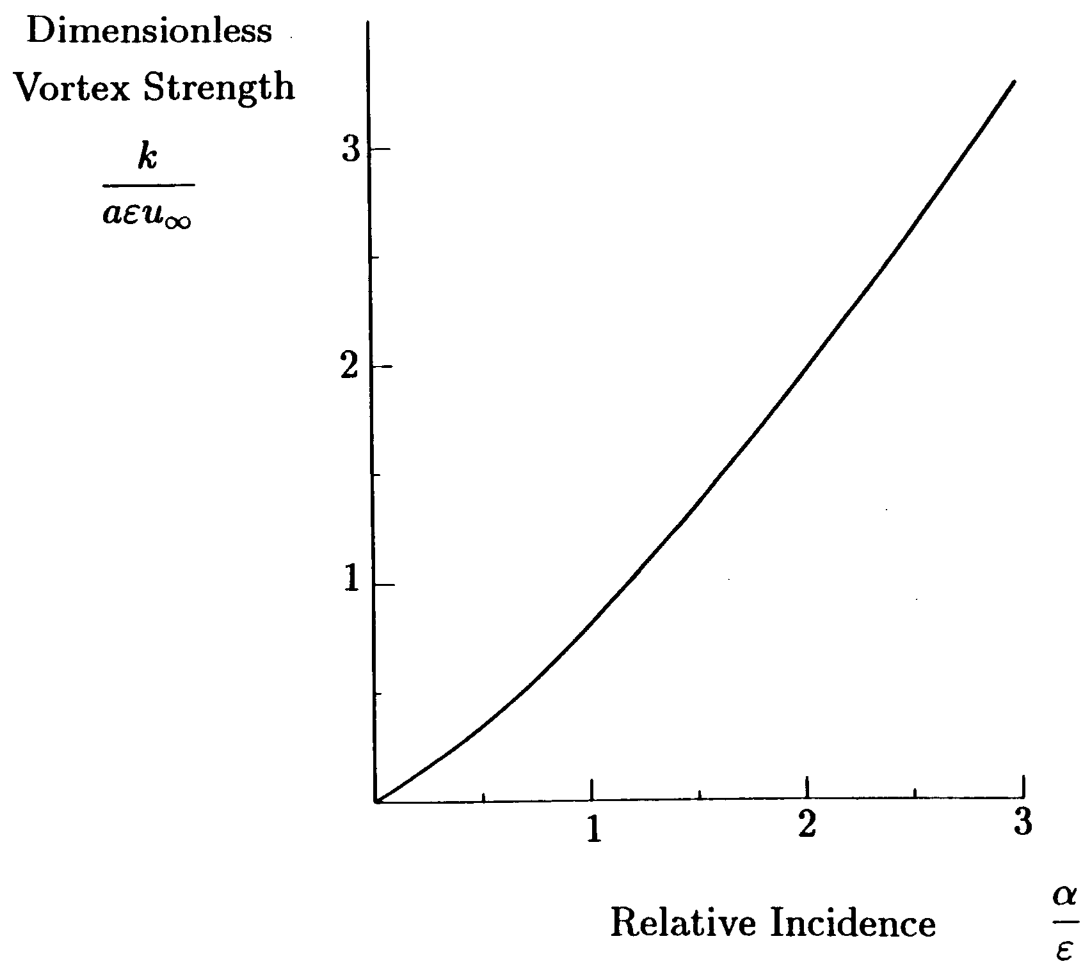

Figure 4.3 Vortex strength vs. relative incidence for a flat delta wing with leading-edge separation.

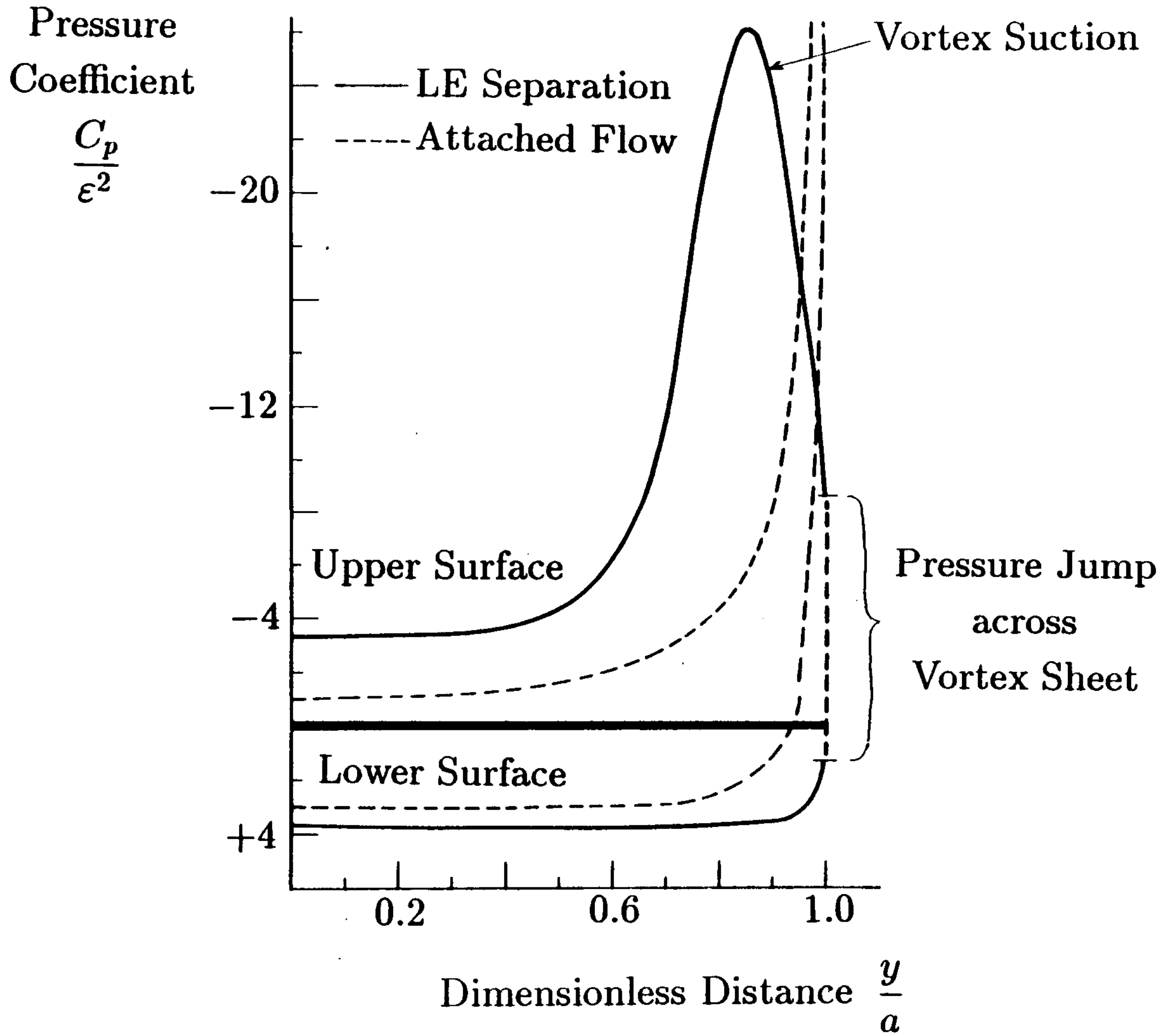

Figure 4.4 Pressure distribution on a flat delta wing with leading-edge separation for $\alpha/\varepsilon = 1$.

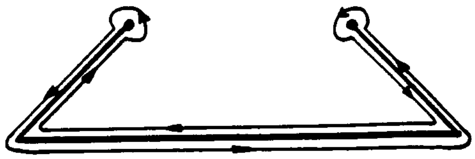

a. z-plane

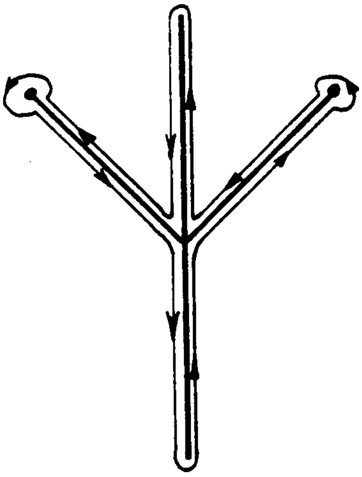

b. ζ-plane

Figure 4.5 Contours of integration for the normal force.

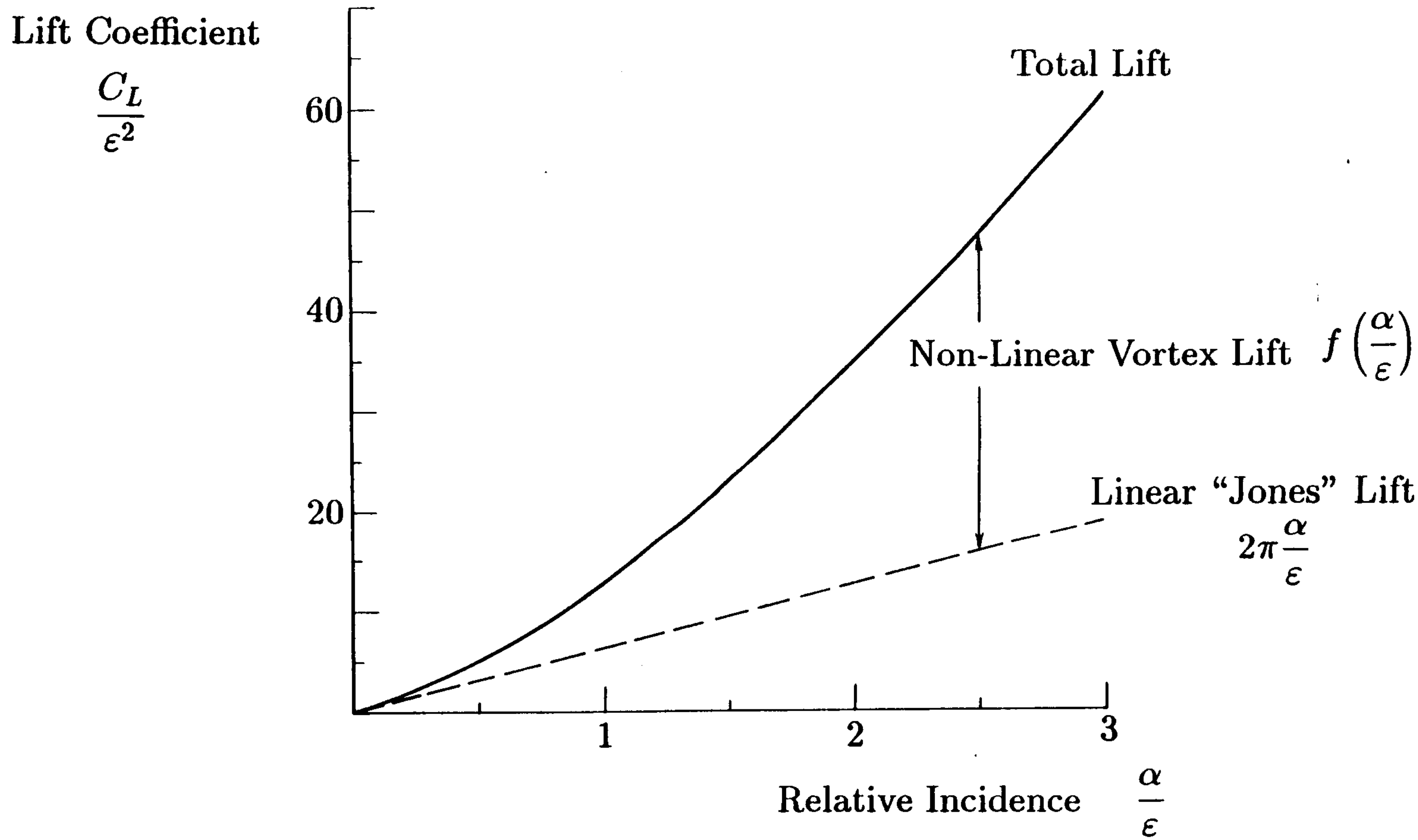

Figure 4.6 Lift vs. relative incidence
for a flat delta wing with leading-edge separation.

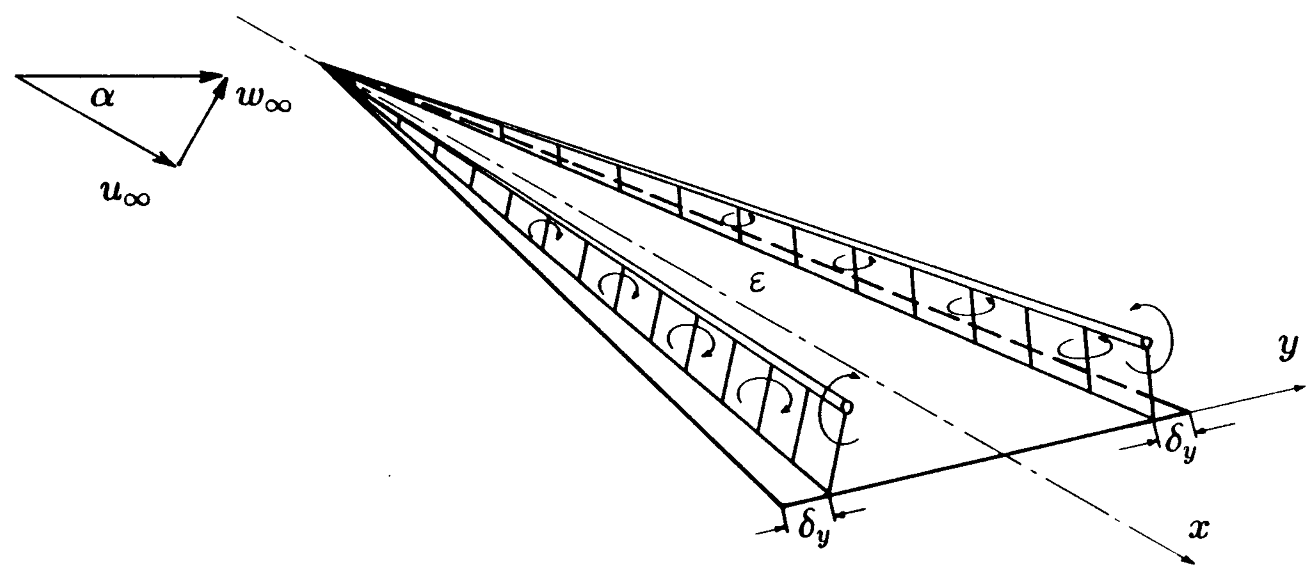

Figure 5.1 "Single-line vortex" model on a flat delta wing with displaced separation.

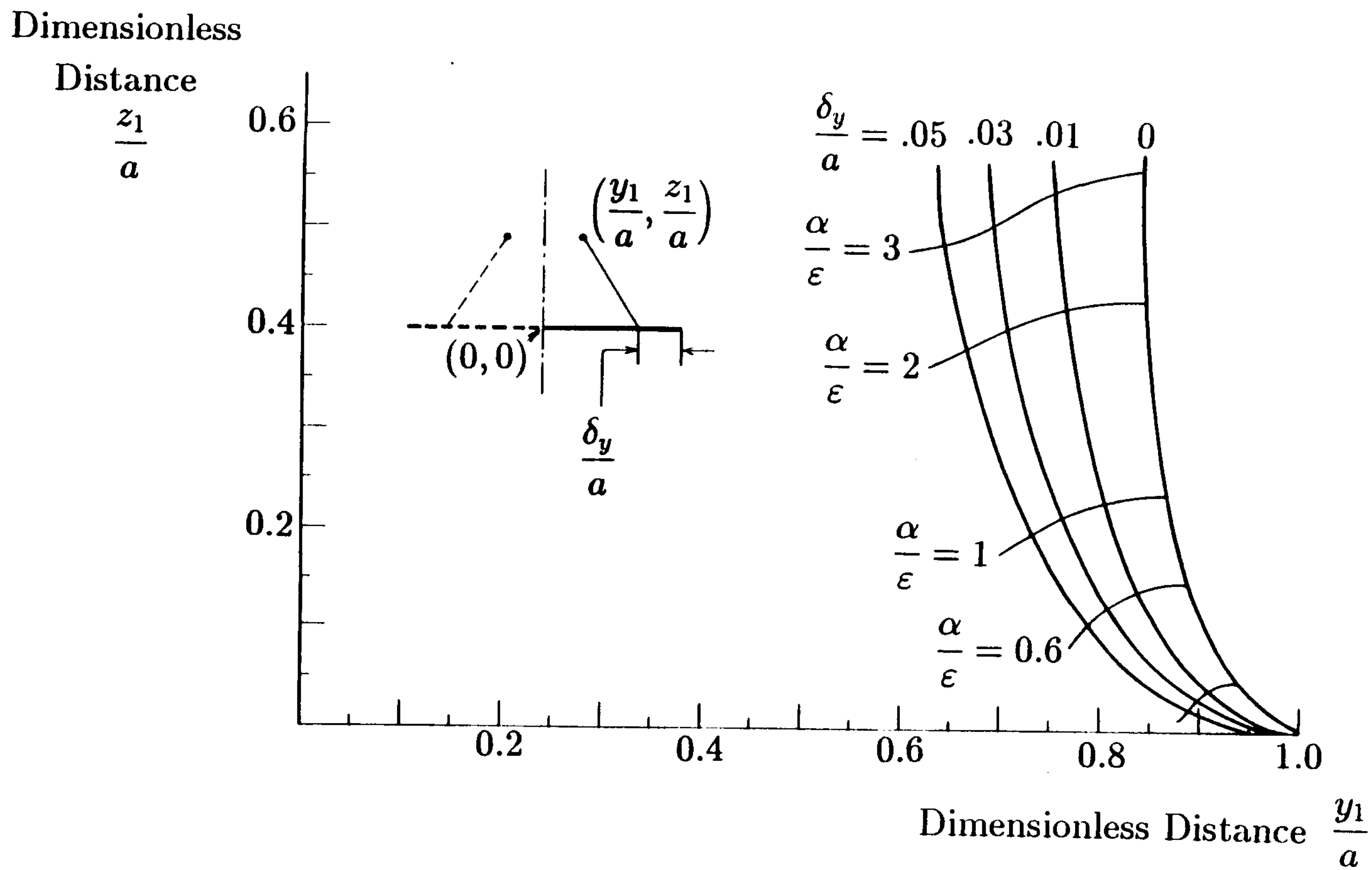

Figure 5.2 Loci of vortex positions for a flat delta wing with displaced separation.

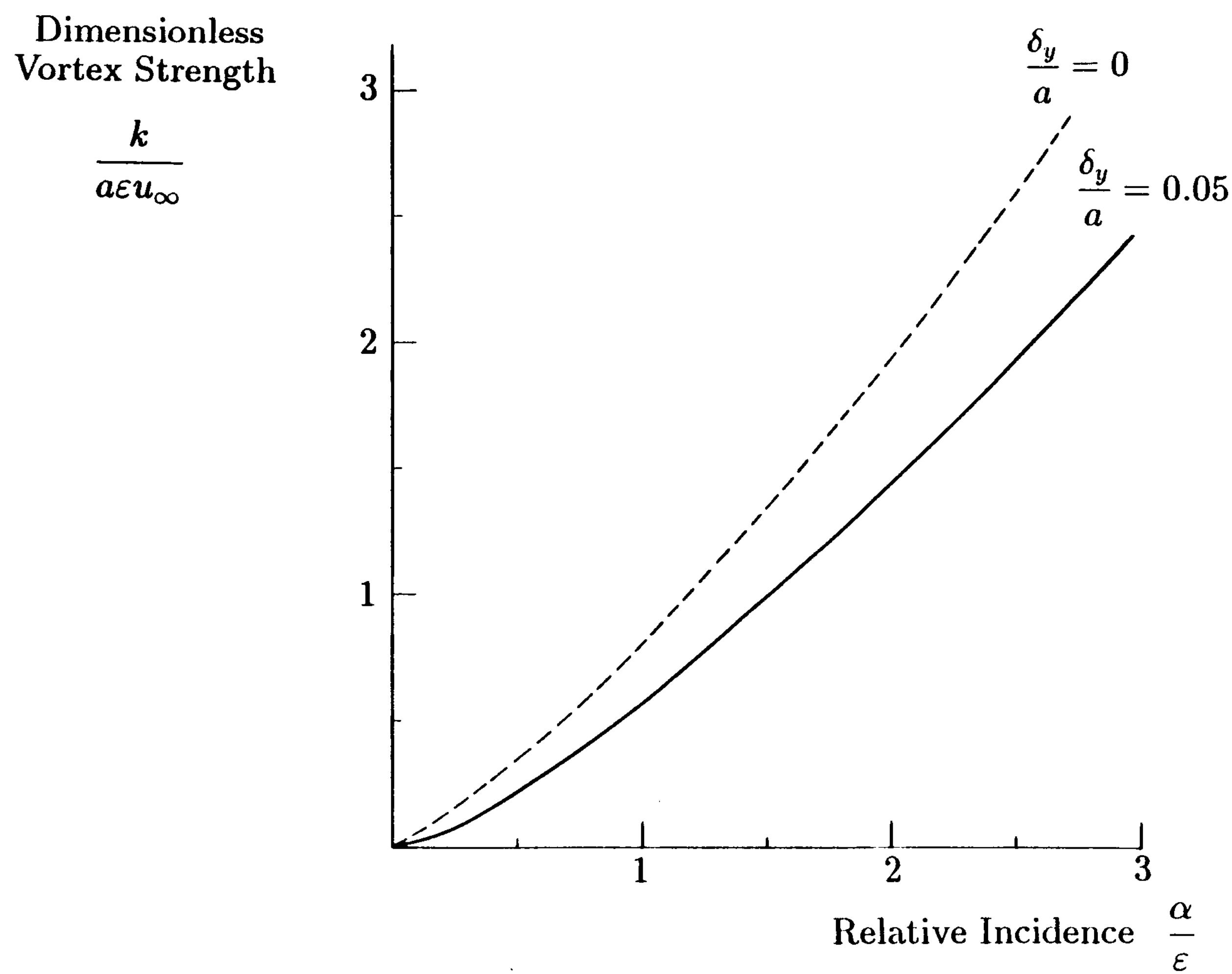

Figure 5.3 Vortex strength vs. relative incidence for a flat delta wing with displaced separation.

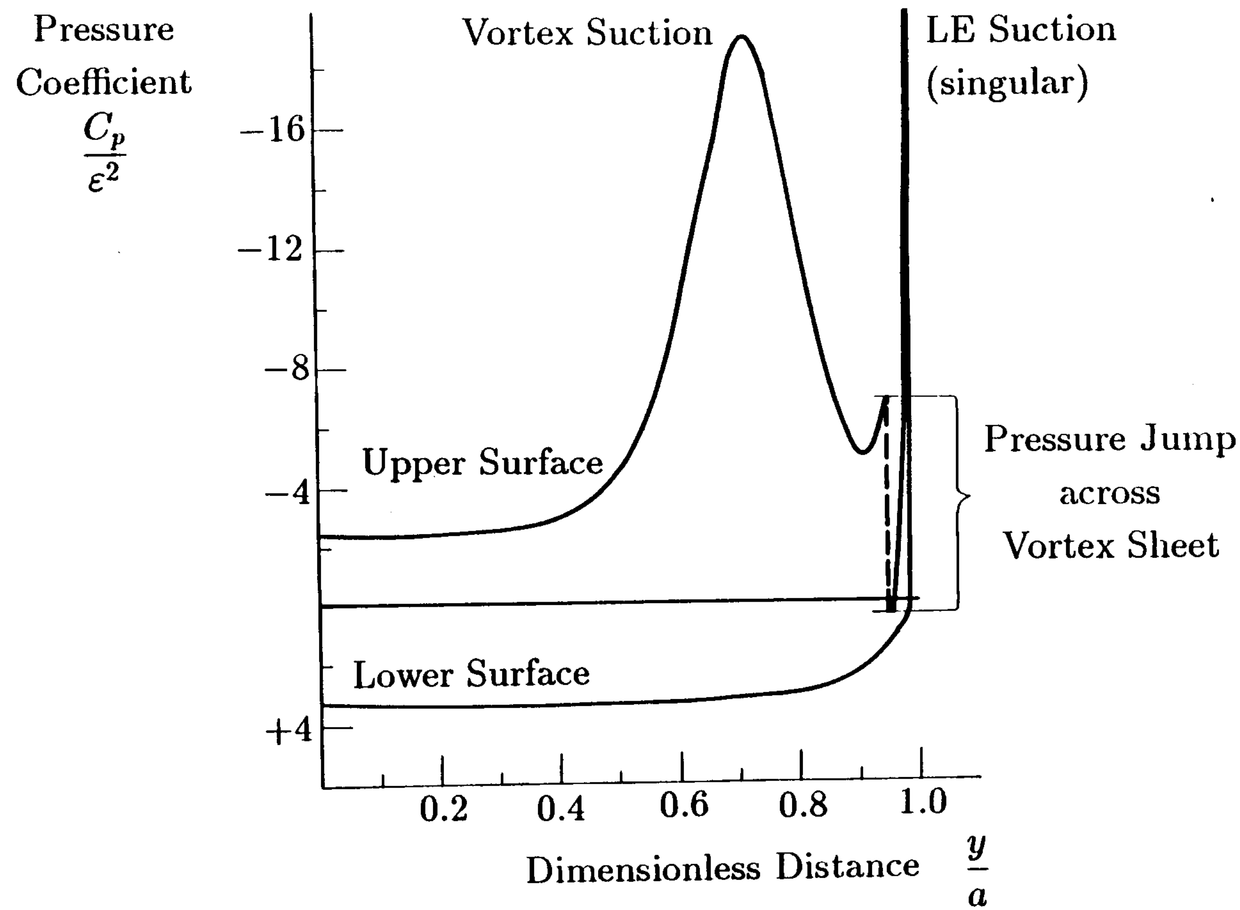

Figure 5.4 Pressure distribution on a flat delta wing with displaced separation ($\delta_y/a = 0.05$) for $\alpha/\varepsilon = 1$.

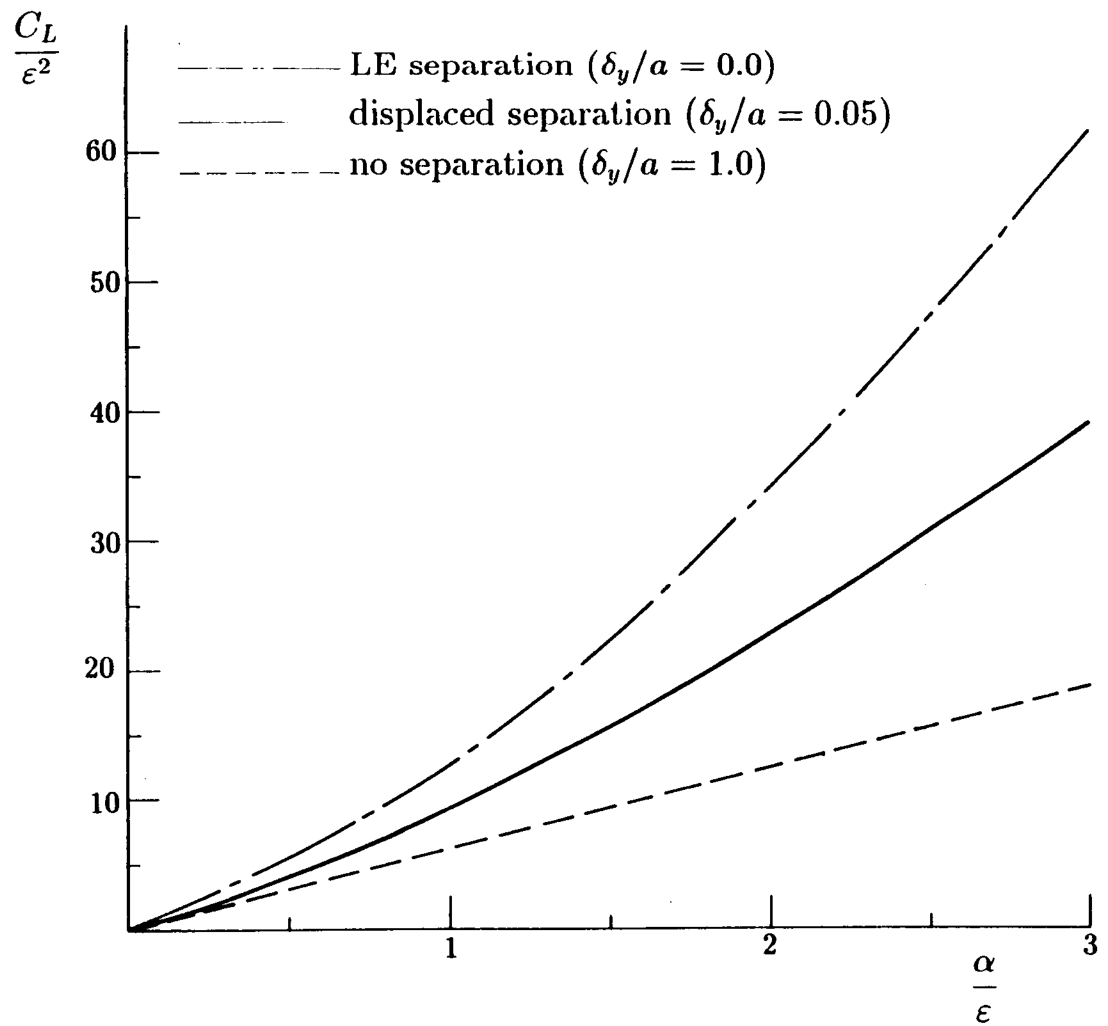

Figure 5.5 Lift vs. relative incidence for a flat delta wing with displaced separation.

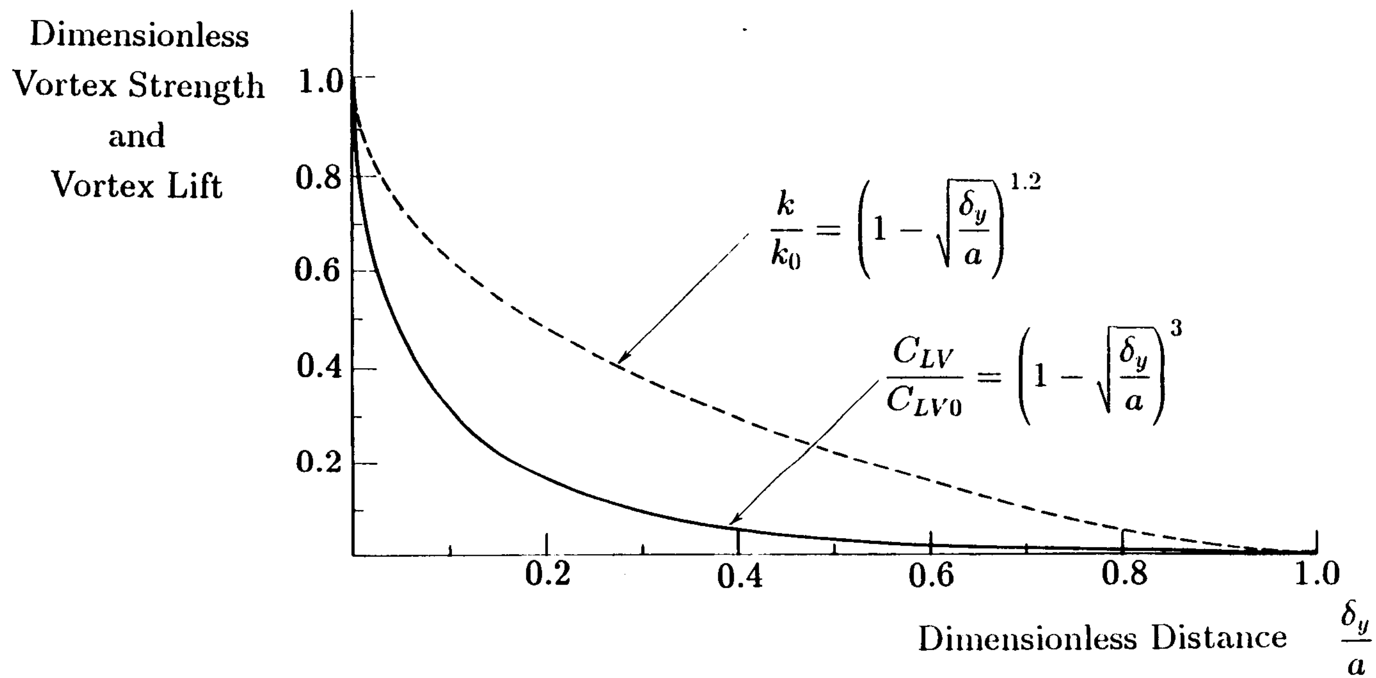

Figure 5.6 Vortex strength and vortex lift vs. separation location for a flat delta wing.

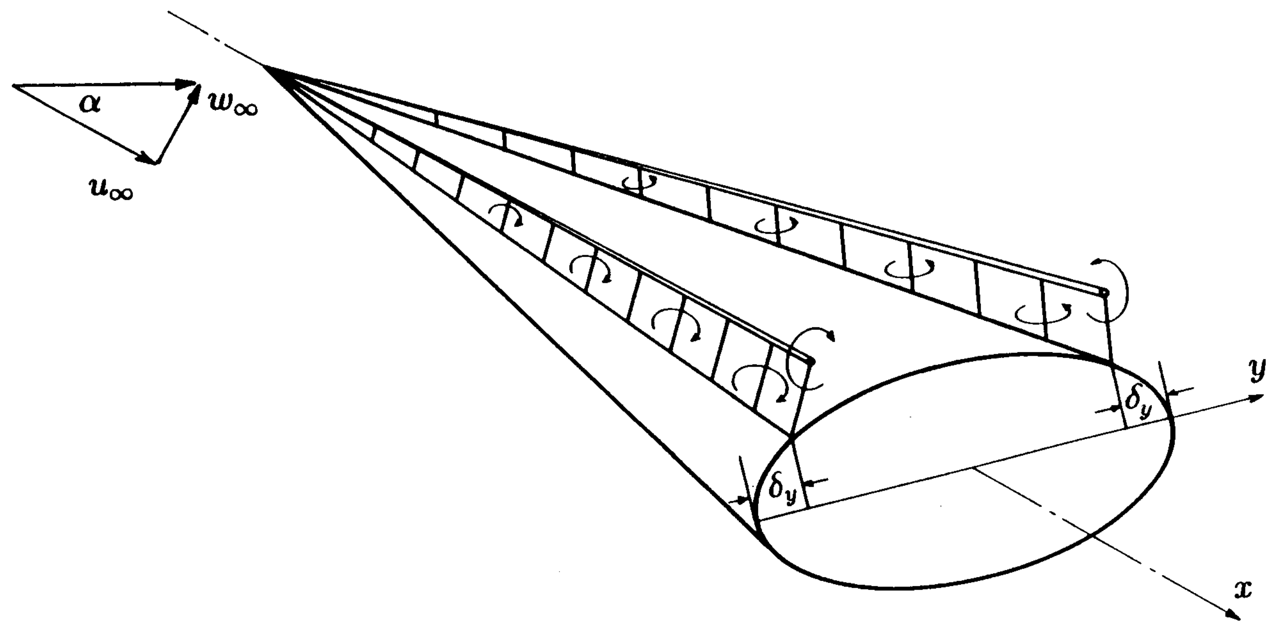

Figure 6.1 "Single-line vortex" model on a delta wing with elliptical cross-section.

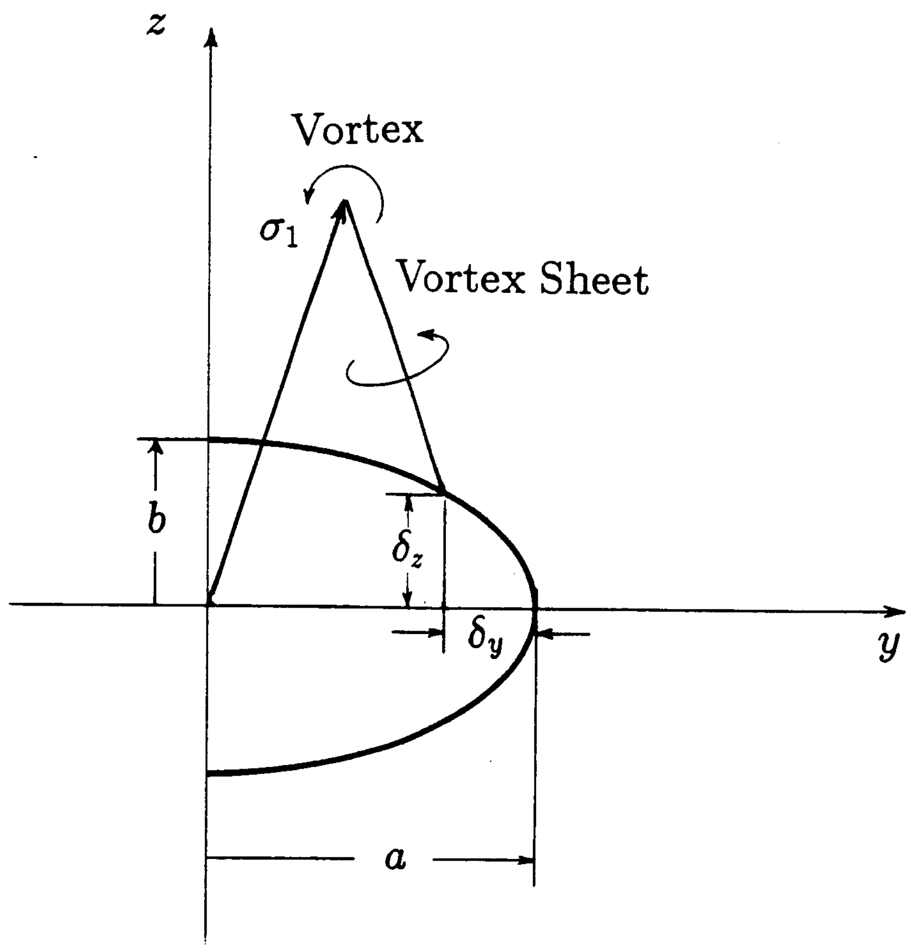

Figure 6.2 Schematic of the details in the cross-plane.

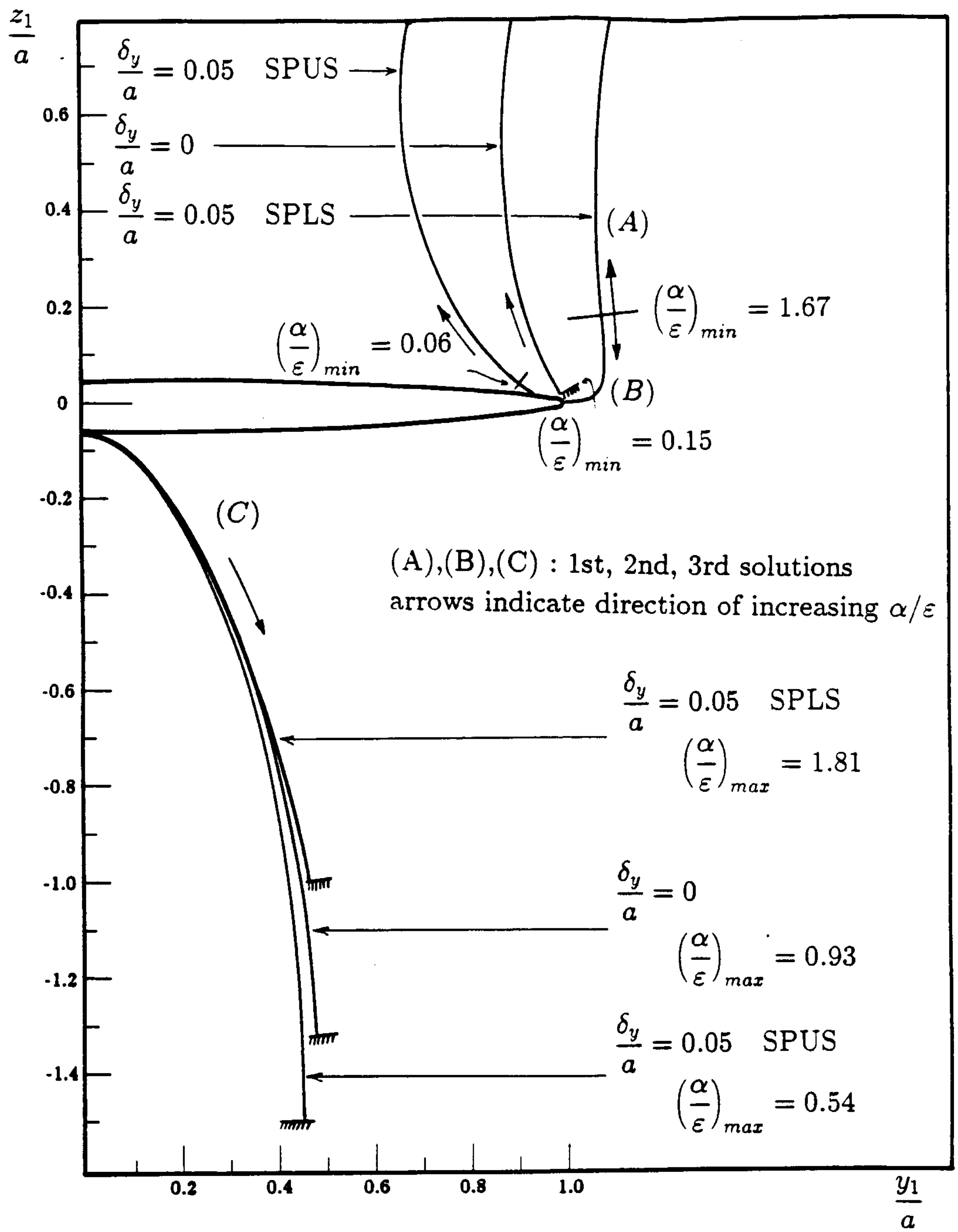

Figure 6.3 Loci of vortex positions
for a delta wing with elliptical cross-section ($b/a = 0.05$).

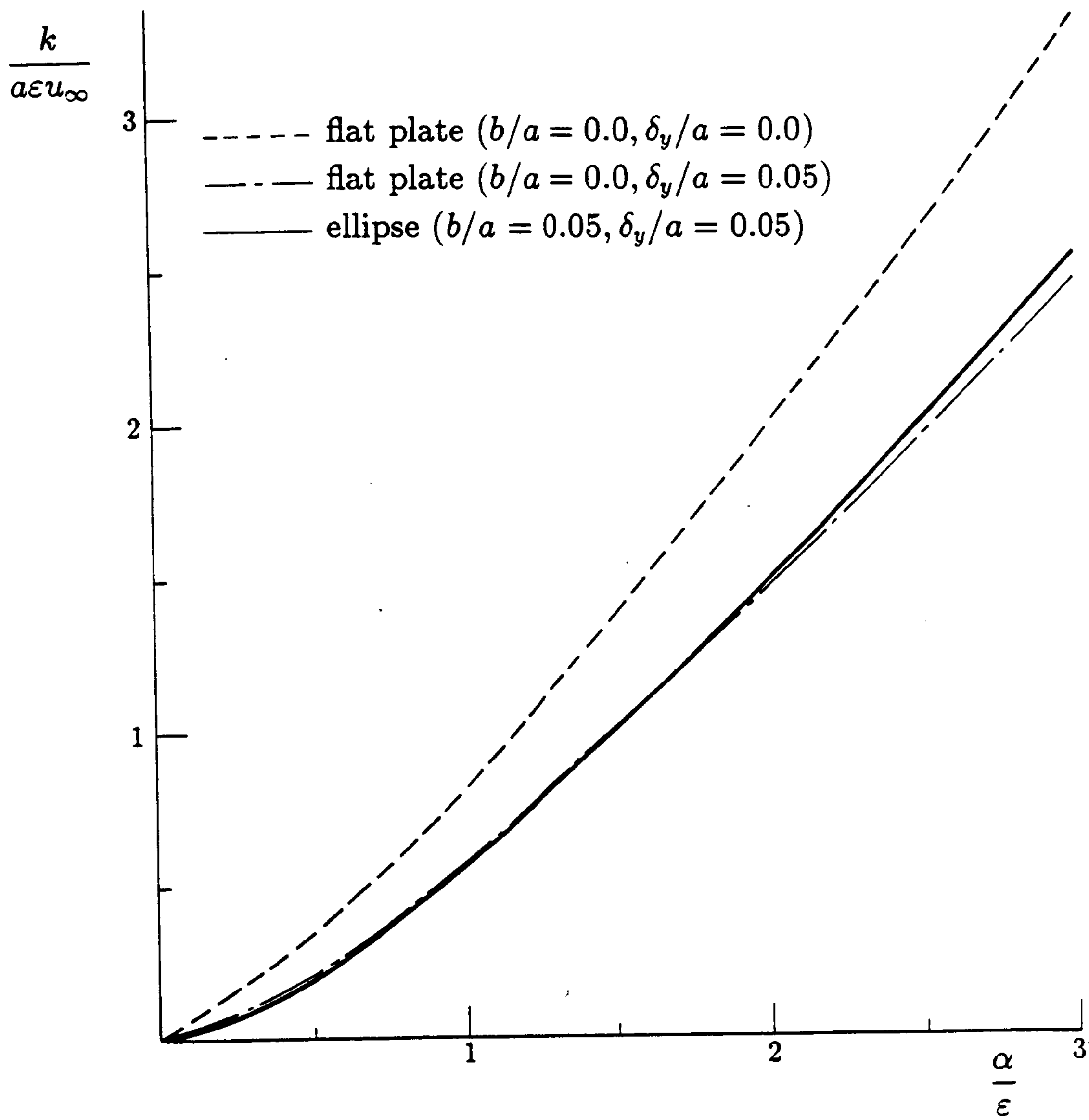

Figure 6.4 Vortex strength vs. relative incidence for a delta wing with elliptical cross-section ($b/a = 0.05$).

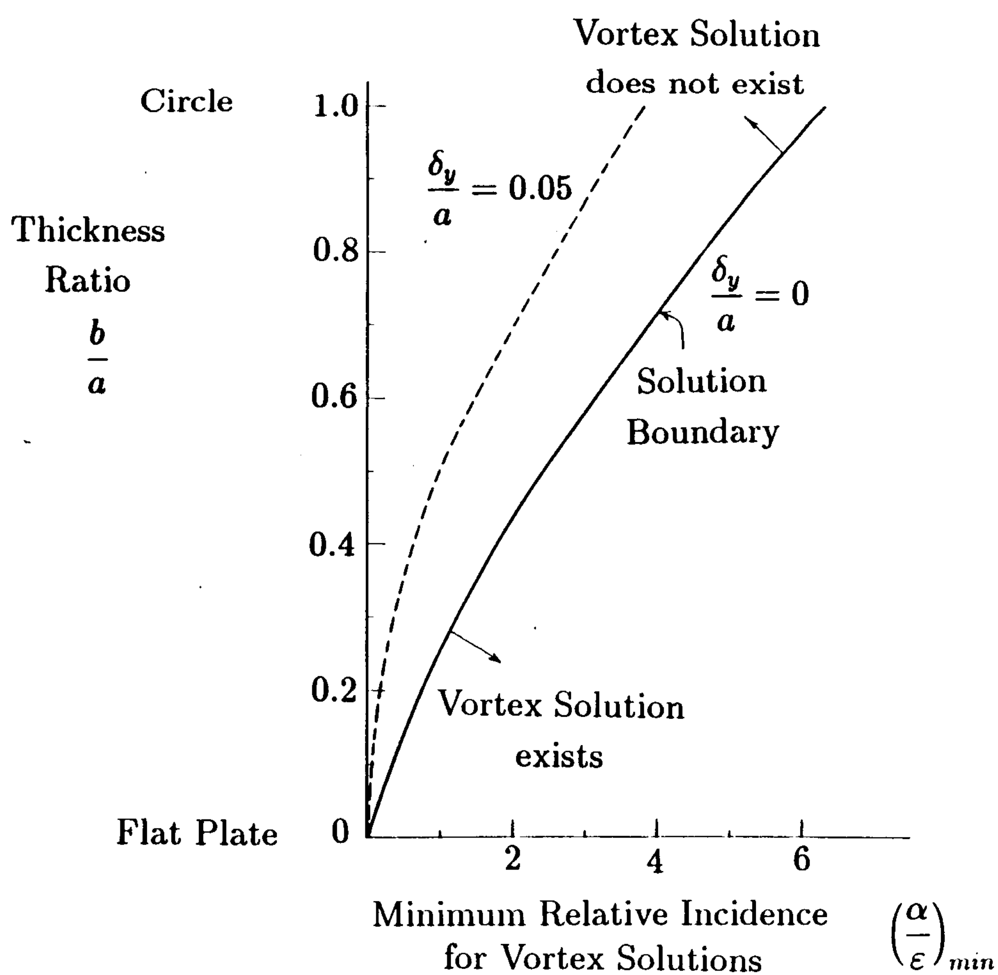

Figure 6.5 Solution boundaries vs. thickness and separation location.

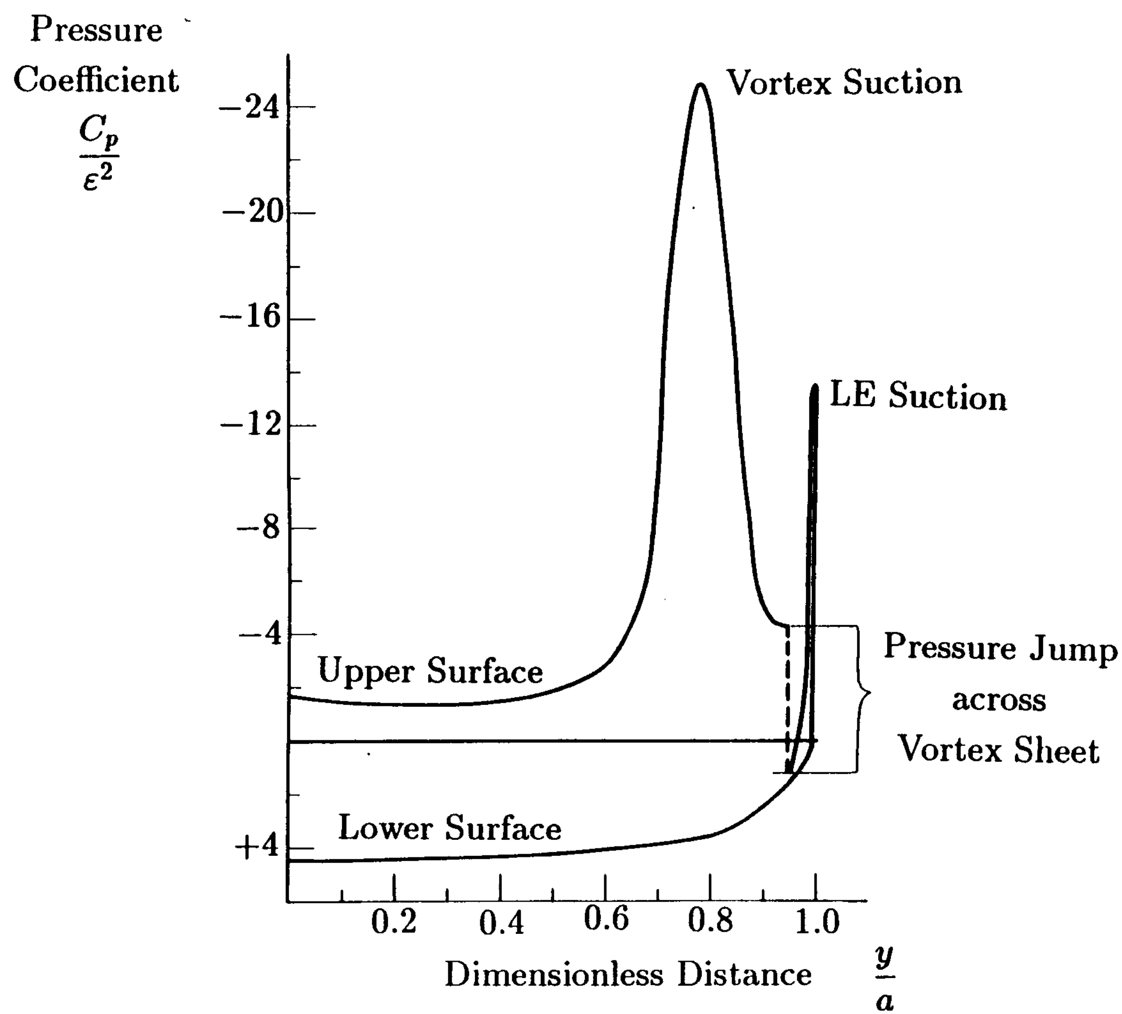

Figure 6.6 Pressure distribution on a delta wing with elliptical cross-section ($b/a = 0.2$, $\delta_y/a = 0.05$) for $\alpha/\varepsilon = 1$.

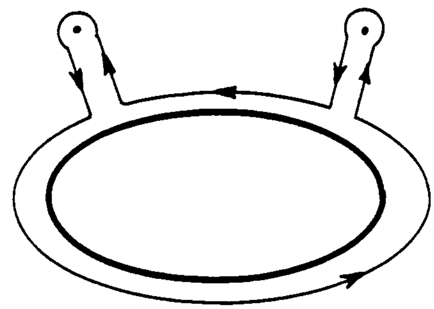

a. σ-plane

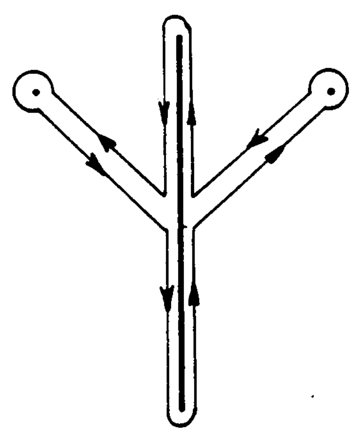

b. ς-plane

Figure 6.7 Contours of integration for the normal force.

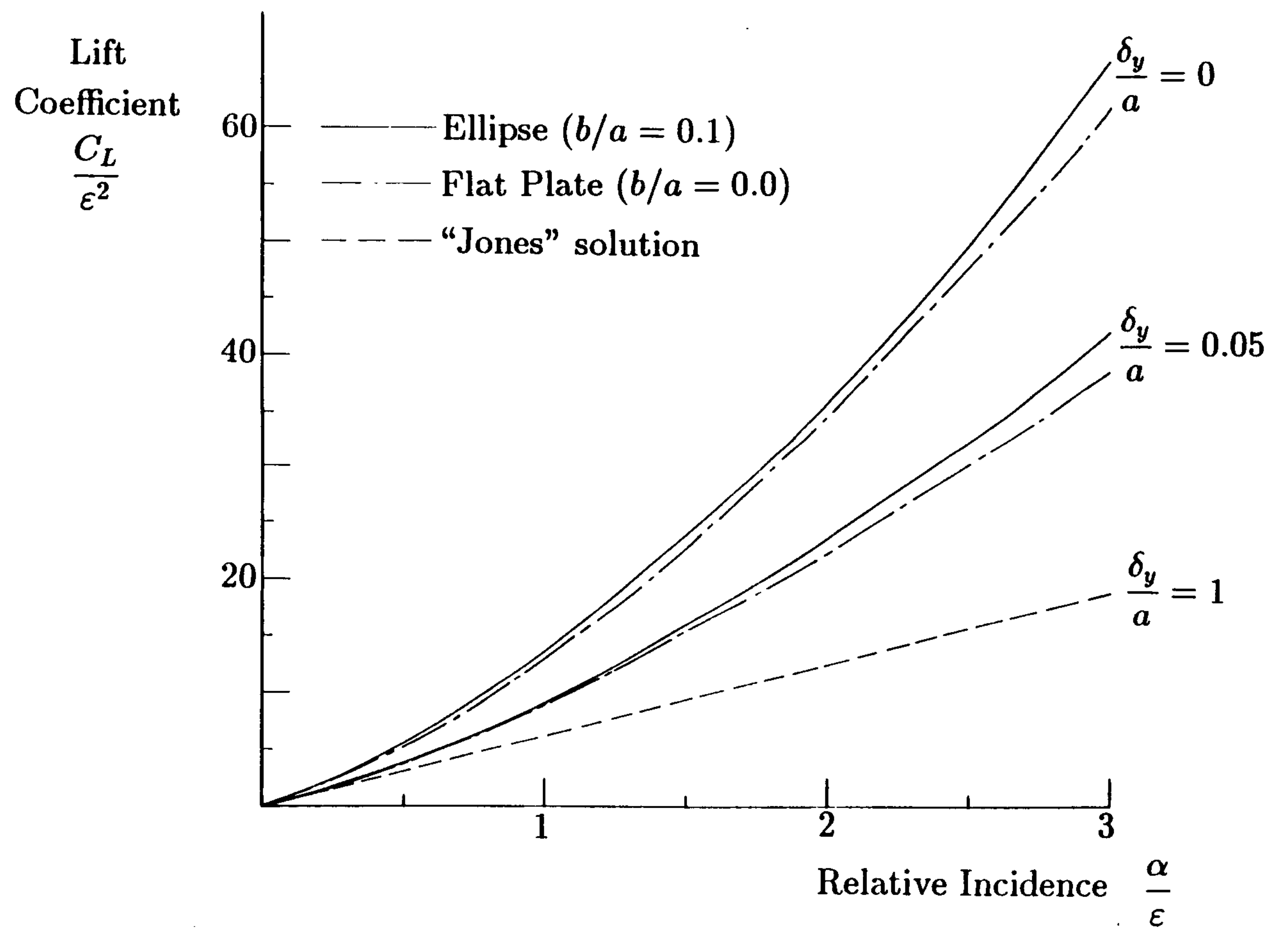

Figure 6.8 Lift vs. relative incidence for delta wings with displaced separation.

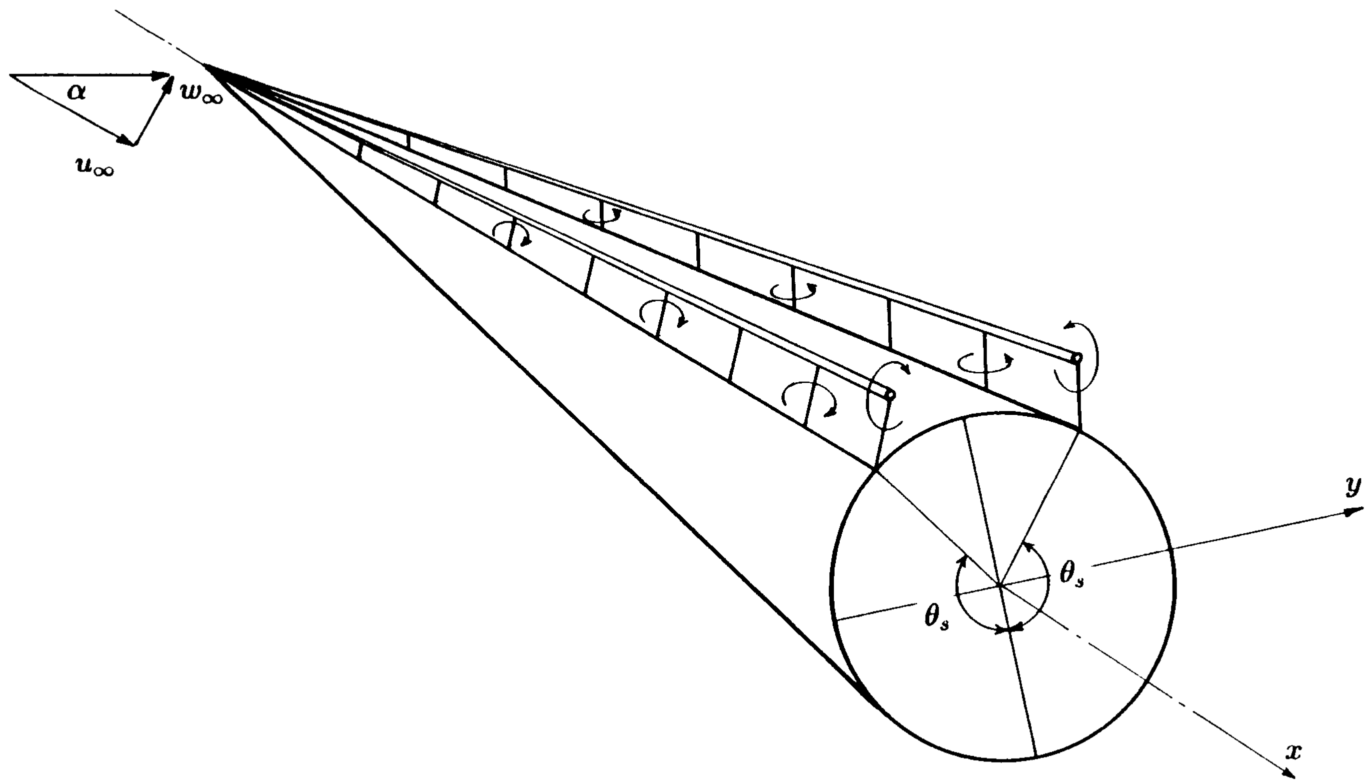

Figure 7.1 "Single-line vortex" model on a circular cone.

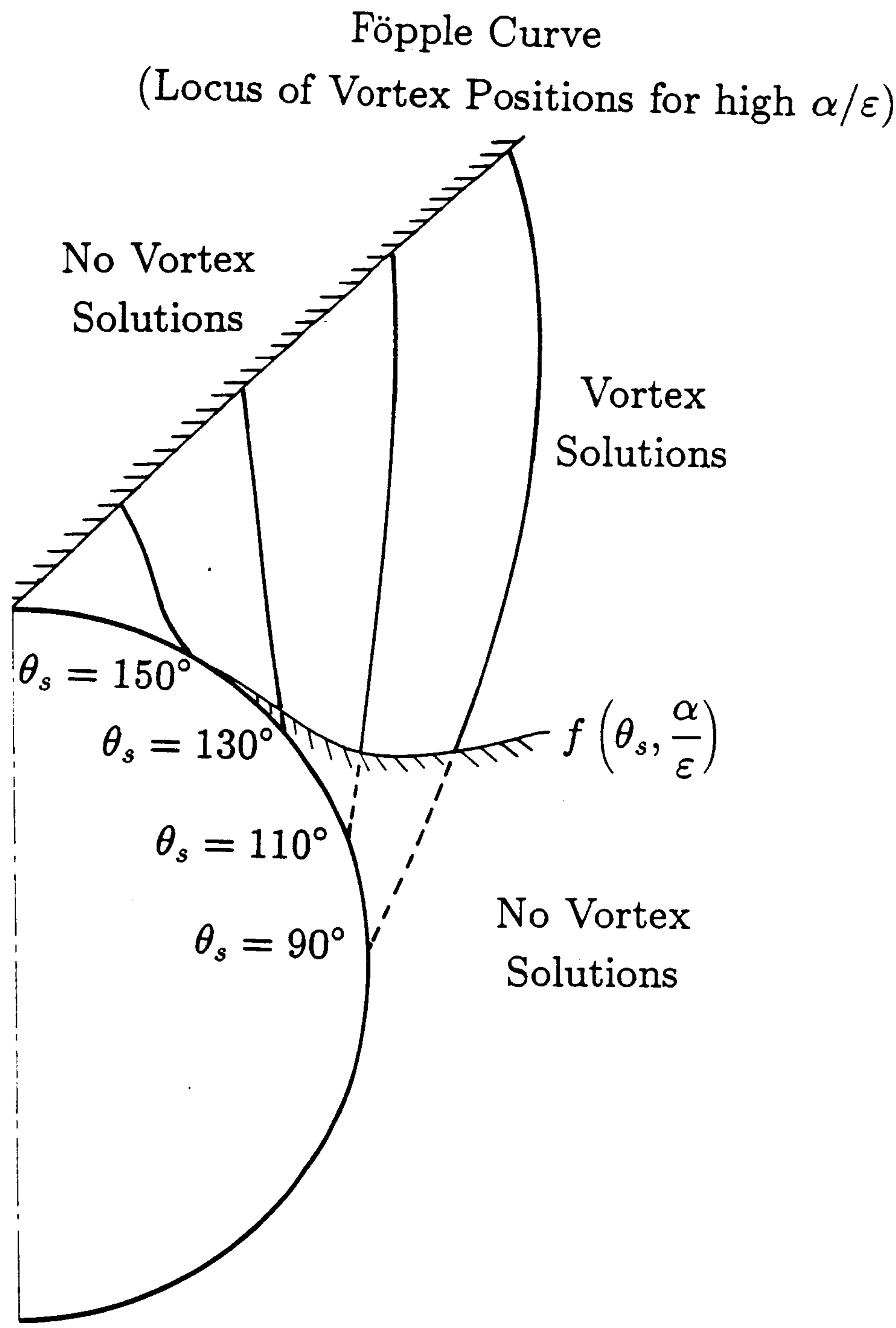

Figure 7.2 Loci of vortex positions on a circular cone.

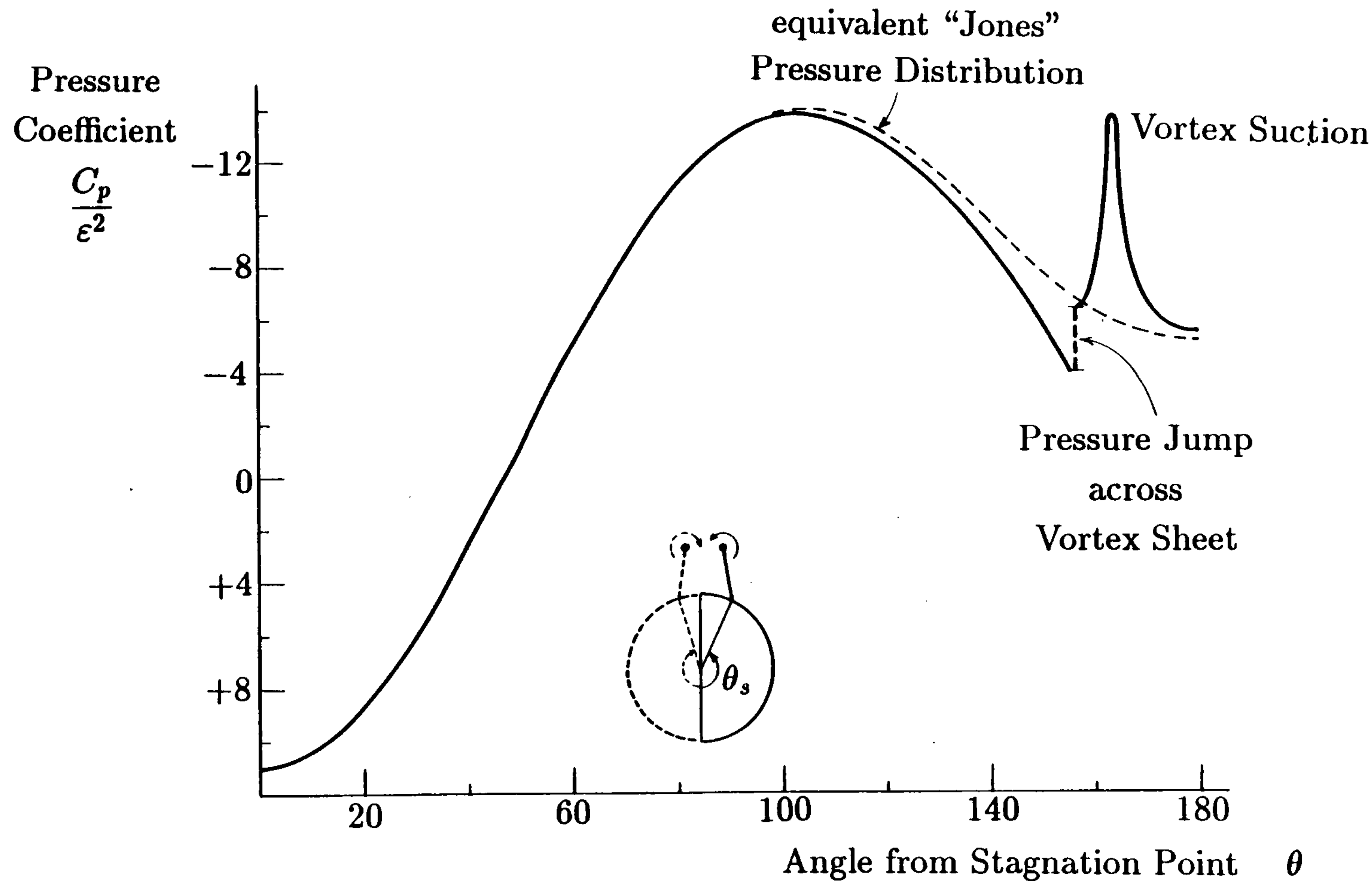

Figure 7.3 Pressure distribution on a circular cone for $\theta_s = 157°$ and $\alpha/\varepsilon = 2$.

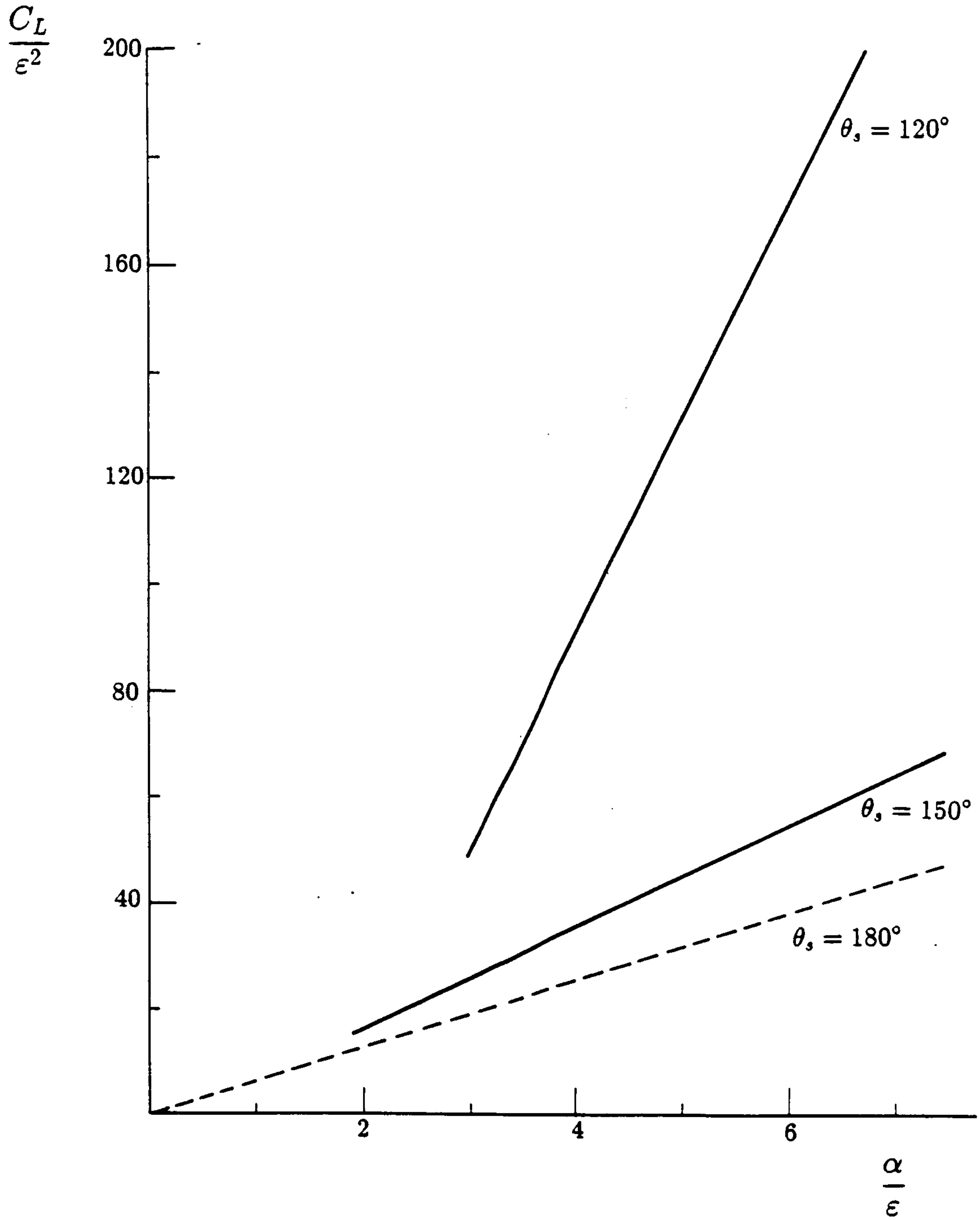

Figure 7.4 Lift vs. relative incidence for various separation angles on a circular cone.

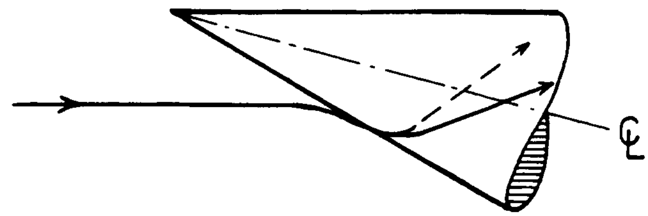

——→ typical streamline at outer edge of BL

- - -→ typical streamline inside BL

Figure 8.1 Secondary flow on a cone at incidence.

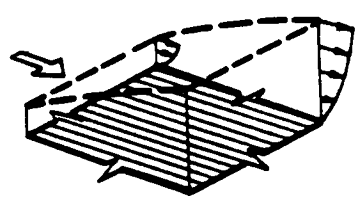

(a) Growth of 2-D BL on a plane.

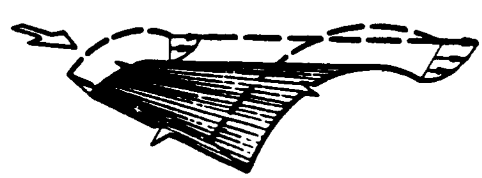

(b) BL growth on a transversely curved surface.

Figure 8.2 Streamline divergence producing a thinner BL.

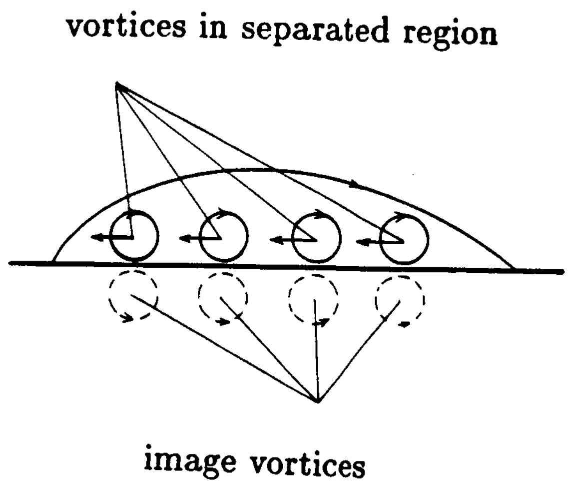

Figure 8.3 The mechanism of vortex coalescence within the BL.

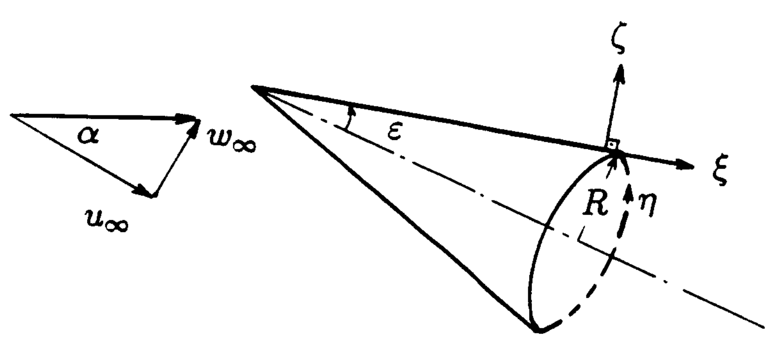

Figure 8.4 Coordinate system for the BL analysis on a circular cone.

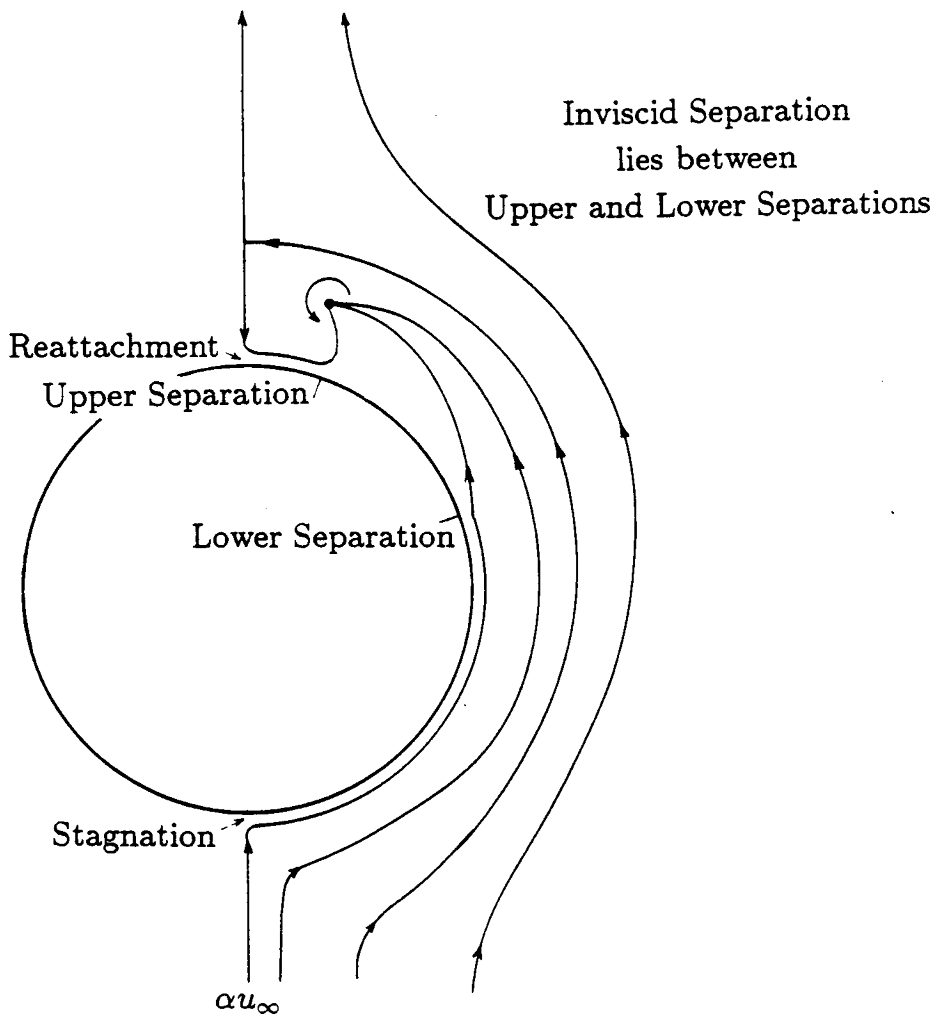

Figure 9.1 Schematic of BL separation in the cross-plane of a circular cone.

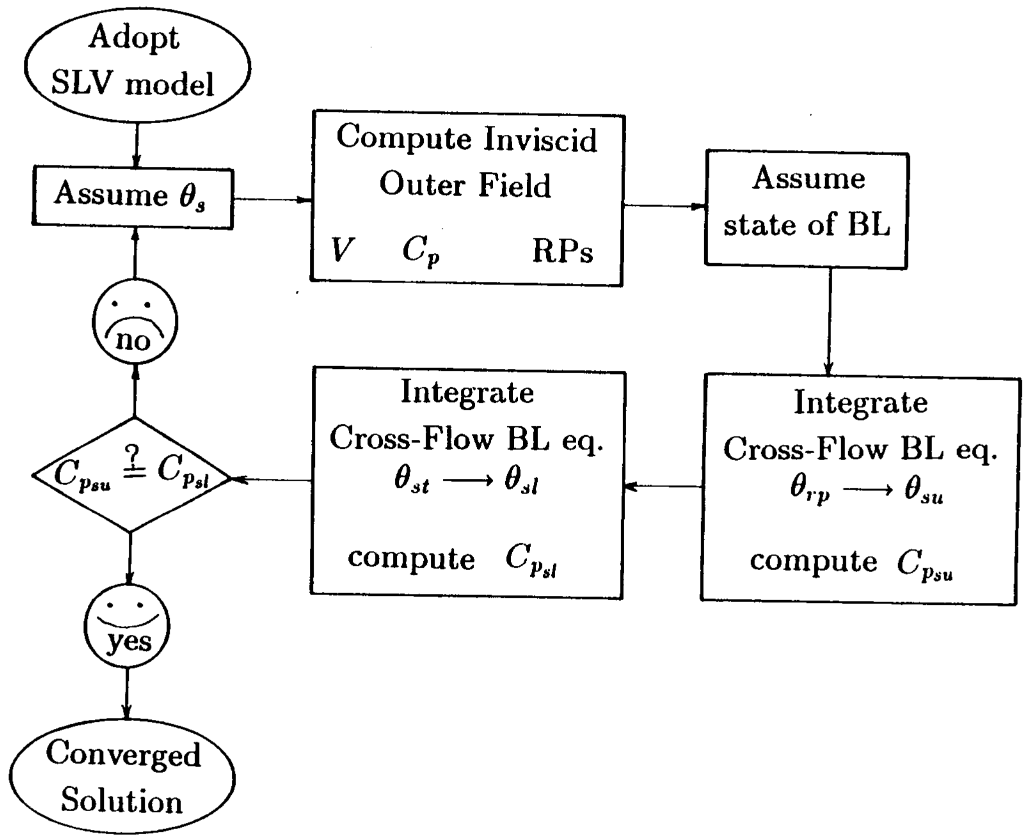

Figure 9.2 Flow chart for viscous/inviscid interaction.

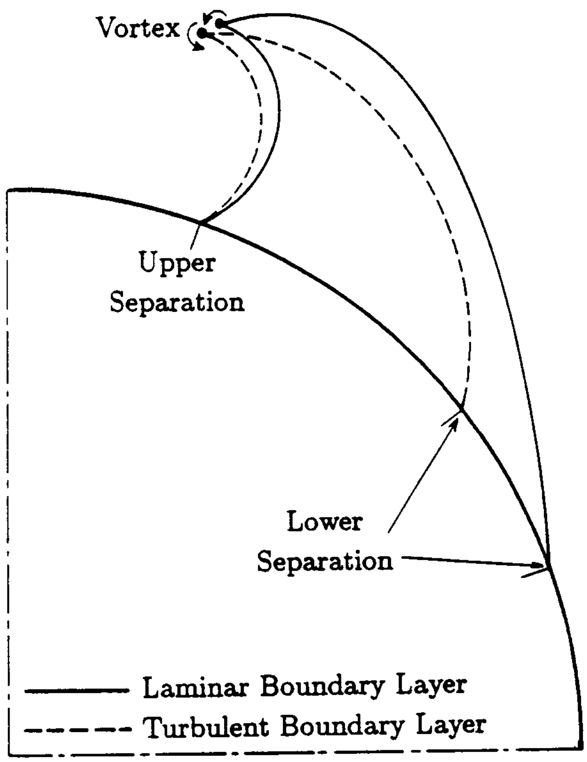

	LAMINAR BOUNDARY LAYER	TURBULENT BOUNDARY LAYER
Lower Separation	109°	127°
Vortex Sheet Location	147°	149°
Upper Separation	160°	160°
Vortex Location	(0.375, 1.285)	(0.349, 1.269)

Figure 9.3 Converged solutions for $\varepsilon = 5°$ and $\alpha = 30°$.

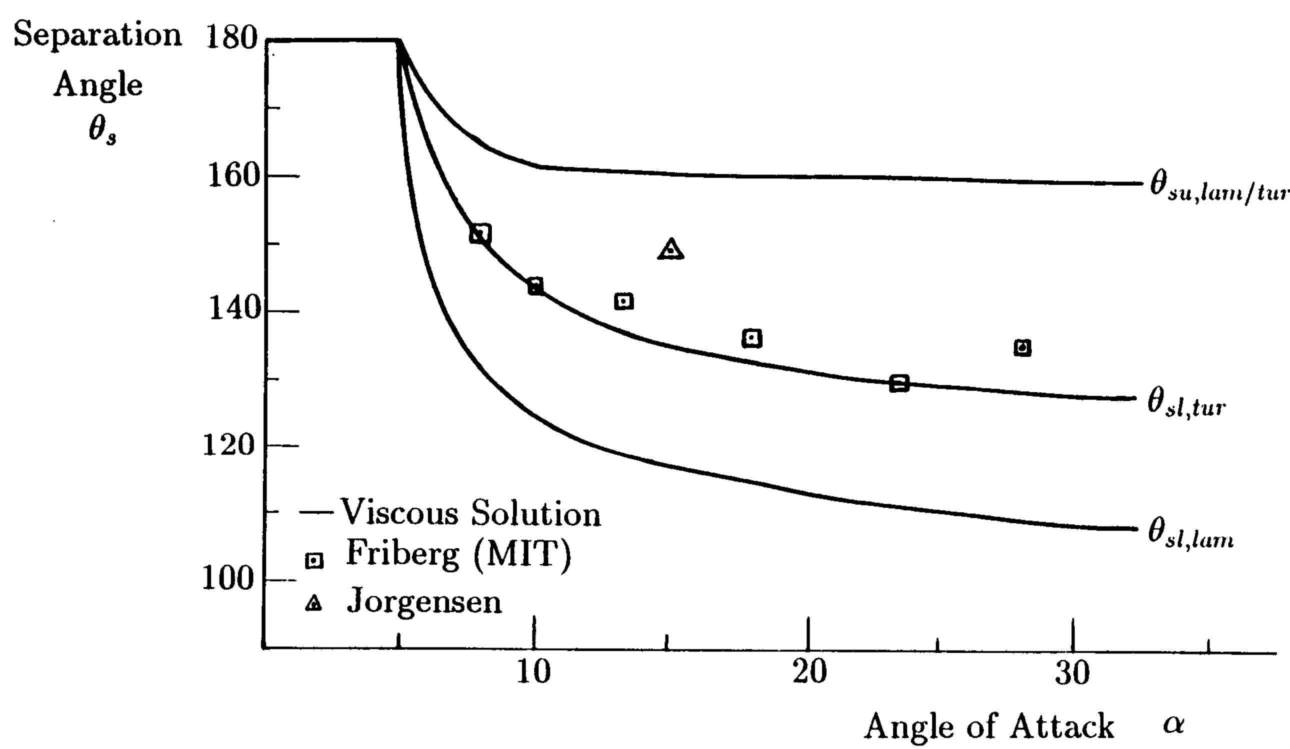

Figure 9.4 Comparison of predicted separation with experiments for a circular cone with $\varepsilon = 5°$.

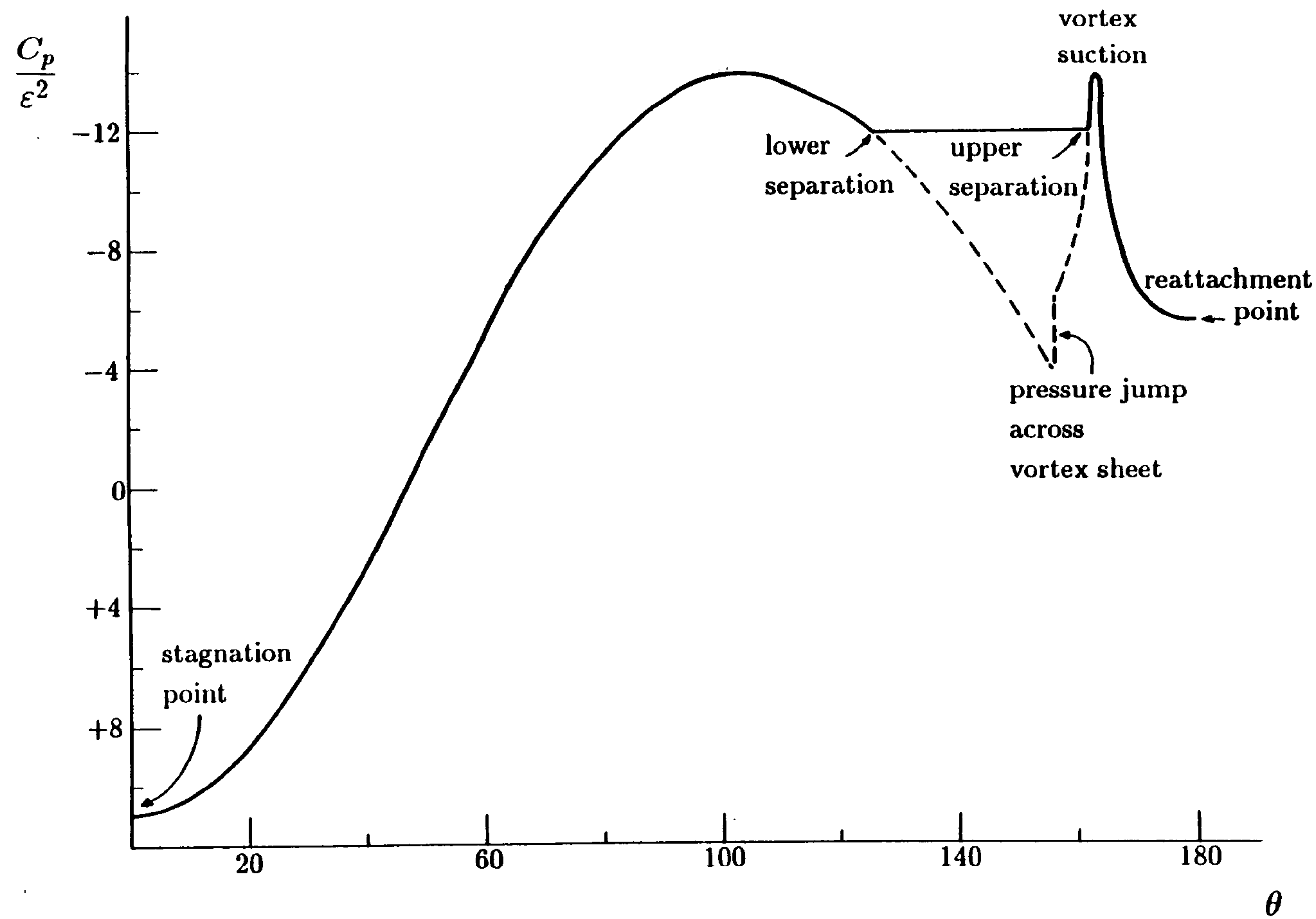

Figure 9.5a Modified pressure distribution on a circular cone for laminar BL ($\alpha/\varepsilon = 2$, $\theta_s = 157°$).

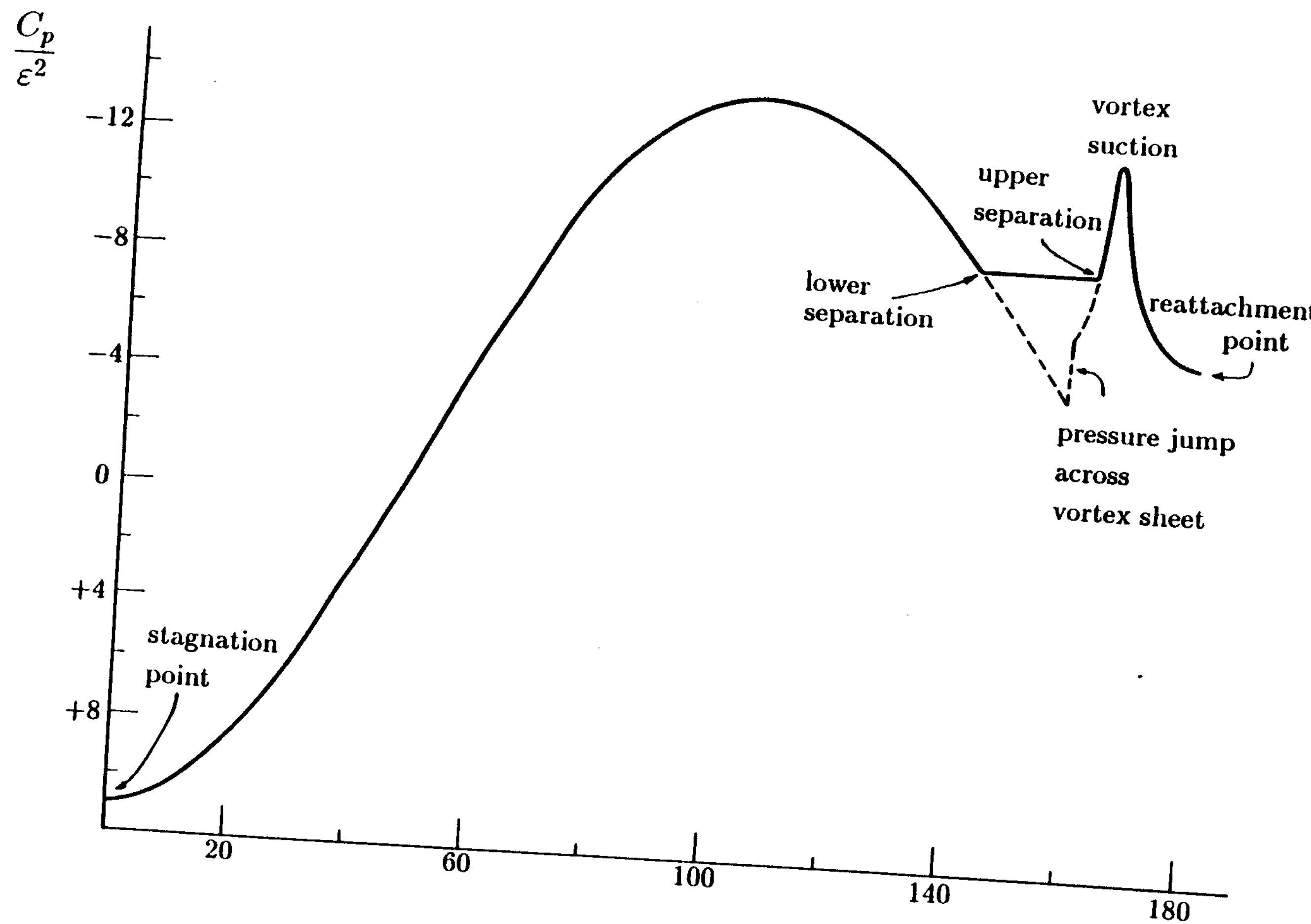

Figure 9.5b Modified pressure distribution on a circular cone for turbulent BL ($\alpha/\varepsilon = 2,\ \theta_s = 159°$).

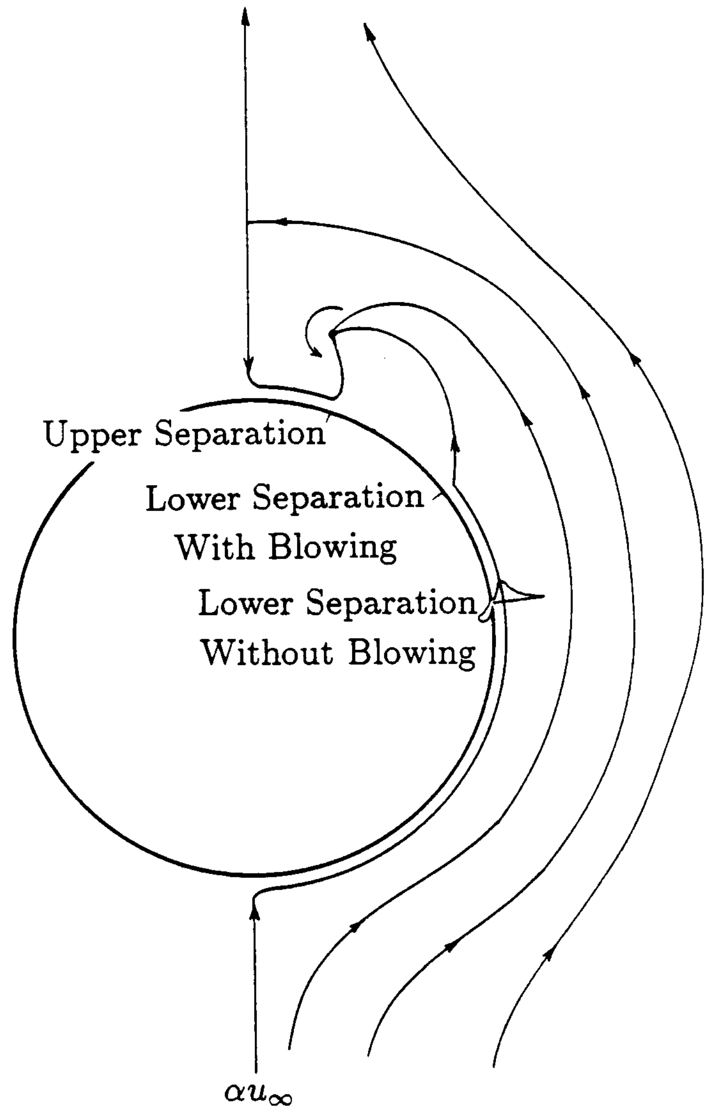

Figure 10.1 Schematic of controlled BL separation with a wall jet in the cross-plane of a circular cone.

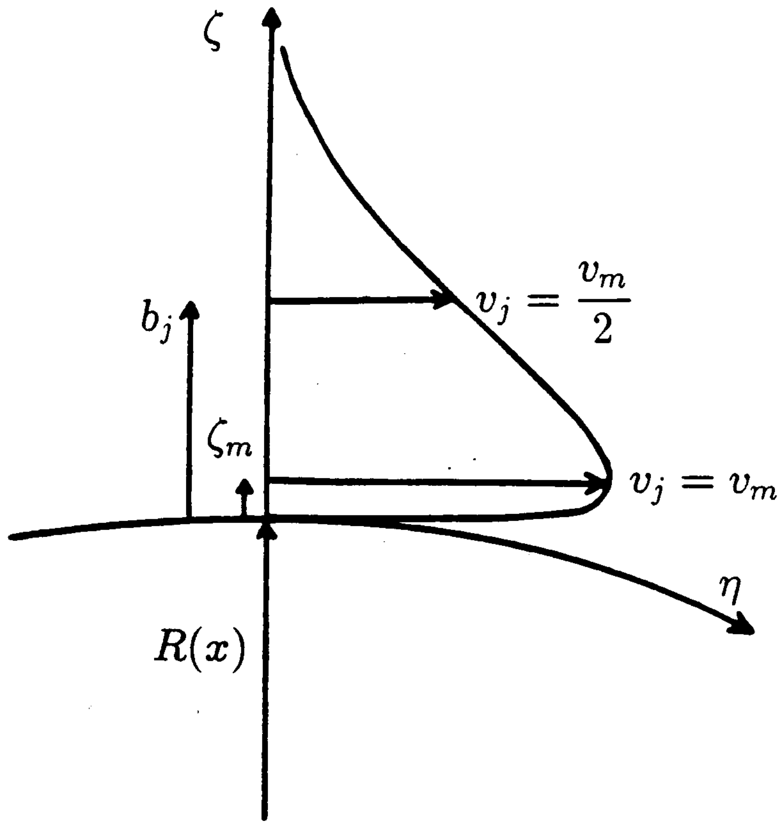

Figure 10.2 Wall jet profile.

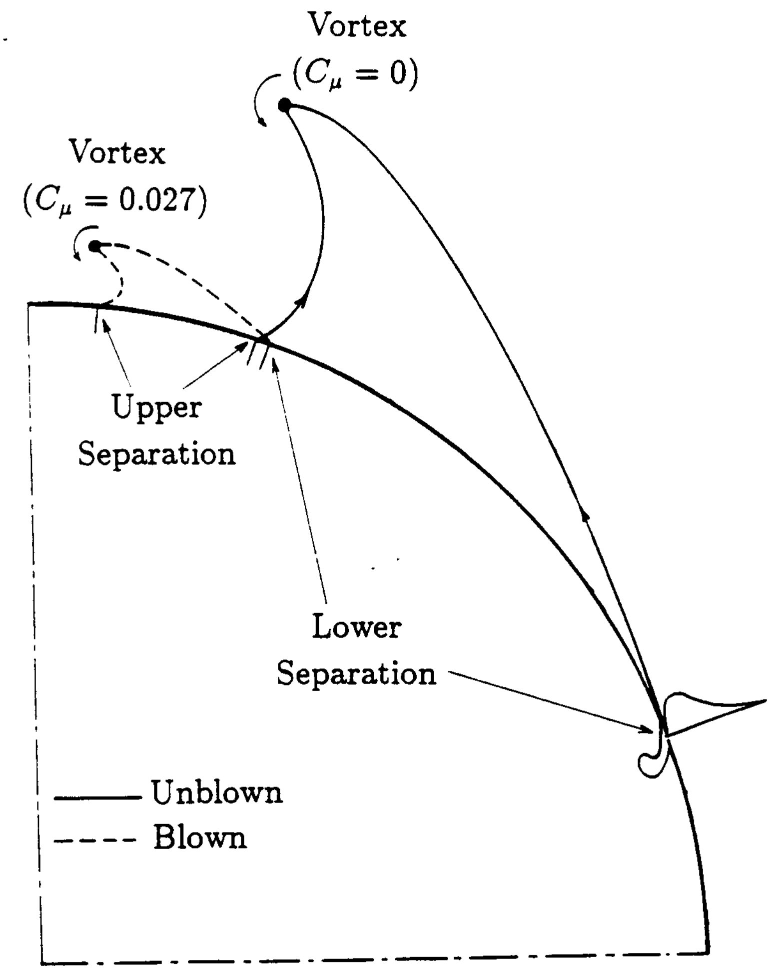

	LAMINAR BOUNDARY LAYER	TURBULENT WALL JET
Blowing Coefficient	0	0.027
Lower Separation	109°	159°
Vortex Sheet Location	147°	170°
Upper Separation	160°	174°
Vortex Location	(0.375, 1.285)	(0.090, 1.079)

Figure 10.3a Converged solutions before and after blowing ($\varepsilon = 5°$, $\alpha = 30°$, laminar BL).

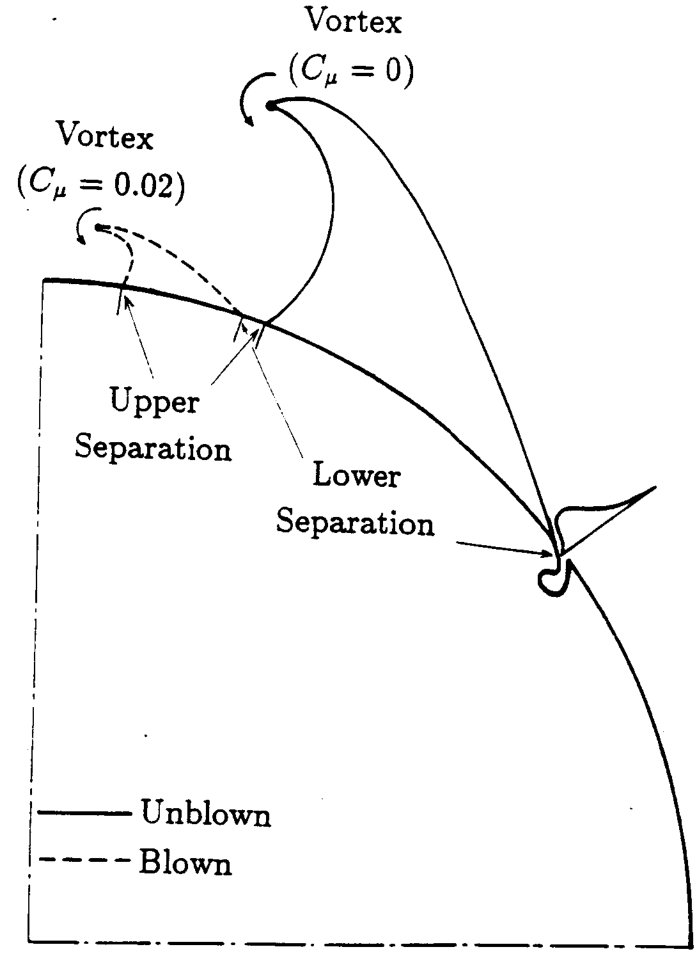

	TURBULENT BOUNDARY LAYER	TURBULENT WALL JET
Blowing Coefficient	0	0.02
Lower Separation	127°	162°
Vortex Sheet Location	149°	170°
Upper Separation	160°	173°
Vortex Location	(0.349, 1.269)	(0.090, 1.079)

Figure 10.3b Converged solutions before and after blowing ($\varepsilon = 5°$, $\alpha = 30°$, turbulent BL).

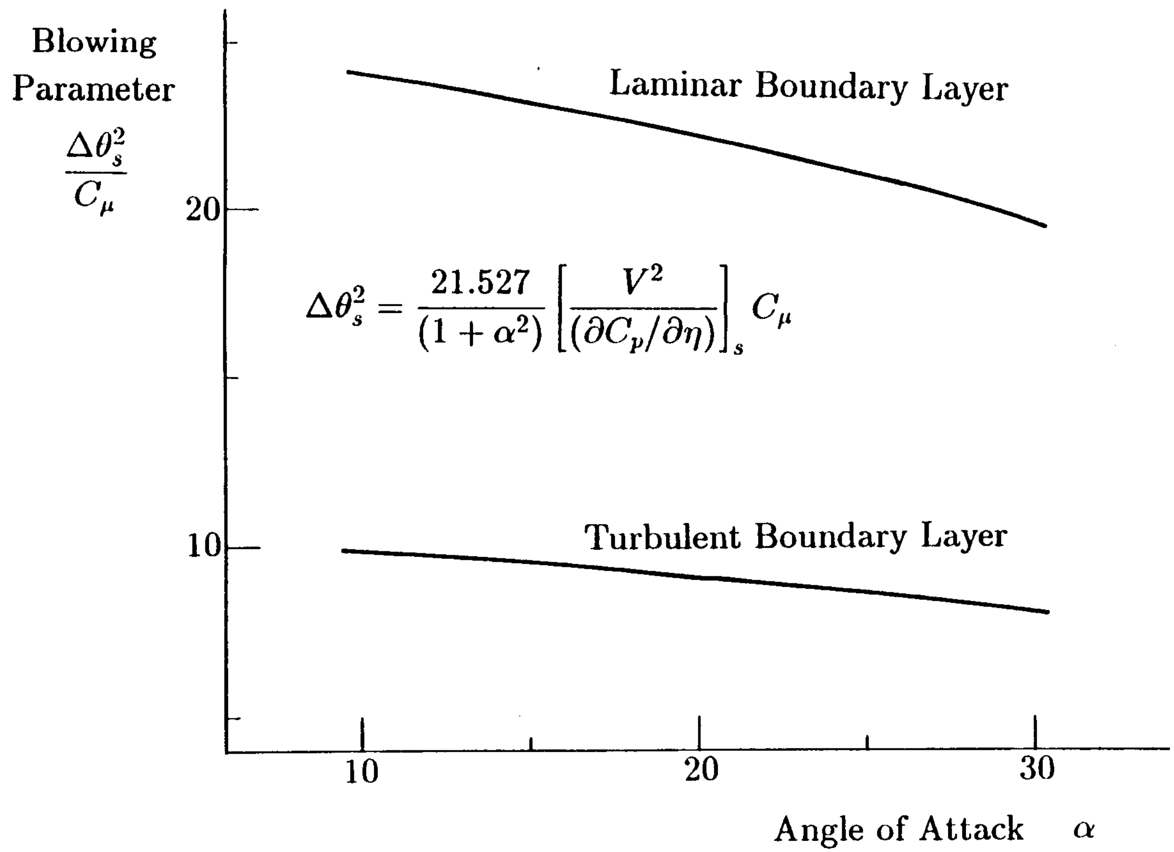

Figure 10.4 Blowing parameter vs. angle of attack.

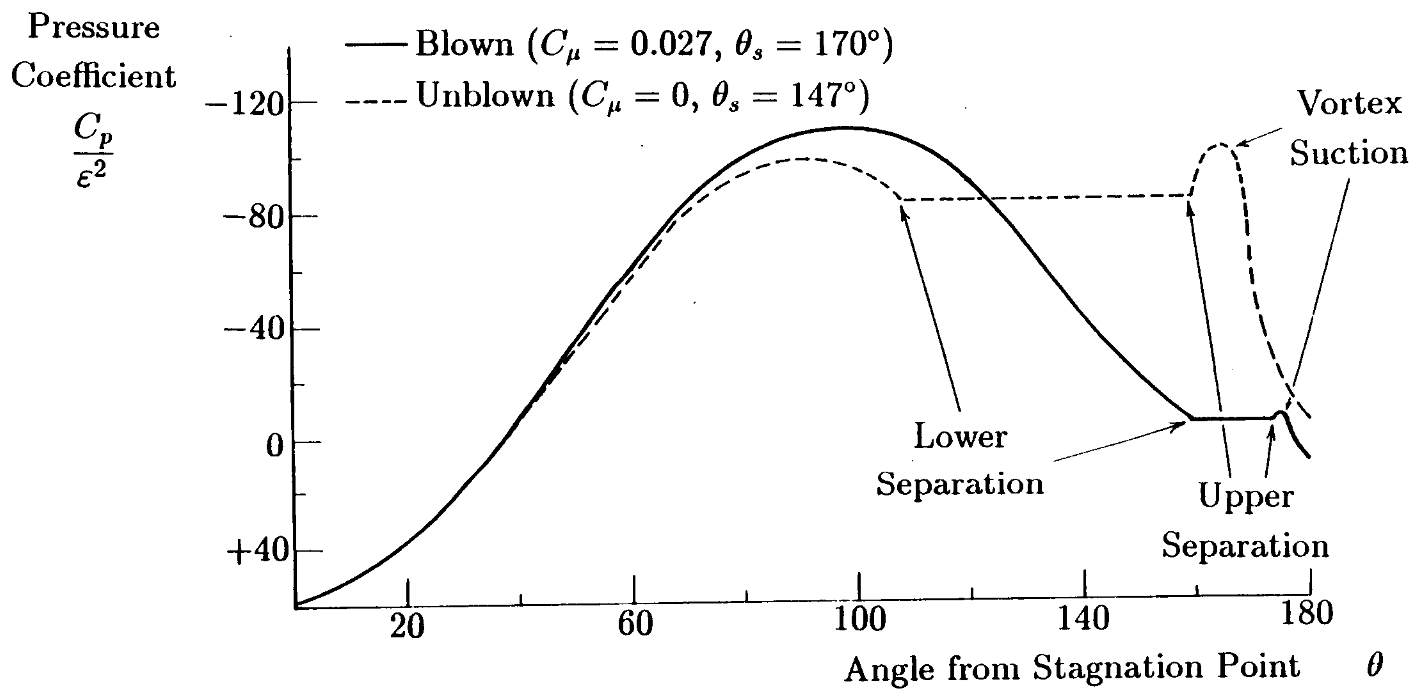

Figure 10.5a Pressure distribution before and after blowing ($\varepsilon = 5°$, $\alpha = 30°$, laminar BL).

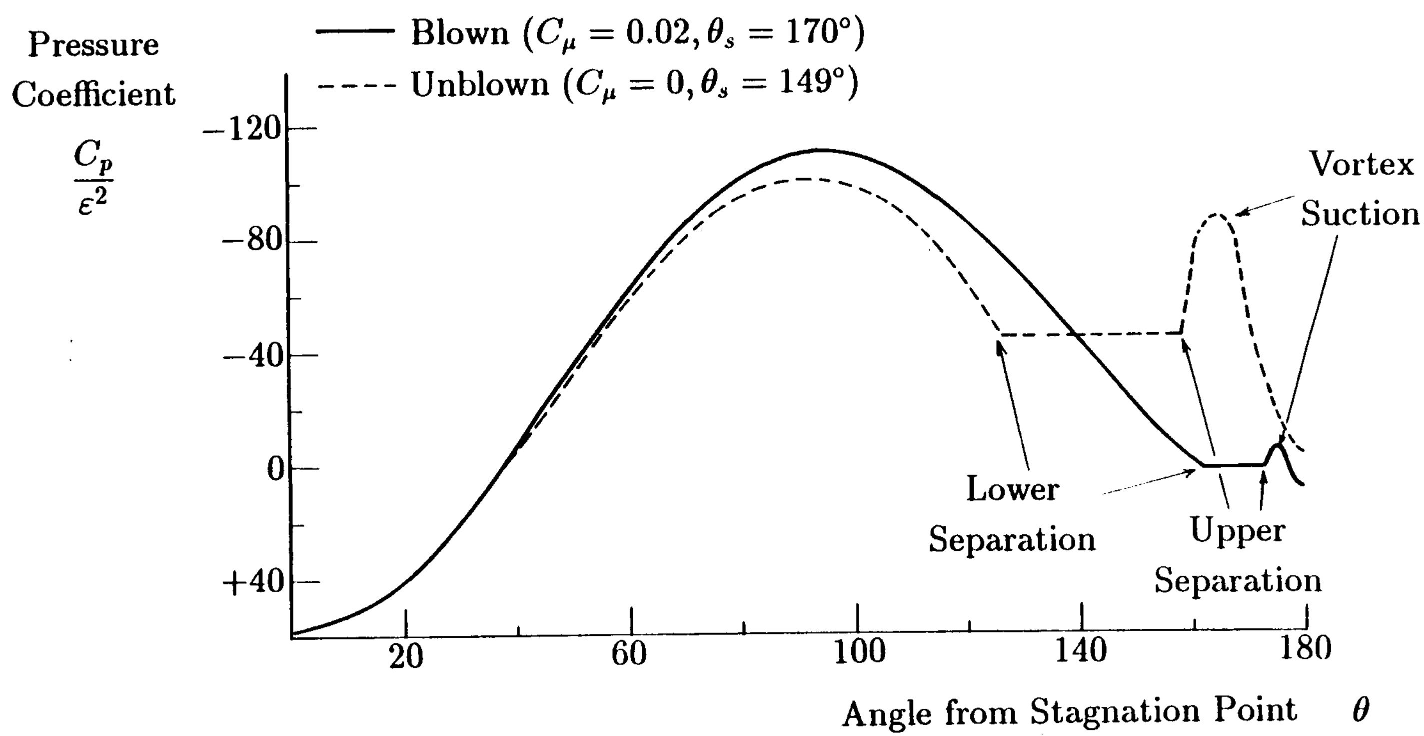

Figure 10.5b Pressure distribution before and after blowing ($\varepsilon = 5°$, $\alpha = 30°$, turbulent BL).

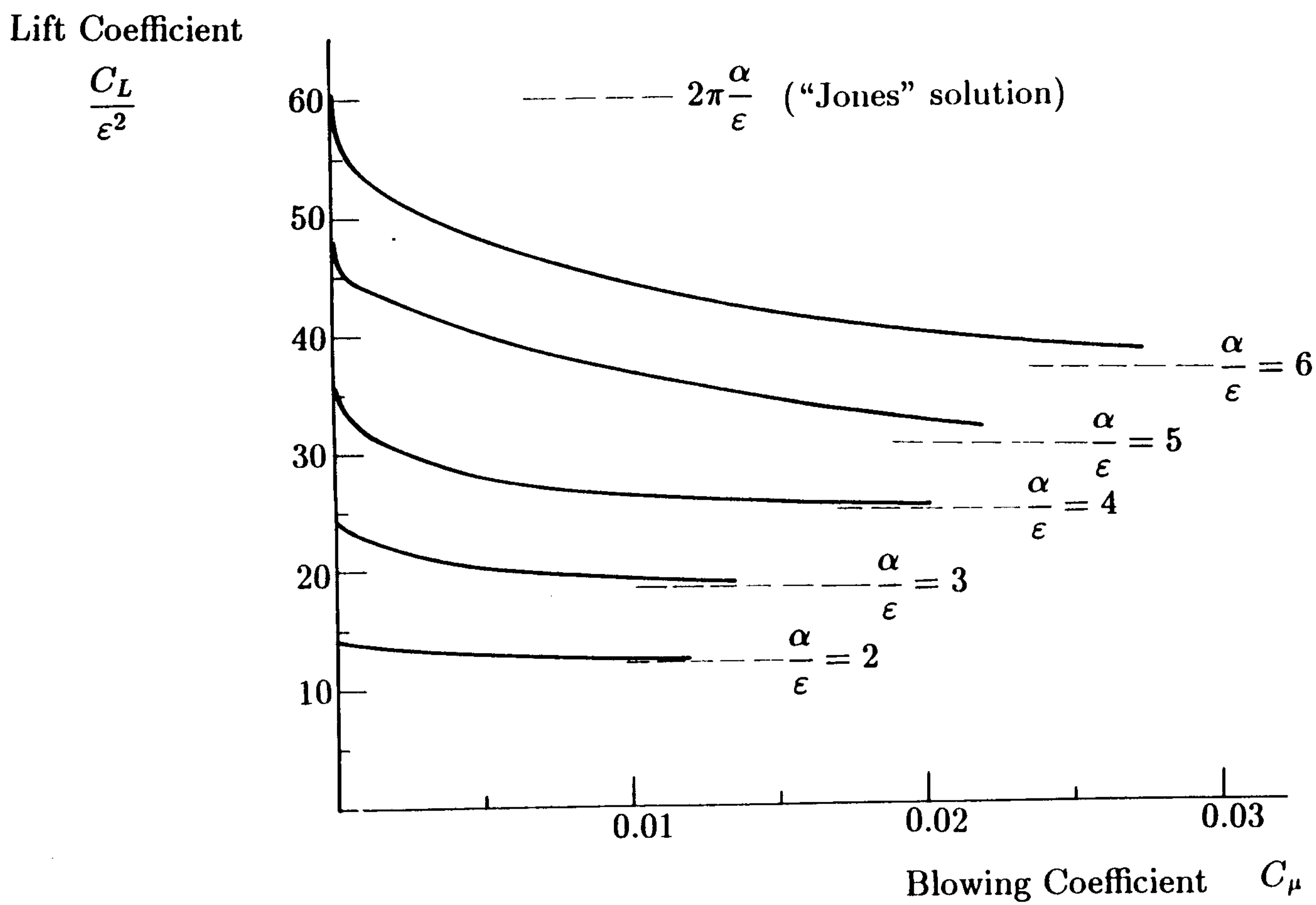

Figure 10.6 Lift vs. blowing.

TABLES

Table 6.1 Summary of scaling laws for displaced separation.

	FLAT PLATE	ELLIPSE $(b/a = 0.1)$
vortex y-coordinate	$y_{10}\left(1-\sqrt{\delta_y/a}\right)$	$y_{10}\left(1-\sqrt{\delta_y/a}\right)$
vortex z-coordinate	$z_{10}\left(1-\sqrt{\delta_y/a}\right)^{0.5}$	z_{10}
vortex strength	$k_0\left(1-\sqrt{\delta_y/a}\right)^{1.2}$	$k_0\left(1-\sqrt{\delta_y/a}\right)^{1.05}$
vortex lift	$C_{LV0}\left(1-\sqrt{\delta_y/a}\right)^{3}$	$C_{LV0}(1-\sqrt{\delta_y/a})^{2.6}$

OVERALL LIFT IS OF THE FORM :

$$\frac{C_L}{\varepsilon^2} = 2\pi\frac{\alpha}{\varepsilon} + \left(\frac{C_{LV0}}{\varepsilon^2}\right)\left(1-\sqrt{\frac{\delta_y}{a}}\right)^{m(b/a)}$$

Table 8.1 Analogy between 2–D and conical BL.

	2–D	CONICAL
momentum	equation	
$\tau_0/\varrho =$	$v_e^2(d\theta_1/dx)+$ $(\delta_1 + 2\theta_1)v_e(dv_e/dx)$	$v_e^2(\partial\theta_{22}/\partial\eta)+$ $v_e(\delta_2 + 2\theta_{22})[(\partial v_e/\partial\eta) + (\varepsilon u_e/R)]$
first	shape factor	
$\Lambda =$	$(\delta^2/\nu)(dv_e/dx)$	$(\delta^2/\nu)[(\partial v_e/\partial\eta) + (\varepsilon u_e/R)]$
second	shape factor	
$K =$	$(\theta_1^2/\delta^2)\Lambda$	$(\theta_{22}^2/\delta^2)\Lambda$
third	shape factor	
$H = f(K)$	(δ_1/θ_1)	(δ_2/θ_{22})
solution		
$\theta^2 =$	$(0.47\nu/v_e^6)\int_0^x v_e^5 dx$	$(0.47\nu/E_L v_e^6)\int_0^\eta E_L v_e^5 d\eta$
$E =$	1	$exp[6\varepsilon\int_0^\eta (u_e/v_e)d\eta]$

Table 10.1 Separation criteria for BL and wall jet.

Laminar Boundary Layer $\left(\frac{\theta_{22}}{\tau_{\eta,0}}\right)\left(\frac{dp}{d\eta}\right) \simeq 0.7$	Turbulent Boundary Layer $\left(\frac{\theta_{22}}{\tau_{\eta,0}}\right)\left(\frac{dp}{d\eta}\right) \simeq 4.7$	Wall Jet $\left(\frac{\zeta_m}{\tau_{\eta,0}}\right)\left(\frac{dp}{d\eta}\right) \simeq 4$
	Typically $\zeta_m \ll \theta_{22}$ And $(\tau_{\eta,0})_{WJ} \gg (\tau_{\eta,0})_{BL}$ So $\left(\frac{dp}{d\eta}\right)_{WJ} \gg \left(\frac{dp}{d\eta}\right)_{BL}$	

APPENDICES

APPENDIX 1

Complex Potential for an Expanding Ellipse

In ref.4, the complex potential for an expanding ellipse is given by

$$\chi_s(\sigma) = u_\infty b_0(x) + \frac{u_\infty}{2\pi}\frac{dS}{dx}\ln\frac{\sigma + \sqrt{\sigma^2 - c^2}}{2} \tag{A1.1}$$

For an elliptical cone the following equations relate the geometrical variables

$$S(x) = \pi ab \tag{A1.2}$$

$$a = x\tan\varepsilon \simeq x\varepsilon \tag{A1.3}$$

$$b = x\tan\delta \simeq x\delta \tag{A1.4}$$

Differentiating eq(A1.2) and using eqs(A1.3) and (A1.4) yields

$$\frac{dS}{dx} \simeq 2\pi x\varepsilon\delta = 2\pi a\delta = 2\pi b\varepsilon \tag{A1.5}$$

The parameter $b_0(x)$ is defined by

$$b_0(x) = a_0(x)\ln\frac{\sqrt{1-M_\infty^2}}{2} - \frac{1}{2}\int_{0^+}^{x}\frac{da_0}{d\xi}\ln(x-\xi)d\xi + \frac{1}{2}\int_{x}^{1^-}\frac{da_0}{d\xi}\ln(\xi-x)d\xi$$

$$-\frac{1}{2}a_0(0^+)\ln x - \frac{1}{2}a_0(1^-)\ln(1-x) \qquad (A1.6)$$

where

$$a_0(x) = \frac{1}{2\pi}\frac{dS}{dx} \simeq b\varepsilon \qquad (A1.7)$$

$$\frac{da_0}{dx} = \frac{1}{2\pi}\frac{d^2S}{dx^2} \simeq \varepsilon\delta$$

For incompressible flow $M_\infty = 0$, so the first integral in eq(A1.6) becomes

$$\frac{1}{2}\varepsilon\delta\int_{0^+}^{x}\ln(x-\xi)d\xi = \frac{1}{2}\varepsilon\delta x(\ln x - 1)$$

The second integral in eq(A1.6) may be written as

$$\frac{1}{2}\varepsilon\delta\int_{x}^{1^-}\ln(\xi-x)d\xi = \frac{1}{2}\varepsilon\delta(1-x)[\ln(1-x)-1]$$

Finally, for the last two terms in eq(A1.6) we have

$$a_0(0^+) = \lim_{x\to 0^+} a_0(x) = 0$$

$$a_0(1^-) = \lim_{x \to 1^-} a_0(x) = \varepsilon\delta$$

Thus, eq(A1.6) reduces to

$$b_0(x) = -\varepsilon\delta \left\{ x \left[\ln 2\sqrt{x(1-x)} - 1 \right] + \frac{1}{2} \right\} \tag{A1.8}$$

Substituting now eqs(A1.5) and (A1.8) into eq(A1.1), the complex potential for an ellipse that expands in a conical manner is obtained

$$\chi_s(\sigma) = -u_\infty \varepsilon\delta \left\{ x \left[\ln 2\sqrt{x(1-x)} - 1 \right] + \frac{1}{2} \right\} + u_\infty b\varepsilon \ln \frac{\sigma + \sqrt{\sigma^2 - c^2}}{2} \tag{A1.9}$$

APPENDIX 2
Distance around the Edge of an Ellipse

The distance of the separation point from the leading edge of an elliptical cross-section may be expressed by the following integral

$$\eta = \int d\eta = \int \sqrt{dy^2 + dz^2} \tag{A2.1}$$

Here, y and z are related by

$$\frac{y^2}{a^2} + \frac{z^2}{b^2} = 1 \Rightarrow \tag{A2.2}$$

$$dz = -\frac{y}{z}\frac{b^2}{a^2}dy \tag{A2.3}$$

$$\frac{y^2}{z^2} = \frac{y^2 a^2}{b^2(a^2 - y^2)} \tag{A2.4}$$

Substituting the above expressions into eq(A2.1) gives

$$\eta = \int_a^{a-\delta_y} \sqrt{1 + \frac{b^2}{a^2}\frac{y^2}{a^2 - y^2}}dy \tag{A2.5}$$

Equation(A2.5) can be simplified, since $a = 1$, and the result is

$$\eta = \int_{1}^{1-\delta_y} \sqrt{1 + b^2 \frac{y^2}{1-y^2}}\, dy \qquad (A2.6)$$

or, since $c^2 = a^2 - b^2 = 1 - b^2$,

$$\eta = \int_{1}^{1-\delta_y} \sqrt{\frac{1 - c^2 y^2}{1-y^2}}\, dy \qquad (A2.7)$$

In order to avoid the evaluation of the elliptic integral of the second kind, the integrand will be simplified further in the following manner

$$\frac{1 - c^2 y^2}{1 - y^2} = \frac{(1+cy)(1-cy)}{(1+y)(1-y)} \simeq \frac{(1+c)(1-cy)}{2(1-y)} \qquad (A2.8)$$

The last equality follows because close to the leading edge $y \simeq 1$.

Note that the above expression is valid for all thicknesses, i.e., from the flat plate case ($c = 1$) to the circle case ($c = 0$). Substituting eq(A2.8) into (A2.7) yields

$$\eta = \sqrt{\frac{1+c}{2}} \int_{1}^{1-\delta_y} \sqrt{\frac{1-cy}{1-y}}\, dy \qquad (A2.9)$$

Integration by parts gives an approximate expression for the distance of the separation point from the leading edge of an elliptical cross-section, as a function of δ_y

$$\eta = -\sqrt{\frac{1+c}{2}} \left\{ \sqrt{(1-c+c\delta_y)\delta_y} + \frac{c-1}{2\sqrt{c}} \ln \frac{[c - c\delta_y - 1 + \sqrt{(1-c+c\delta_y)c\delta_y}\ ]^2}{(1-c)(1-c+c\delta_y)} \right\} \qquad (A2.10)$$

APPENDIX 3

Evaluation of the Derivative $d\chi/da$

For the term χ_{s2} in eq(6.2) the derivative with respect to x can be evaluated directly from

$$\frac{d\chi_{s2}}{dx} = -u_\infty \varepsilon \frac{b}{x}\left\{\ln\left[2\sqrt{x(1-x)}\right] - \frac{1}{2(1-x)}\right\} \tag{A3.1}$$

For the rest of the complex potential $(\chi_{cf} + \chi_{s1})$, we have

$$\frac{d\chi}{da} = \frac{\partial\chi}{\partial\theta}\frac{d\theta}{da} + \frac{\partial\chi_{cf}}{\partial\theta_1}\frac{d\theta_1}{da} + \frac{\partial\chi_{cf}}{\partial\bar{\theta}_1}\frac{d\bar{\theta}_1}{da} + \frac{\partial\chi_{cf}}{\partial k}\frac{dk}{da} + \frac{\partial\chi_{cf}}{\partial R}\frac{dR}{da} + \frac{\partial\chi_{s1}}{\partial b}\frac{db}{da} \tag{A3.2}$$

and since $\theta_1, \bar{\theta}_1$ (or $\sigma_1, \bar{\sigma}_1$), k, a and b are all linear functions of x

$$\frac{d\theta_1}{da} = \frac{\theta_1}{a} \tag{A3.3}$$

$$\frac{d\bar{\theta}_1}{da} = \frac{\bar{\theta}_1}{a} \tag{A3.4}$$

$$\frac{dR}{da} = \frac{R}{a} \tag{A3.5}$$

$$\frac{db}{da} = \frac{b}{a} \tag{A3.6}$$

Equation(6.9) can be solved for the vortex strength

$$k = \frac{(\theta_s + \bar{\theta}_1)(\theta_s - \theta_1)(\theta_s\bar{\theta}_1 - R^2)(\theta_s\theta_1 + R^2)}{\theta_s^2(\theta_1 + \bar{\theta}_1)(R^2 - \theta_1\bar{\theta}_1)} u_\infty \alpha \tag{A3.7}$$

and differentiation with respect to a gives

$$\frac{dk}{da} = \frac{k}{a} \tag{A3.8}$$

In a similar manner, differentiating eqs(6.1) and (6.3) gives the following expressions

$$\frac{\partial \chi}{\partial \theta} = -\imath u_\infty \alpha \left(1 + \frac{R^2}{\theta^2}\right) - \imath k \left(\frac{1}{\theta - \theta_1} - \frac{1}{\theta + \bar{\theta}_1} + \frac{\theta_1}{\theta\theta_1 + R^2} - \frac{\bar{\theta}_1}{\theta\bar{\theta}_1 - R^2}\right) + u_\infty b \frac{\varepsilon}{\theta} \tag{A3.9}$$

$$\frac{\partial \chi_{cf}}{\partial \theta_1} = \imath k \left(\frac{1}{\theta - \theta_1} - \frac{\theta}{\theta\theta_1 + R^2}\right) + \imath \frac{k}{\theta_1} \tag{A3.10}$$

$$\frac{\partial \chi_{cf}}{\partial \bar{\theta}_1} = \imath k \left(\frac{1}{\theta + \bar{\theta}_1} + \frac{\theta}{\theta\bar{\theta}_1 - R^2}\right) - \imath \frac{k}{\bar{\theta}_1} \tag{A3.11}$$

$$\frac{\partial \chi_{cf}}{\partial k} = -\imath \ln \left(\frac{\bar{\theta}_1}{\theta_1} \frac{(\theta - \theta_1)}{(\theta + \bar{\theta}_1)} \frac{(\theta\theta_1 + R^2)}{(\theta\bar{\theta}_1 - R^2)}\right) \tag{A3.12}$$

$$\frac{\partial \chi_{cf}}{\partial R} = \imath \frac{2Ru_\infty \alpha}{\theta} - 2\imath k R \left(\frac{1}{\theta\theta_1 + R^2} + \frac{1}{\theta\bar{\theta}_1 - R^2}\right) \tag{A3.13}$$

$$\frac{\partial \chi_{s1}}{\partial b} = u_\infty \varepsilon \ln \theta \tag{A3.14}$$

Finally, from fig(2.2)

$$\frac{d\theta}{da} = \frac{d\theta}{dc}\frac{dc}{da} = -\frac{c^2}{2a\sqrt{\sigma^2 - c^2}} \tag{A3.15}$$

$$\frac{d\theta}{d\sigma} = \frac{1}{2}\left(1 + \frac{\sigma}{\sqrt{\sigma^2 - c^2}}\right) \tag{A3.16}$$

APPENDIX 4

Three-Dimensional Boundary Layer Equations

A4.1 Equations

Using an orthogonal system, which is not less general but simplifies matters considerably, the expression for a general element of length, is given by

$$(ds)^2 = h_1^2(d\xi)^2 + h_2^2(d\eta)^2 + h_3^2(d\zeta)^2 \qquad (A4.1)$$

where the metric coefficients are in general functions of all three coordinates

$$h_1 = h_1(\xi, \eta, \zeta)$$

$$h_2 = h_2(\xi, \eta, \zeta)$$

$$h_3 = h_3(\xi, \eta, \zeta)$$

ξ and η lie and are defined on the surface over which the boundary layer is flowing, while ζ extends into the layer.

When the surface is regular, and not excessively curved in comparison with the boundary layer thickness

$$h_1 = h_1(\xi, \eta)$$

$$h_2 = h_2(\xi, \eta)$$

$$h_3 = h_3(\xi, \eta)$$

If (ξ, η, ζ) are known functions of some Cartesian system (x, y, z), then

$$\left(\frac{1}{h_1}\right)^2 = \left(\frac{\partial \xi}{\partial x}\right)^2 + \left(\frac{\partial \xi}{\partial y}\right)^2 + \left(\frac{\partial \xi}{\partial z}\right)^2 \tag{A4.2a}$$

$$\left(\frac{1}{h_2}\right)^2 = \left(\frac{\partial \eta}{\partial x}\right)^2 + \left(\frac{\partial \eta}{\partial y}\right)^2 + \left(\frac{\partial \eta}{\partial z}\right)^2 \tag{A4.2b}$$

$$\left(\frac{1}{h_3}\right)^2 = \left(\frac{\partial \zeta}{\partial x}\right)^2 + \left(\frac{\partial \zeta}{\partial y}\right)^2 + \left(\frac{\partial \zeta}{\partial z}\right)^2 \tag{A4.2c}$$

The boundary layer equations in a general system of orthogonal curvilinear coordinates like the one just described, can be written as follows :

continuity equation

$$\frac{\partial}{\partial \xi}(h_2 h_3 u) + \frac{\partial}{\partial \eta}(h_1 h_3 v) + \frac{\partial}{\partial \zeta}(h_1 h_2 w) = 0 \tag{A4.3}$$

momentum equation in the ξ - direction

$$\frac{u}{h_1}\frac{\partial u}{\partial \xi} + \frac{v}{h_2}\frac{\partial u}{\partial \eta} + \frac{w}{h_3}\frac{\partial u}{\partial \zeta} + \frac{uv}{h_1 h_2}\frac{\partial h_1}{\partial \eta} - \frac{v^2}{h_1 h_2}\frac{\partial h_2}{\partial \xi} = -\frac{1}{\varrho h_1}\frac{\partial p}{\partial \xi} + \frac{1}{\varrho h_3}\frac{\partial \tau_\xi}{\partial \zeta} \tag{A4.4}$$

momentum equation in the η - direction

$$\frac{u}{h_1}\frac{\partial v}{\partial \xi}+\frac{v}{h_2}\frac{\partial v}{\partial \eta}+\frac{w}{h_3}\frac{\partial v}{\partial \zeta}+\frac{uv}{h_1h_2}\frac{\partial h_2}{\partial \xi}-\frac{u^2}{h_1h_2}\frac{\partial h_1}{\partial \eta}=-\frac{1}{\varrho h_2}\frac{\partial p}{\partial \eta}+\frac{1}{\varrho h_3}\frac{\partial \tau_\eta}{\partial \zeta} \qquad (A4.5)$$

momentum equation in the ζ - direction

$$\frac{\partial p}{\partial \zeta}=0 \qquad (A4.6)$$

For the derivation of the above equations, the flow has been assumed steady, incompressible with neither body forces nor Coriolis acceleration terms. The pressure gradient components may also be written as

$$\frac{1}{\varrho h_1}\frac{\partial p}{\partial \xi}=-\frac{u_e}{h_1}\frac{\partial u_e}{\partial \xi}-\frac{v_e}{h_2}\frac{\partial u_e}{\partial \eta}-\frac{u_e v_e}{h_1h_2}\frac{\partial h_1}{\partial \eta}+\frac{v_e^2}{h_1h_2}\frac{\partial h_2}{\partial \xi} \qquad (A4.7)$$

$$\frac{1}{\varrho h_2}\frac{\partial p}{\partial \eta}=-\frac{u_e}{h_1}\frac{\partial v_e}{\partial \xi}-\frac{v_e}{h_2}\frac{\partial v_e}{\partial \eta}-\frac{u_e v_e}{h_1h_2}\frac{\partial h_2}{\partial \xi}+\frac{u_e^2}{h_1h_2}\frac{\partial h_1}{\partial \eta} \qquad (A4.8)$$

A4.2 Boundary Conditions

(i) At the surface of the body ($\zeta = 0$), the "no-slip" condition is

$$u=v=w=0 \qquad (A4.9)$$

(ii) At the outer edge of the boundary layer ($\zeta \to \infty$), the velocity should match that of the external flow

$$u \to u_e(\xi, \eta) \tag{A4.10a}$$

$$v \to v_e(\xi, \eta) \tag{A4.10b}$$

$$w \to 0 \tag{A4.10c}$$

A4.3 Choice of the Coordinate System

The equations in section (A4.1) are complicated mainly because of the presence of the metric coefficients h_1, h_2, h_3 and their derivatives. It is therefore imperative that the coordinate system is chosen in such a way as to simplify both the differential equations as well as the boundary conditions.

A first simplification applicable in boundary layer studies, is to restrict the general orthogonal system which was defined in section (A4.1), by setting

$$h_3(\xi, \eta) = 1 \tag{A4.11}$$

which implies that ζ represents an actual distance measured along a straight normal from the surface. As a result, only the choice of the two remaining surface coordinates ξ and η needs to be made.

References 45–48 have an extensive discussion on the various possibilities for the choice of the two remaining coordinate axes. The problem which exists most of the times, is that there is usually one coordinate system in which the boundary layer equations take the simplest form, and another one which offers the simplest boundary conditions. For the circular cone for example, since it is a developable surface (i.e., it can be rolled out into a plane without being stretched after suitable cuts have been made), a cartesian coordinate system exists such that $h_1 = h_2 = 1$. However, none of the coordinates of this system lies along the cone generators so the simple "conical flow" boundary conditions are lost. Thus, the best choice seems to be an orthogonal coordinate system consisting of geodesics (surface curves connecting succesive points along the shortest route possible) and geodesic parallels. Then, the metric coefficient for the coordinates which are geodesics becomes

$$h_1(\xi, \eta) = 1 \tag{A4.12}$$

and eq(A4.1) now reads

$$(ds)^2 = (d\xi)^2 + h_2^2(d\eta)^2 + (d\zeta)^2 \tag{A4.13}$$

APPENDIX 5

Solution of the Boundary Layer Equation

A5.1 Laminar Boundary Layer

For the laminar boundary layer the shear stress is given by

$$\tau_{\eta L} = \mu \frac{\partial v}{\partial \zeta} = \varrho \nu \frac{\partial v}{\partial \zeta} \tag{A5.1}$$

If we define a dimensionless coordinate across the boundary layer

$$\lambda \equiv \frac{\zeta}{\delta(\xi, \eta)} \tag{A5.2}$$

then it may be written

$$\frac{v}{v_e} = f(\lambda) = a_1\lambda + b_1\lambda^2 + c_1\lambda^3 + d_1\lambda^4 \qquad \text{for} \qquad 0 \leq \lambda \leq 1 \tag{A5.3}$$

The constants a_1, b_1, c_1, d_1 will be evaluated from the boundary conditions.

The first boundary condition eq(A4.9), applied at $\lambda = 0$ reduces eq(A4.5) to

$$\frac{\partial \tau_\eta}{\partial \zeta} = \frac{1}{\varepsilon\xi}\frac{\partial p}{\partial \eta} \tag{A5.4}$$

Combining now eqs(A5.1),(A5.4) and (A4.8) yields

$$\nu\frac{\partial^2 v}{\partial\zeta^2} = -\frac{v_e}{\varepsilon\xi}\left(\frac{\partial v_e}{\partial\eta} + \varepsilon u_e\right) \tag{A5.5}$$

The first pressure gradient parameter may be defined in a manner analogous to that for the two-dimensional boundary layer

$$\Lambda_\eta \equiv \frac{\delta^2}{a\nu}\left(\frac{\partial v_e}{\partial\eta} + \varepsilon u_e\right) \tag{A5.6}$$

Then eq(A5.5) reduces to

$$\nu\frac{\partial^2 v}{\partial\zeta^2} = -v_e\frac{\nu}{\delta^2}\Lambda_\eta$$

Evaluation of the second derivative on the left side by means of eq(A5.3) yields

$$b_1 = -\frac{1}{2}\Lambda_\eta \tag{A5.7a}$$

The second boundary condition eqs(A4.10), applied at $\lambda = 1$ gives $v = v_e, \partial v/\partial\zeta = 0$ and $\partial^2 v/\partial\zeta^2 = 0$. When these conditions are expressed in terms of eq(A5.3), yield repsectively

$$f(1) = 1 \Rightarrow a_1 + b_1 + c_1 + d_1 = 1 \tag{A5.7b}$$

$$f'(1) = 0 \Rightarrow a_1 + 2b_1 + 3c_1 + 4d_1 = 0 \tag{A5.7c}$$

$$f''(1) = 0 \Rightarrow b_1 + 3c_1 + 6d_1 = 0 \tag{A5.7d}$$

Solving now the system of eqs(A5.7) gives

$$a_1 = 2 + \frac{\Lambda_\eta}{6} \tag{A5.7e}$$

$$c_1 = -2 + \frac{\Lambda_\eta}{2} \tag{A5.7f}$$

$$d_1 = 1 - \frac{\Lambda_\eta}{6} \tag{A5.7g}$$

Substitution of eqs(A5.7) into (A5.3) shows that

$$\frac{u}{u_e} = F(\lambda) \tag{A5.8a}$$

$$\frac{v}{v_e} = F(\lambda) + \Lambda_\eta G(\lambda) \tag{A5.8b}$$

where the functions F and G are exactly the same as in the two-dimensional flow

$$F(\lambda) = 1 - (1-\lambda)^3(1+\lambda) \tag{A5.9a}$$

$$G(\lambda) = \frac{1}{6}\lambda(1-\lambda)^3 \tag{A5.9b}$$

Thus, the dimensionless quantities of interest will also have the same form as their two-dimensional counterparts

$$\frac{\delta_1}{\delta} = \int_0^1 (1-F)d\lambda = 0.3 \tag{A5.10a}$$

$$\frac{\delta_2}{\delta} = \int_0^1 (1-F-\Lambda_\eta G)d\lambda = 0.3 - 0.00833\Lambda_\eta \tag{A5.10b}$$

$$\frac{\theta_{11}}{\delta} = \int_0^1 F(1-F)d\lambda = 0.11746 \tag{A5.10c}$$

$$\frac{\theta_{22}}{\delta} = \int_0^1 (F+\Lambda_\eta G)(1-F-\Lambda_\eta G)d\lambda = 0.11746 - 0.00106\Lambda_\eta - 0.00011\Lambda_\eta^2 \tag{A5.10d}$$

$$\frac{\theta_{12}}{\delta} = \int_0^1 (1-F)(F+\Lambda_\eta G)d\lambda = 0.11746 - 0.0036\Lambda_\eta \tag{A5.10e}$$

$$\frac{\theta_{21}}{\delta} = \int_0^1 F(1-F-\Lambda_\eta G)d\lambda = 0.11746 - 0.0047\Lambda_\eta \tag{A5.10f}$$

Notice that Λ_η does not appear in the right side of functions which depend only on the axial flow, since there is no pressure gradient in the ξ - direction.

The friction coefficient is now defined by

$$C_{f\eta} \equiv \frac{\tau_\eta}{\frac{1}{2}\varrho v_e^2} \tag{A5.11}$$

from which it may be written

$$\frac{\tau_\eta \delta}{\mu v_e} = \frac{\tau_\eta}{\varrho v_e^2}\frac{\delta v_e}{\nu} = \frac{1}{2}C_{f\eta}\frac{\delta v_e}{\nu} = 2 + \frac{\Lambda_\eta}{6} \tag{A5.12}$$

Cross-flow separation occurs when $\tau_\eta = 0$, or, when $\Lambda_\eta = -12$, while stagnation points correspond to $\Lambda_\eta = +7.052$.

Multiplying now eq(8.15) by $(\theta_{22}/\nu v_e)$ yields

$$\frac{v_e \theta_{22}}{R\nu}\frac{\partial \theta_{22}}{\partial \eta} + \frac{\theta_{22}^2}{R\nu}\left(2 + \frac{\delta_2}{\theta_{22}}\right)\left(\frac{\partial v_e}{\partial \eta} + \varepsilon u_e\right) = \frac{\tau_\eta \delta}{\mu v_e}\frac{\theta_{22}}{\delta} \tag{A5.13}$$

which is identical in form with the corresponding equation for the two-dimensional boundary layer, eq(10.26) in ref.40. Following the same procedure for its solution as in the two-dimensional case, one may define the second pressure gradient parameter as

$$K_{\eta L} \equiv \frac{\theta_{22}^2}{R\nu}\left(\frac{\partial v_e}{\partial \eta} + \varepsilon u_e\right) \tag{A5.14}$$

Combining now eqs(A5.6) and (A5.14) gives

$$K_{\eta L} = \theta_{22}^2 \frac{\Lambda_\eta}{\delta^2} \tag{A5.14a}$$

which, when combined with eq(A5.10d) yields

$$K_{\eta L} = \frac{1}{3969}\left(\frac{37}{5} - \frac{\Lambda_\eta}{15} - \frac{\Lambda_\eta^2}{144}\right)^2 \Lambda_\eta \qquad (A5.14b)$$

The boundary layer shape factor is defined by

$$H_{2L} \equiv \frac{\delta_2}{\theta_{22}} \qquad (A5.15)$$

and using eqs(A5.10b)and (A5.10d) it can be written as

$$H_{2L} = \frac{0.3 - 0.00833\Lambda_\eta}{0.11746 - 0.00106\Lambda_\eta - 0.00011\Lambda_\eta^2} = f_1(K_{\eta L}) \qquad (A5.15a)$$

Equations(A5.10d) and (A5.12) also combine to give

$$\frac{\tau_\eta \delta}{\mu v_e}\frac{\theta_{22}}{\delta} = \left(2 + \frac{\Lambda_\eta}{6}\right)\left(\frac{37}{5} - \frac{\Lambda_\eta}{15} - \frac{\Lambda_\eta^2}{144}\right)\frac{1}{63} = f_2(K_{\eta L}) \qquad (A5.16)$$

Now eq(A5.13) can be written as

$$\frac{1}{2}\frac{d}{d\eta}\left(\frac{\theta_{22}^2}{R\nu}\right) v_e + K_{\eta L}[2 + f_1(K_{\eta L})] = f_2(K_{\eta L}) \qquad (A5.17)$$

and if the function F is introduced in a manner analogous to that for the two-dimensional case

$$\begin{aligned} F(K_{\eta L}) &= 2f_2(K_{\eta L}) - 4K_{\eta L} - 2K_{\eta L} f_1(K_{\eta L}) \\ &= \frac{2}{63}\left(\frac{37}{5} - \frac{\Lambda_\eta}{15} - \frac{\Lambda_\eta^2}{144}\right)\left[2 - \frac{116}{315}\Lambda_\eta + \left(\frac{2}{945} + \frac{1}{120}\right)\Lambda_\eta^2 + \frac{2}{9072}\Lambda_\eta^3\right] \end{aligned} \qquad (A5.18)$$

eq(A5.17) finally becomes

$$\frac{d}{d\eta}\left(\frac{\theta_{22}^2}{R\nu}\right) = \frac{F(K_{\eta L})}{v_e} \tag{A5.19}$$

which is a non-linear ordinary differential equation for $(\theta_{22}^2/R\nu)$. The function $F(K_{\eta L})$ can be approximated by a straight line

$$F(K_{\eta L}) = c_L - d_L K_{\eta L} \tag{A5.20}$$

where c_L and d_L are constants. When this is done, eq(A5.19) transforms into

$$\frac{d\omega_L}{d\eta} + \omega_L\left[(d_L - 1)\frac{1}{v_e}\frac{dv_e}{d\eta} + d_L\varepsilon\frac{u_e}{v_e}\right] = c_L \tag{A5.21}$$

where

$$\omega_L \equiv \frac{v_e\theta_{22}^2}{a\nu} \tag{A5.22}$$

The integrating factor for eq(A5.21) is

$$exp\left[\int_0^\eta P_L(\eta)d\eta\right] = v_e^{d_L-1}E_L \tag{A5.23}$$

where

$$E_L \equiv exp\left[d_L\varepsilon\int_0^\eta \frac{u_e}{v_e}d\eta\right] \tag{A5.24}$$

and

$$P_L(\eta) \equiv (d_L - 1)\frac{1}{v_e}\frac{dv_e}{d\eta} + d_L\varepsilon\frac{u_e}{v_e} \tag{A5.25}$$

Then the solution to eq(A5.21) is written as

$$\omega_L = \frac{c_L \int\limits_0^\eta v_e^{d_L-1} E_L d\eta}{v_e^{d_L-1} E_L} \tag{A5.26}$$

Using the dimensionless velocities defined in eqs(8.17) the solution may be expressed in the following way

$$\theta_{22}^2 = \frac{Rc_L\nu}{E_L u_\infty}\frac{1}{V^{d_L}}\int\limits_0^\eta E_L V^{d_L-1} d\eta \tag{A5.27}$$

where

$$E_L \equiv exp\left[d_L\varepsilon\int\limits_0^\eta \frac{U}{V} d\eta\right] \tag{A5.28}$$

The condition for separation in laminar flow is written in terms of the pressure gradient parameters

$$\Lambda_\eta = -12 \Rightarrow K_{\eta L} = -0.157 \tag{A5.29}$$

and from the definition of $K_{\eta L}$ in eq(A5.14) we get

$$\frac{c_L}{E_L V^{d_L}}\left(\frac{dV}{d\eta}+\varepsilon U\right)\int_0^{\eta} E_L V^{d_L-1} d\eta = -0.157 \qquad (A5.30)$$

The constants c_L and d_L have the same values as for the two-dimensional laminar boundary layer (i.e., $c_L = 0.47$ and $d_L = 6$). These values may be substituted into eq(A5.30), and the "separation criterion for laminar flow" can be expressed as

$$SC_L \equiv E_L^{-1} V^{-6}\left(\frac{dV}{d\eta}+\varepsilon U\right)\int_0^{\eta_s} E_L V^5 d\eta = -0.334 \qquad (A5.32)$$

For sufficiently slender bodies and small angles of attack it may be assumed

$$u_e \simeq u_\infty \Rightarrow U \simeq 1.0 \qquad (A5.33)$$

so

$$SC_L = E_L^{-1} V^{-6}\left(\frac{dV}{d\eta}+\varepsilon\right)\int_0^{\eta_s} E_L V^5 d\eta = -0.334 \qquad (A5.32a)$$

where

$$E_L = exp\left[6\varepsilon\int_0^{\eta}\frac{d\eta}{V}\right] \qquad (A5.28a)$$

To avoid infinite values of E_L at the reattachment points, the velocity will be approximated by a linear expression near these points

$$V = \omega_{0L}\eta \qquad \text{where} \qquad \omega_{0L} = const \tag{A5.34}$$

when this is done E_L becomes

$$E_L = exp\left[6\varepsilon \int_0^{\eta} \frac{dV}{V}\frac{d\eta}{dV}\right]$$

and since $(d\eta/dV = 1/\omega_{0L} = const$ the right side of the previous equation can be integrated to give

$$E_L = V^{(6\varepsilon/\omega_{0L})} \tag{A5.35}$$

Finally eq(A5.32a) gives

$$SC_L = \frac{1}{6} \tag{A5.36}$$

which is the limit of SC_L as η approaches a reattachment point.

A5.2 Turbulent Boundary Layer

The procedure for the solution of the boundary layer equations for turbulent flow is similar to the one outlined in the previous section for the laminar case. The differences are mainly due to the fact that the turbulent boundary layer grows thicker than the laminar one, as was explained in section (8.3)

For the turbulent case it is necessary to define, as in the two-dimensional case, the following parameters

$$Re_\eta \equiv \frac{v_e \theta_{22}}{\nu} \tag{A5.37}$$

$$K_{\eta T} \equiv \frac{\theta_{22}}{R v_e} Re_\eta^{\frac{5}{4}} \left(\frac{dv_e}{d\eta} + \varepsilon u_e \right) \tag{A5.38}$$

$$H_{2T} \equiv \frac{\delta_2}{\theta_{22}} = g_1(K_{\eta T}) \tag{A5.39}$$

$$\frac{1}{2} C_{f\eta} = \frac{\tau_\eta}{\varrho v_e^2} = Re^{-\frac{5}{4}} g_2(K_{\eta T}) \tag{A5.40}$$

Substituting eqs(A5.37) through (A5.40) into (A5.13) yields after some algebra

$$\frac{1}{R} \frac{d}{d\eta} (\theta_{22} Re_\eta^{\frac{5}{4}}) = F(K_{\eta T}) - \frac{5}{4} \frac{\theta_{22}}{R v_e} Re_\eta^{\frac{5}{4}} \varepsilon u_e \tag{A5.41}$$

where

$$F(K_{\eta T}) \equiv 2.25 g_2 - (3.25 + 2.25 g_1) K_{\eta T} \tag{A5.42}$$

It must be noted that $F(K_{\eta T})$ is again the same function as in the two-dimensional case, and it may be approximated by a straight line

$$F(K_{\eta T}) = c_T - d_T K_{\eta T} \tag{A5.43}$$

When this is done, eq(A5.41) transforms into

$$\frac{d\omega_T}{d\eta} + \omega_T \left[\left(d_T + \frac{5}{4} \right) \varepsilon \frac{u_e}{v_e} + d_T \frac{1}{v_e} \frac{dv_e}{d\eta} \right] = Rc_T \tag{A5.44}$$

where

$$\omega_T \equiv \theta_{22} Re_\eta^{\frac{5}{4}} \tag{A5.45}$$

The integrating factor for eq(A5.44) is

$$exp \left[\int_{\eta_{tr}}^{\eta} P_T(\eta) d\eta \right] = E_T v_e^{d_T} \tag{A5.46}$$

where

$$E_T \equiv exp \left[\varepsilon \left(d_T + \frac{5}{4} \right) \int_{\eta_{tr}}^{\eta} \frac{u_e}{v_e} d\eta \right] \tag{A5.47}$$

and

$$P_T(\eta) \equiv \left(d_T + \frac{5}{4}\right)\varepsilon\frac{u_e}{v_e} + \frac{d_T}{v_e}\frac{dv_e}{d\eta} \tag{A5.48}$$

Then the solution to eq(A5.44) is written as

$$\omega_T = \frac{Rc_T\left[\int\limits_{\eta_{tr}}^{\eta} E_T v_e^{d_T} d\eta + c_2\right]}{E_T v_e^{d_T}} \tag{A5.49}$$

or, using the same dimensionless terms defined by eqs(8.17) as well as $c_T = 0.016$ and $d_T = 4$ (same values as for the two-dimensional boundary layer)

$$E_T = exp\left[5.25\varepsilon\int\limits_{\eta_{tr}}^{\eta}\frac{U}{V}d\eta\right] \tag{A5.50}$$

$$\theta_{22}^{2.25} = \left(\frac{\nu}{u_\infty}\right)^{1.25}\frac{0.016R}{E_T V^{5.25}}\left[\int\limits_{\eta_{tr}}^{\eta} E_T V^4 d\eta + c_2\right] \tag{A5.51}$$

The constant of integration c_2 may be determined by equating θ_{22} from eq(A5.51) with its value for laminar flow, both being evaluated at the transition point. This yields

$$c_2 = 26.729\nu^{-0.125}E_L^{-1.125}V^{9.5}\left[\int\limits_{0}^{\eta_{tr}} E_L V^5 d\eta\right]^{1.125} \tag{A5.52}$$

Separation of the turbulent boundary layer occurs when $K_{\eta T} = -0.06$ as for the two-dimensionlal case. Using eqs(A5.38) and (A5.51) this condition translates to

$$SC_T \equiv \frac{1}{E_T V^5}\left(\frac{dV}{d\eta} + \varepsilon U\right)\left[\int_{\eta_{tr}}^{\eta_s} E_T V^4 d\eta + c_2\right] = -3.75 \tag{A5.53}$$

assuming again that $U \simeq 1$, eqs(A5.47) and (A5.53) reduce to

$$E_T = exp\left[5.25\varepsilon \int_{\eta_{tr}}^{\eta} \frac{d\eta}{V}\right] \tag{A5.47a}$$

$$SC_T = \frac{1}{E_T V^5}\left(\frac{dV}{d\eta} + \varepsilon\right)\left[\int_{\eta_{tr}}^{\eta_s} E_T V^4 d\eta + c_2\right] = -3.75 \tag{A5.53a}$$

The linearity assumption for the velocity near reattachment points is employed again

$$V = \omega_{0T}\eta \qquad \text{where} \qquad \omega_{0T} = const \tag{A5.54}$$

and the result is now

$$E_T = V^{5.25(\varepsilon/\omega_{0T})} \tag{A5.55}$$

Substitution of the above approximations into eq(A5.53a) yields

$$SC_T = \frac{\omega_{0T} + \varepsilon}{5(\omega_{0T} + \varepsilon) + 0.25\varepsilon} \tag{A5.56}$$

and since ε is small, the second term in the denominator may be neglected leaving

$$SC_T = \frac{1}{5} \tag{A5.57}$$

which is the limit of SC_T as η approaches a reattachment point for a slender cone, assuming that the boundary layer is turbulent from its start.

APPENDIX 6

Program Listings

This appendix contains five main FORTRAN programs :

A. PROGRAM VORTEX-CIRCLE

B. PROGRAM V-CP ELLIPSE

C. PROGRAM V-CP CIRCLE

D. PROGRAM K-CL

E. PROGRAM BL

The function of each program, as well as the function of each subroutine within the main programs, is explained with comments wherever is appropriate.

```
      PROGRAM VORTEX-CIRCLE
C     ------------------------------------------------------------
C     THIS PROGRAM SOLVES THE SYSTEM OF EQUATIONS CONSISTING OF
C     THE SEPARATION AND FORCE-FREE CONDITIONS, FOR THE RIGHT
C     VORTEX POSITION. A CIRCULAR CROSS-SECTION IS CONSIDERED,
C     AND THE VORTEX SYSTEM CAN BE EITHER SYMMETRICAL OR
C     ASYMMETRICAL.
C     ------------------------------------------------------------
      IMPLICIT REAL*8 (A-H,O-Z)
      DIMENSION H(10),RHS(10),WORK(10),X(10),XOLD(10),Z(10)
      DIMENSION RJAC(10,10),OA(10,10),IPVT(10)
C     ------------------------------------------------------------
C     OUTPUT
C     ------------------------------------------------------------
C     X        IS THE SOLUTION OF THE SYSTEM IN VECTOR FORM
C     ------------------------------------------------------------
C     RJAC     IS THE JACOBIAN OF THE SYSTEM
C     RHS      IS THE RIGHT HAND SIDE OF THE EQ. : RJAC*H=RHS
C              IN VECTOR FORM
C     H        IS THE DIFFERENCE : XNEW-XOLD
C     ACC      IS AN ESTIMATE OF THE MACHINE ACCURACY
C     ------------------------------------------------------------
C     INPUT
C     ------------------------------------------------------------
      OPEN(UNIT=6, FILE='TTY:',STATUS='NEW')
    1 CONTINUE
C
C     NDIM     IS THE DECLARED ROW DIMENSION OF THE JACOBIAN
C     N        IS THE ORDER OF THE MATRIX
C     NMAX     IS THE MAX ALLOWABLE # OF ITERATIONS
C
      N=4
      NDIM=4
      NMAX=25
      WRITE(5,40)
   40 FORMAT( ' GIVE THE RATIO ALFA/EPSILON ')
      READ(5,100)AE
      WRITE(5,41)
   41 FORMAT( ' GIVE THE ASSUMED SEPARATION ANGLE ON THE RIGHT')
      READ(5,100)SEPAR1
      WRITE(5,42)
   42 FORMAT( ' GIVE THE ASSUMED SEPARATION ANGLE ON THE LEFT')
      READ(5,100)SEPAR2
C     ------------------------------------------------------------
C     INITIAL GUESS
C     ------------------------------------------------------------
      WRITE(5,50)
   50 FORMAT( ' GIVE Y10 ')
      READ(5,100) X(1)
      WRITE(5,51)
   51 FORMAT( ' GIVE Z10 ')
      READ(5,100) X(2)
      WRITE(5,52)
   52 FORMAT( ' GIVE Y20 ')
      READ(5,100) X(3)
      WRITE(5,53)
```

```
 53     FORMAT( ' GIVE Z20 ')
        READ(5,100) X(4)
100     FORMAT(F)
C       ----------------------------------------------------------
        A=1.0D0
        GP=3.141592654D0
        SEP1=SEPAR1*GP/180.0D0
        SEP2=(180.0D0-SEPAR2)*GP/180.0D0
C       ----------------------------------------------------------
C       ESTIMATE MACHINE ACCURACY
C       ----------------------------------------------------------
        ACC=1.0D0
140     ACC=0.5D0*ACC
        ACCU=ACC+1.0D0
        IF (ACCU.GT.1.0D0) GO TO 140
C       ----------------------------------------------------------
C       PRINT INITIAL GUESS
C       ----------------------------------------------------------
        DO 200 I=1,N
        WRITE (5,150) I,X(I)
150     FORMAT(' X(',I1,')=',F10.3)
200     CONTINUE
C       ----------------------------------------------------------
        NITER=0
        NCONV=0
C       ----------------------------------------------------------
C       LOOP FOR EACH ITERATION
C       ----------------------------------------------------------
250     CONTINUE
        DO 260 I=1,N
        XOLD(I)=X(I)
260     CONTINUE
C       ----------------------------------------------------------
C       FORM THE JACOBIAN MATRIX AND THE RHS VECTOR
C       ----------------------------------------------------------
        CALL JACOB(NDIM,N,AE,SEP1,SEP2,X,RJAC,RHS)
300     FORMAT (1X,4F15.8)
C       ----------------------------------------------------------
C       SOLVE THE SYSTEM RJAC*H=RHS
C       ----------------------------------------------------------
        CALL DECOMP(NDIM,N,RJAC,COND,IPVT,WORK,OA,Z)
C
C       THE SYSTEM WILL BE SOLVED ONLY IF RJAC IS WELL CONDITIONED
C
        CONDI=COND+1.0D0
        IF (CONDI.EQ.COND) GO TO 390
        GO TO 420
390     WRITE (5,400)
400     FORMAT(' MATRIX IS SINGULAR TO WORKING PRECISION. ')
        GO TO 710
420     CONTINUE
        CALL SOLVE(NDIM,N,RJAC,RHS,IPVT,H)
```

```
C     --------------------------------------------------------------
C     COMPUTE NEW VECTOR X
C     --------------------------------------------------------------
      DO 450 I=1,N
      X(I)=X(I)+H(I)
450   CONTINUE
      NITER=NITER+1
      WRITE (6,470) NITER, (X(I),I=1,N)
470   FORMAT (1X,I3,8F9.5)
C     --------------------------------------------------------------
C     CHECK FOR CONVERGENCE
C     --------------------------------------------------------------
      DO 500 I=1,N
      IF(ABS((XOLD(I)-X(I))/XOLD(I)).LE.1.E-5)NCONV=NCONV+1
500   CONTINUE
      IF (NCONV.EQ.N) GO TO 600
      IF (NITER.LT.NMAX) GO TO 250
      WRITE (5,520)
520   FORMAT(' SOLUTION DOES NOT CONVERGE ')
      WRITE(5,521)
521   FORMAT(' WITHIN THE SPECIFIED NUMBER OF ITERATIONS  ')
      GO TO 710
C     --------------------------------------------------------------
C     WRITE SOLUTION
C     --------------------------------------------------------------
600   WRITE (5,650)
650   FORMAT(///,' THE SOLUTION OF THE SYSTEM IS : '//)
      DO 700 I=1,N
      WRITE (5,670) I,X(I)
670   FORMAT(' X(',I1,')=',F15.5)
700   CONTINUE
      R1=DSQRT(X(1)**2+X(2)**2)
      R2=DSQRT(X(3)**2+X(4)**2)
      WRITE(5,705)R1,R2
705   FORMAT(2F15.5)
710   WRITE(5,750)
750   FORMAT(/,' DO YOU WANT TO CONTINUE ? (1 FOR YES-0 FOR NO)>',$)
      READ(6,*) ILOG
      IF(ILOG.EQ.1)GO TO 1
      STOP
      END


      SUBROUTINE SPLIT(AE,SEP1,SEP2,Y1,Z1,Y2,Z2,U,W,JF)
C     --------------------------------------------------------------
C     THIS SUBROUTINE SPLITS A COMPLEX FUNCTION INTO ITS
C     REAL AND IMAGINARY PARTS.
C     --------------------------------------------------------------
      EXTERNAL F
      REAL*8 Y1,Y2,Z1,Z2,SEP1,SEP2,U,W
      COMPLEX*8 S1,S2,V,F
      S1=CMPLX(Y1,Z1)
      S2=CMPLX(Y2,Z2)
      V=F(AE,SEP1,SEP2,S1,S2,JF)
      U=REAL(V)
      W=AIMAG(V)
      RETURN
      END
```

```
      SUBROUTINE JACOB(NDIM,N,AE,SEP1,SEP2,X,RJAC,RHS)
C     ------------------------------------------------------------
C     THIS SUBROUTINE COMPUTES THE JACOBIAN OF THE GIVEN
C     SYSTEM OF EQUATIONS.
C     ------------------------------------------------------------
      IMPLICIT REAL*8 (A-H,O-Z)
      DIMENSION RJAC(N,N),RHS(N),X(N)
      Y1=X(1)
      Z1=X(2)
      Y2=X(3)
      Z2=X(4)
      DYZ=0.001D0
      CALL SPLIT(AE,SEP1,SEP2,Y1,Z1,Y2,Z2,FR1,FI1,1)
      CALL SPLIT(AE,SEP1,SEP2,Y1,Z1,Y2,Z2,FR2,FI2,2)
      RHS(1)=-FR1
      RHS(2)=-FI1
      RHS(3)=-FR2
      RHS(4)=-FI2
C     ------------------------------------------------------------
C     CALCULATE THE DERIVATIVES WITH RESPECT TO Y1
C     ------------------------------------------------------------
      Y1N=Y1+DYZ
      CALL SPLIT(AE,SEP1,SEP2,Y1N,Z1,Y2,Z2,FR1Y1,FI1Y1,1)
      CALL SPLIT(AE,SEP1,SEP2,Y1N,Z1,Y2,Z2,FR2Y1,FI2Y1,2)
      RJAC(1,1)=(FR1Y1-FR1)/DYZ
      RJAC(2,1)=(FI1Y1-FI1)/DYZ
      RJAC(3,1)=(FR2Y1-FR2)/DYZ
      RJAC(4,1)=(FI2Y1-FI2)/DYZ
C     ------------------------------------------------------------
C     CALCULATE THE DERIVATIVES WITH RESPECT TO Z1
C     ------------------------------------------------------------
      Z1N=Z1+DYZ
      CALL SPLIT(AE,SEP1,SEP2,Y1,Z1N,Y2,Z2,FR1Z1,FI1Z1,1)
      CALL SPLIT(AE,SEP1,SEP2,Y1,Z1N,Y2,Z2,FR2Z1,FI2Z1,2)
      RJAC(1,2)=(FR1Z1-FR1)/DYZ
      RJAC(2,2)=(FI1Z1-FI1)/DYZ
      RJAC(3,2)=(FR2Z1-FR2)/DYZ
      RJAC(4,2)=(FI2Z1-FI2)/DYZ
C     ------------------------------------------------------------
C     CALCULATE THE DERIVATIVES WITH RESPECT TO Y2
C     ------------------------------------------------------------
      Y2N=Y2+DYZ
      CALL SPLIT(AE,SEP1,SEP2,Y1,Z1,Y2N,Z2,FR1Y2,FI1Y2,1)
      CALL SPLIT(AE,SEP1,SEP2,Y1,Z1,Y2N,Z2,FR2Y2,FI2Y2,2)
      RJAC(1,3)=(FR1Y2-FR1)/DYZ
      RJAC(2,3)=(FI1Y2-FI1)/DYZ
      RJAC(3,3)=(FR2Y2-FR2)/DYZ
      RJAC(4,3)=(FI2Y2-FI2)/DYZ
C     ------------------------------------------------------------
C     CALCULATE THE DERIVATIVES WITH RESPECT TO Z2
C     ------------------------------------------------------------
      Z2N=Z2+DYZ
      CALL SPLIT(AE,SEP1,SEP2,Y1,Z1,Y2,Z2N,FR1Z2,FI1Z2,1)
      CALL SPLIT(AE,SEP1,SEP2,Y1,Z1,Y2,Z2N,FR2Z2,FI2Z2,2)
```

```
      RJAC(1,4)=(FR1Z2-FR1)/DYZ
      RJAC(2,4)=(FI1Z2-FI1)/DYZ
      RJAC(3,4)=(FR2Z2-FR2)/DYZ
      RJAC(4,4)=(FI2Z2-FI2)/DYZ
C     ----------------------------------------------------------------
      RETURN
      END


      COMPLEX FUNCTION F(AE,SEP1,SEP2,S1,S2,JF)
C     ----------------------------------------------------------------
      REAL*8 SEP1,SEP2
      COMPLEX*8 S1,S2,CS1,CS2,SP1,SP2,CSP1,CSP2,Q1,Q2
      COMPLEX*8 A1,A2,A3,A4,B1,B2,B3,B4,C1,C2,C3,C4
      COMPLEX*8 D1,D3,E1,E3,H1,H3,G1,G3,F1,F2
C     ----------------------------------------------------------------
      A=1.0
C     ----------------------------------------------------------------
      SP1=A*CMPLX(COS(SEP1),SIN(SEP1))
      SP2=A*CMPLX(COS(SEP2),SIN(SEP2))
      CS1=CONJG(S1)
      CS2=CONJG(S2)
      CSP1=CONJG(SP1)
      CSP2=CONJG(SP2)
      A1=1.0+A**2/SP1**2
      A2=1.0+A**2/SP2**2
      A3=1.0+A**2/CSP2**2
      A4=1.0+A**2/CSP1**2
      B1=1.0/(SP1-S1)-CS1/(SP1*CS1-A**2)
      B2=1.0/(SP2-S1)-CS1/(SP2*CS1-A**2)
      B3=1.0/(CS2-CSP2)+S2/(S2*CSP2-A**2)
      B4=1.0/(CS2-CSP1)+S2/(S2*CSP1-A**2)
      C1=1.0/(SP1-S2)-CS2/(SP1*CS2-A**2)
      C2=1.0/(SP2-S2)-CS2/(SP2*CS2-A**2)
      C3=1.0/(CS1-CSP2)+S1/(S1*CSP2-A**2)
      C4=1.0/(CS1-CSP1)+S1/(S1*CSP1-A**2)
      D1=(2.0*CS1-CSP1)/A
      D3=(SP2-2.0*S2)/A
      E1=1.0+A**2/S1**2
      E3=1.0+A**2/CS2**2
      H1=-CS1/(S1*CS1-A**2)
      H3=S2/(S2*CS2-A**2)
      G1=1.0/(S1-S2)-CS2/(S1*CS2-A**2)
      G3=1.0/(CS1-CS2)+S1/(S1*CS2-A**2)
      Q1=(A1*C2-A2*C1)/(B2*C1-B1*C2)
      Q2=(A3*C4-A4*C3)/(C3*B4-C4*B3)
      F1=(0,1)*(Q1*H1-Q2*G1+E1)+(D1-A/S1)/AE
      F2=(0,1)*(Q2*H3-Q1*G3+E3)+(D3+A/CS2)/AE
      IF (JF.EQ.1) F=F1
      IF (JF.EQ.2) F=F2
      RETURN
      END
```

```
      SUBROUTINE SOLVE(NDIM,N,A,B,IPVT,X)
C     ---------------------------------------------------------------
      IMPLICIT REAL*8 (A-H,O-Z)
      DIMENSION A(NDIM,N),B(N),IPVT(N),X(N)
C
C     SOLUTION OF LINEAR SYSTEM, A*X=B
C     DO NOT USE IF DECOMP HAS DETECTED SINGULARITY
C
C     INPUT..
C
C       NDIM = DECLARED ROW DIMENSION OF ARRAY CONTAINING A
C
C       N = ORDER OF MATRIX.
C
C       A = TRIANGULARIZED MATRIX OBTAINED FROM DECOMP
C
C       B = RIGHT HAND SIDE VECTOR
C
C       IPVT = PIVOT VECTOR OBTAINED FROM DECOMP
C
C     OUTPUT..
C
C       X = SOLUTION VECTOR,X.
C
      INTEGER KB,KM1,NM1,KP1,I,K,M
      REAL T
      DO 1 I=1,N
      X(I)=B(I)
 1    CONTINUE
C
C     FORWARD ELIMINATION
C
      IF(N.EQ.1) GO TO 50
      NM1=N-1
      DO 20 K=1,NM1
      KP1=K+1
      M=IPVT(K)
      T=X(M)
      X(M)=X(K)
      X(K)=T
      DO 10 I=KP1,N
      X(I)=X(I)+A(I,K)*T
 10   CONTINUE
 20   CONTINUE
C
C     BACK SUBSTITUTION
C
      DO 40 KB=1,NM1
      KM1=N-KB
      K=KM1+1
      X(K)=X(K)/A(K,K)
      T=-X(K)
      DO 30 I=1,KM1
      X(I)=X(I)+A(I,K)*T
 30   CONTINUE
 40   CONTINUE
 50   X(1)=X(1)/A(1,1)
      RETURN
      END
```

```
      SUBROUTINE DECOMP(NDIM,N,A,COND,IPVT,WORK,OA,Z)
C     ---------------------------------------------------------------
      IMPLICIT REAL*8 (A-H,O-Z)
      DIMENSION A(NDIM,N),IPVT(N),OA(NDIM,N),WORK(N),Z(N)
C
C     DECOMPOSES A REAL MATRIX BY GAUSSIAN ELIMINATION
C     AND ESTIMATES THE CONDITION OF THE MATRIX.
C
C     USE SOLVE TO COMPUTE SOLUTIONS TO LINEAR SYSTEMS.
C
C     INPUT..
C
C       NDIM = DECLARED ROW DIMENSION OF THE ARRAY CONTAINING A.
C
C       N = ORDER OF THE MATRIX.
C
C       A = MATRIX TO BE TRIANGULARIZED.
C
C     OUTPUT..
C
C       A CONTAINS AN UPPER TRIANGULAR MATRIX U AND A PERMUTED
C        VERSION OF A LOWER TRIANGULAR MATRIX I-L SO THAT
C        (PERMUTATION MATRIX)*A = L*U
C
C       COND = AN ESTIMATE OF THE CONDITION OF A.
C         FOR THE LINEAR SYSTEM A*X =B, CHANGES IN A AND B
C         MAY CAUSE CHANGES COND TIMES AS LARGE
C         IF COND+1.0 .EQ. COND , A IS SINGULAR TO WORKING
C         PRECISION. COND IS SET TO 1.0E+32 IF EXACT
C         SINGULARITY IS DETECTED.
C
C       IPVT = THE PIVOT VECTOR.
C         IPVT(K) = THE INDEX OF THE K-TH PIVOT ROW
C         IPVT(N) = (-1)**(NUMBER OF INTERCHANGES)
C
C     WORK , Z .. THESE VECTORS MUST BE DECLARED AND
C     INCLUDED IN THE  CALL. THEIR INPUT CONTENTS ARE IGNORED.
C               THEIR OUTPUT CONTENTS ARE USUALLY UNIMPORTANT.
C
C       OA.. THE ORIGINAL N*N MATRIX
C
C     THE DETERMINANT OF A CAN BE OBTAINED ON OUTPUT BY
C       DET(A) = IPVT(N) * A(1,1) * A(2,2) * ... * A(N,N).
C
      REAL EK,T,ANORM,YNORM,ZNORM
      INTEGER NM1,I,J,K,KP1,KB,KM1,M
C
      DO 1 I=1,N
      DO 1 J=1,N
      OA(I,J)=A(I,J)
  1   CONTINUE
C
      IPVT(N) = 1
      IF (N.EQ.1) GO TO 80
      NM1 = N - 1
C
```

```
C       COMPUTE 1-NORM OF A
C
        ANORM = 0.0
        DO 10 J=1,N
        T=0.0
        DO 5 I=1,N
        T=T+ABS(A(I,J))
 5      CONTINUE
        IF (T.GT.ANORM) ANORM=T
 10     CONTINUE
C
C       GAUSSIAN ELIMINATION WITH PARTIAL PIVOTING
C
        DO 35 K=1,NM1
        KP1=K+1
C
C       FIND PIVOT
C
        M=K
        DO 15 I=KP1,N
        IF(ABS(A(I,K)).GT.ABS(A(M,K))) M=I
 15     CONTINUE
        IPVT(K) = M
        IF (M.NE.K) IPVT(N) =-IPVT(N)
        T = A(M,K)
        A(M,K) = A(K,K)
        A(K,K) = T
C
C       SKIP STEP IF PIVOT IS ZERO
C
        IF (T.EQ.0.0) GO TO 35
C
C       COMPUTE MULTIPLIERS
C
        DO 20 I=KP1,N
        A(I,K) = -A(I,K)/T
 20     CONTINUE
C
C       INTERCHANGE AND ELIMINATE BY COLUMNS
C
        DO 30 J=KP1,N
        T=A(M,J)
        A(M,J)=A(K,J)
        A(K,J)=T
        IF (T.EQ.0.0) GO TO 30
        DO 25 I=KP1,N
        A(I,J)=A(I,J)+A(I,K)*T
 25     CONTINUE
 30     CONTINUE
 35     CONTINUE
C
C       COND = (1-NORM OF A)*(AN ESTIMATE OF 1-NORM OF A-INVERSE)
C       ESTIMATE OBTAINED BY ONE STEP OF INVERSE ITERATION FOR THE
C       SMALL SINGULAR VECTOR. THIS INVOLVES SOLVING TWO SYSTEMS
C       OF EQUATIONS,(A-TRANSPOSE)*Y = E AND A*Z = Y WHERE E
C       IS A VECTOR OF +1 OR -1 CHOSEN TO CAUSE GROWTH IN Y.
C       ESTIMATE = (1-NORM OF Z)/(1-NORM OF Y)
C
```

```
C         SOLVE (A-TRANSPOSE)*Y = E
C
          DO 50 K=1,N
          T=0.0
          IF (K.EQ.1)GO TO 45
          KM1=K-1
          DO 40 I=1,KM1
          T=T+A(I,K)*WORK(I)
 40       CONTINUE
 45       EK=1.0
          IF(T.LT.0.0) EK=-1.0
          IF(A(K,K).EQ.0.0) GO TO 90
          WORK(K)=-(EK+T)/A(K,K)
 50       CONTINUE
          DO 60 KB=1,NM1
          K=N-KB
          T=0.0
          KP1=K+1
          DO 55 I=KP1,N
          T=T+A(I,K)*WORK(K)
 55       CONTINUE
          WORK(K)=T
          M=IPVT(K)
          IF (M.EQ.K) GO TO 60
          T=WORK(M)
          WORK(M)=WORK(K)
          WORK(K)=T
 60       CONTINUE
C
          YNORM=0.0
          DO 65 I=1,N
          YNORM=YNORM+ABS(WORK(I))
 65       CONTINUE
C
C         SOLVE A*Z = Y
C
          CALL SOLVE(NDIM,N,A,WORK,IPVT,Z)
C
          ZNORM=0.0
          DO 70 I=1,N
          ZNORM=ZNORM+ABS(Z(I))
 70       CONTINUE
C
C         ESTIMATE CONDITION
C
          COND=ANORM*ZNORM/YNORM
          IF (COND.LT.1.0) COND=1.0
          RETURN
C
C         1-BY-1
C
 80       COND=1.0
          IF (A(1,1).NE.0.0) RETURN
C
C         EXACT SINGULARITY
C
 90       COND=1.0E+32
          RETURN
          END
```

```
      PROGRAM V-CP ELLIPSE
C     ------------------------------------------------------------
C     THIS PROGRAM COMPUTES THE VELOCITY AND PRESSURE DISTRIBUTIONS
C     ON THE SURFACE OF A CONICAL BODY OF ELLIPTICAL OR FLAT
C     CROSS-SECTION WITH SEPARATED FLOW.
C     ------------------------------------------------------------
      COMPLEX CV1,CV2,CV3,CV4,CV5,CV6,G,G1,G2,Q,QA,Q1,Q2,QF,S,SP,SP1
      COMPLEX S1,S2,T,TA,T1,T1A,T2,T2A,TS,VCF,WT,WT1,WT2,WR,WB,WA,WQ
C     ------------------------------------------------------------
C     DATA
C     ------------------------------------------------------------
      OPEN(UNIT=6, FILE='TTY:',STATUS='NEW')
      WRITE (5,10)
 10   FORMAT( ' GIVE THE CONE SEMIAPEX ANGLE ')
      READ (5,95) EPSILO
      WRITE (5,20)
 20   FORMAT( ' GIVE THE THICKNESS RATIO ')
      READ (5,95) B
      WRITE (5,30)
 30   FORMAT( ' GIVE THE ANGLE OF ATTACK ')
      READ (5,95) ALFA
      WRITE (5,40)
 40   FORMAT( ' GIVE THE DISPLACEMENT OF THE SP ')
      READ (5,95) DY
      WRITE (5,50)
 50   FORMAT( ' GIVE THE VORTEX POSITION ')
      READ (5,95) S1
      WRITE (5,60)
 60   FORMAT(/,' WHICH SURFACE ? (-1 FOR LOWER-+1 FOR UPPER)>',$)
      READ (6,*) SURF
 95   FORMAT(2F)
      A=1.0
      PI=3.14159
C     ------------------------------------------------------------
      AE=ALFA/EPSILO
      C=SQRT(A**2-B**2)
      R=(A+B)/2
      ALF=ALFA*PI/180.0
      EPS=EPSILO*PI/180.0
C     ------------------------------------------------------------
C     WHEN THE SP IS ON THE UPPER SURFACE  DZ > 0
C     WHEN THE SP IS ON THE LOWER SURFACE  DZ < 0
C     ------------------------------------------------------------
      DZ=(B/A)*SQRT(DY*(2*A-DY))
      X=A/EPS
      Y=0.0
100   CONTINUE
C     ------------------------------------------------------------
C     FOR THE UPPER SURFACE  Z > 0
C     FOR THE LOWER SURFACE  Z < 0
C     ------------------------------------------------------------
      Z=SURF*B*SQRT(1-(Y/A)**2)
      S=Y+(0,1)*Z
      S2=CONJG(S1)
C     ------------------------------------------------------------
C     FOR THE UPPER SURFACE  G > 0
C     FOR THE LOWER SURFACE  G < 0
C     ------------------------------------------------------------
```

```
      IF (B.EQ.0.0) SUR=SURF
      IF (B.GT.0.0) SUR=+1.0
      G=SUR*CSQRT(S**2-C**2)
      G1=CSQRT(S1**2-C**2)
      G2=CSQRT(S2**2-C**2)
      T=(S+G)/2
      T1=(S1+G1)/2
      T2=(S2+G2)/2
      SP1=CSQRT((A-DY)**2+2*DZ*(A-DY)*(0,1)-DZ**2-C**2)
      SP=0.5*(A-DY+(0,1)*DZ+SP1)
      Q1=(SP+T2)*(SP-T1)*(SP*T2-R**2)*(SP*T1+R**2)
      Q2=SP**2*(T1+T2)*(R**2-T1*T2)
      Q=(Q1/Q2)*ALF
      QF=1/(T-T1)-1/(T+T2)+T1/(T*T1+R**2)-T2/(T*T2-R**2)
      TA=-C**2/(2*A*G)
      T1A=T1/A
      T2A=T2/A
      RA=R/A
      BA=B/A
      QA=Q/A
      TS=(1+S/G)/2
      WT=-(0,1)*ALF*(1+R**2/T**2)-(0,1)*Q*QF+B*EPS/T
      WT1=(0,1)*Q*(1/(T-T1)-T/(T*T1+R**2)+1/T1)
      WT2=(0,1)*Q*(1/(T+T2)+T/(T*T2-R**2)-1/T2)
C     ------------------------------------------------------------
      CV1=CLOG(T-T1)
      CV1R=REAL(CV1)
      CV1I=AIMAG(CV1)
      IF (SURF.EQ.+1.0.AND.Y.GE.(1-DY)) CV1I=CV1I-2*PI
      DCV1I=ABS(CV1I-CV1IO)
      IF (SURF.EQ.+1.0.AND.DCV1I.GT.4.0) CV1I=CV1I+2*PI
C     IF (SURF.EQ.+1.0.AND.Y.GE.(1-DY)) CV1I=CV1I-2*PI
      CV1=CMPLX(CV1R,CV1I)
      CV1IO=AIMAG(CV1)
      WRITE(5,150)Y,CV1I
C     ------------------------------------------------------------
      CV2=CLOG(T+T2)
      CV3=CLOG(T*T1+R**2)
      CV4=CLOG(T*T2-R**2)
      CV5=CLOG(T1)
      CV6=CLOG(T2)
      WQ=-(0,1)*(CV1-CV2+CV3-CV4+CV6-CV5)
      WR=2*(0,1)*R*ALF/T-2*(0,1)*Q*R*(1/(T*T1+R**2)+1/(T*T2-R**2))
      WB=EPS*CLOG(T)
      WA=WT*TA+WT1*T1A+WT2*T2A+WQ*QA+WR*RA+WB*BA
      VXS=EPS*(B/X)*(ALOG(2*SQRT(X*(1-X)))-1/(2*(1-X)))
      VX=EPS*REAL(WA)-VXS
      VCF=WT*TS
      VY=REAL(VCF)
      VZ=-AIMAG(VCF)
      VEL=SQRT(VX**2+VY**2+VZ**2)
      CP=ALF**2-2*VX-VY**2-VZ**2
      CPEE=CP/EPS**2
      WRITE(21,150)Y,CPEE
150   FORMAT(2F10.3)
      Y=Y+0.01
      IF(Y.LE.1.0)GO TO 100
      STOP
      END
```

```
      PROGRAM V-CP CIRCLE
C     ---------------------------------------------------------------
C     THIS PROGRAM COMPUTES THE VELOCITY AND PRESSURE DISTRIBUTIONS
C     ON THE SURFACE OF A CIRCULAR CONE WITH SEPARATED FLOW
C     FOR THE CASE OF AN ASSYMETRICAL VORTEX SYSTEM.
C     FROM THE OUTPUT, ONE CAN ALSO DETERMINE
C     THE POSITION OF THE STAGNATION, SEPARATION AND
C     REATTACHMENT POINTS.
C     ---------------------------------------------------------------
      COMPLEX A1,A2,A3,A4,B1,B2,B3,B4,C1,C2,C3,C4
      COMPLEX CS1,CS2,CSP1,CSP2,D1,D2,D3,D4,D5
      COMPLEX DWA,DWS,DWS1,DWS2,DWS3,K1,K2,S,S1,S2,SP1,SP2
      COMPLEX WA,WA1,WA2,WA3,WK1,WK2,WS1,WS2,WCS1,WCS2
C     ---------------------------------------------------------------
C     DATA
C     ---------------------------------------------------------------
      OPEN (UNIT=6,FILE='TTY:',STATUS='NEW')
    1 CONTINUE
      WRITE (5,10)
   10 FORMAT ( ' GIVE THE SEMIAPEX ANGLE ')
      READ (5,100) EPSILO
      WRITE (5,20)
   20 FORMAT ( ' GIVE THE ANGLE OF ATTACK ')
      READ (5,100) ALFA
      WRITE (5,30)
   30 FORMAT ( ' GIVE THE SEPARATION ANGLE ON THE RIGHT ')
      READ (5,100) SEPAR1
      WRITE (5,40)
   40 FORMAT ( ' GIVE THE SEPARATION ANGLE ON THE LEFT ')
      READ (5,100) SEPAR2
      WRITE (5,50)
   50 FORMAT ( ' GIVE THE RIGHT VORTEX POSITION ')
      READ (5,100) S1
      WRITE (5,60)
   60 FORMAT ( ' GIVE THE LEFT VORTEX POSITION ')
      READ (5,100) S2
      WRITE (5,70)
   70 FORMAT ( ' GIVE THE INTERVAL STEP ')
      READ(5,100) DETA
  100 FORMAT (2F)
      PI=3.141592654
C     ---------------------------------------------------------------
      EPS=EPSILO*PI/180.0
      ALF=ALFA*PI/180.0
      SEP1=SEPAR1*PI/180.0
      SEP2=(180.0-SEPAR2)*PI/180.0
      DET=DETA*PI/180.0
C     ---------------------------------------------------------------
      A=1.0
      SP1=A*CMPLX(COS(SEP1),SIN(SEP1))
      SP2=A*CMPLX(COS(SEP2),SIN(SEP2))
      CS1=CONJG(S1)
      CS2=CONJG(S2)
      CSP1=CONJG(SP1)
      CSP2=CONJG(SP2)
```

```
      ETA=-90.0
150   ET=ETA*PI/180.0
      Y=A*COS(ET)
      Z=A*SIN(ET)
      S=CMPLX(Y,Z)
      A1=1+A**2/SP1**2
      A2=1+A**2/SP2**2
      B1=1/(SP1-S1)-CS1/(CS1*SP1-A**2)
      B2=1/(SP2-S1)-CS1/(CS1*SP2-A**2)
      C1=1/(SP1-S2)-CS2/(CS2*SP1-A**2)
      C2=1/(SP2-S2)-CS2/(CS2*SP2-A**2)
      K1=ALF*(A1*C2-A2*C1)/(B2*C1-B1*C2)
      K2=ALF*(A1*B2-A2*B1)/(C1*B2-C2*B1)
      WA2=-2*(0,1)*K1*A/(S*CS1-A**2)
      WA3=+2*(0,1)*K2*A/(S*CS2-A**2)
      WS1=+K1*(0,1)/(S-S1)
      WS2=-K2*(0,1)/(S-S2)
      WCS1=+(0,1)*K1*A**2/(CS1*(S*CS1-A**2))
      WCS2=-(0,1)*K2*A**2/(CS2*(S*CS2-A**2))
C     ------------------------------------------------------------
      D1=CLOG(S)
C     ------------------------------------------------------------
      D2=CLOG(S-S2)
      D2R=REAL(D2)
      D2I=AIMAG(D2)
      IF (ET.GE.SEP2) D2I=D2I+2*PI
      D2=CMPLX(D2R,D2I)
C     ------------------------------------------------------------
      D3=CLOG(S-S1)
      D3R=REAL(D3)
      D3I=AIMAG(D3)
      IF (ET.GE.SEP1) D3I=D3I+2*PI
      D3=CMPLX(D3R,D3I)
C     ------------------------------------------------------------
      D4=CLOG(S-A**2/CS2)
      D4R=REAL(D4)
      D4I=AIMAG(D4)
      DD4I=ABS(D4I-D4IO)
      IF (DD4I.GT.4.0) D4I=D4I+2*PI
      D4=CMPLX(D4R,D4I)
      D4IO=AIMAG(D4)
C     ------------------------------------------------------------
      D5=CLOG(S-A**2/CS1)
      D5R=REAL(D5)
      D5I=AIMAG(D5)
      DD5I=ABS(D5I-D5IO)
      IF (DD5I.GT.4.0) D5I=D5I+2*PI
      D5=CMPLX(D5R,D5I)
      D5IO=AIMAG(D5)
C     ------------------------------------------------------------
      WK1=-(0,1)*(D3-D5)
      WK2=+(0,1)*(D2-D4)
C     ------------------------------------------------------------
      DWS2=-K1*(0,1)*(1/(S-S1)-CS1/(S*CS1-A**2))
      DWS3=+K2*(0,1)*(1/(S-S2)-CS2/(S*CS2-A**2))
C     ------------------------------------------------------------
```

```
      WA1=2*(0,1)*ALF*(A/S)
      WA=WA1+WA2+WA3+EPS*D1
      DWS1=-ALF*(0,1)*(1+A**2/S**2)
      DWA=WA+WS1*S1+WS2*S2+WCS1*CS1+WCS2*CS2+WK1*K1+WK2*K2
      DWS=DWS1+DWS2+DWS3+EPS*(A/S)
      VX=EPS*REAL(DWA)
      VY=+REAL(DWS)
      VZ=-AIMAG(DWS)
      CP=ALF**2-2*VX-VY**2-VZ**2
      CPEE=CP/EPS**2
      WRITE (6,200) ETA,CPEE
200   FORMAT (2F10.3)
      ETA=ETA+DETA
      IF (ETA.LE.90.0) GO TO 150
      WRITE (5,300)
300   FORMAT(/,' DO YOU WANT TO CONTINUE ?(1 FOR YES-0 FOR NO)>',$)
      READ (6,*) ILOG
      IF (ILOG.EQ.1) GO TO 1
      STOP
      END
```

```
      PROGRAM K-CL
C     ------------------------------------------------------------
C     THIS PROGRAM COMPUTES THE VORTEX STRENGTH K
C     AND THE LIFT COEFFICIENT CL
C     FOR A CONICAL BODY WITH ELLIPTICAL OR CIRCULAR
C     CROSS-SECTION, EXHIBITING LEADING EDGE SEPARATION.
C     ------------------------------------------------------------
      COMPLEX S,G1,G2,TH1,TH2,T,T1,QK1,QK2,QK,FL
C     ------------------------------------------------------------
C     DATA
C     ------------------------------------------------------------
C     AE      :  relative incidence
C     S       :  vortex position in the physical plane
C     B       :  ellipse semi-minor axis
C                (0 for a flat plate, 1 for a circle)
C     PARAM   :  = separation angle (for a circle)
C                = distance of separation from the leading edge
                   (for an ellipse or a flat plate)
C     ------------------------------------------------------------
      OPEN (UNIT=6, FILE='TTY:',STATUS='NEW')
      A=1.0
      P=3.14159
 100  CONTINUE
      WRITE (5,200)
 200  FORMAT (/,' Enter AE, S(complex), B, PARAM below.')
      READ (6,*) AE, S, B, PARAM
C     ------------------------------------------------------------
C     JONES LIFT (linear with angle of attack)
C     ------------------------------------------------------------
      CL1=2*P*AE
C     ------------------------------------------------------------
C     VORTEX LIFT (non-linear with angle of attack)
C     ------------------------------------------------------------
      C=SQRT(A**2-B**2)
      R=(A+B)/2
      G1=CSQRT(S**2-C**2)
      G2=CSQRT(CONJG(S)**2-C**2)
      TH1=S+G1
      TH2=CONJG(S)+G2
      IF (B.LT.1.0) GO TO 10
      THS=PARAM
      THSR=THS*P/180.0
      DY=A*(1-COS(THSR))
      DZ=A*SIN(THSR)
      GO TO 20
  10  DY=PARAM
      DZ=B*SQRT(1-(A-DY)**2)
  20  T1=A-DY+(0,1)*DZ
      T=(T1+CSQRT((A-DY)**2+2*(0,1)*(A-DY)*DZ-DZ**2-C*C))/2
      QK1=(0.25*TH2**2+T*TH2-R**2)/((T+0.5*TH2)*(0.5*T*TH2-R**2))
      QK2=(R**2+T*TH1-0.25*TH1**2)/((T-0.5*TH1)*(0.5*T*TH1+R**2))
      QK=T**2/(T**2+R**2)*(QK1-QK2)
      VK=1/QK
      IF (B.EQ.1.0) GO TO 250
```

```
      FL=(1+(A+B)/(A-B))*G1+(1-(A+B)/(A-B))*S
      GO TO 260
250   FL=2*G1
260   CL2=(4*P*AE/(QK*A**2))*REAL(FL)
      CL=CL1+CL2
      WRITE (5,300) VK,CL
300   FORMAT (2F20.3)
      WRITE (5,400)
400   FORMAT(/,' Do you want to continue ? (1 for yes - 0 for no) >',$)
      READ (6,*) ILOG
      IF (ILOG.EQ.1) GO TO 100
      STOP
      END
```

```
      PROGRAM BL
C     -------------------------------------------------------------
C     THIS PROGRAM INTEGRATES THE CROSS-FLOW BOUNDARY LAYER EQUATION
C     FROM A STAGNATION (OR REATTACHMENT POINT) TO THE REGION WHERE
C     THE FLOW IS EXPECTED TO SEPARATE,
C     ON THE SURFACE OF A CIRCULAR CONE WITH SEPARATED FLOW,
C     FOR EITHER SYMMETRICAL OR ASSYMETRICAL VORTEX SYSTEMS.
C     IN ORDER TO SATISFY KELVIN'S THEOREM, THE VORTEX (K1-K2)
C     SUGGESTED BY THE CIRCLE THEOREM FOR THE ASSYMETRICAL CASE
C     HAS NOT BEEN INCLUDED.
C     THE VELOCITY AND PRESSURE AT EACH POINT ARE
C     CALCULATED BY SUBROUTINE VEL.
C     FOR THE CASE OF A LAMINAR BOUNDARY LAYER
C     THE SEPARATION POINT IS REACHED WHEN THE VALUE OF THE
C     FUNCTION SC (SEPARATION CRITERION) IS -0.334 .
C     FOR THE CASE OF A TURBULENT BOUNDARY LAYER
C     THE SEPARATION POINT IS REACHED WHEN THE VALUE OF THE
C     FUNCTION SC (SEPARATION CRITERION) IS -3.75 .
C     -------------------------------------------------------------
      COMPLEX S1,S2
      EXTERNAL EI,SCI
C     -------------------------------------------------------------
C     DATA
C     -------------------------------------------------------------
      OPEN(UNIT=6, FILE='TTY:',STATUS='NEW')
  1   CONTINUE
      WRITE (5,3)
  3   FORMAT(/,' STATUS OF BL ? (0 FOR LAMINAR-1 FOR TURBULENT)>',$)
      READ (6,*) NBL
      WRITE (5,11)
 11   FORMAT( ' GIVE THE ANGLE OF ATTACK ')
      READ (5,20) ALFA
      WRITE (5,12)
 12   FORMAT( ' GIVE THE CONE SEMIAPEX ANGLE ')
      READ (5,20) EPSILO
      WRITE (5,13)
 13   FORMAT( ' GIVE THE SEPARATION ANGLE ON THE RIGHT ')
      READ (5,20) SEPAR1
      WRITE (5,14)
 14   FORMAT( ' GIVE THE SEPARATION ANGLE ON THE LEFT ')
      READ (5,20) SEPAR2
      WRITE (5,15)
 15   FORMAT( ' GIVE THE RIGHT VORTEX POSITION ')
      READ (5,20) S1
      WRITE (5,16)
 16   FORMAT( ' GIVE THE LEFT VORTEX POSITION ')
      READ (5,20) S2
      WRITE (5,17)
 17   FORMAT( ' GIVE STAGNATION POINT LOCATION ')
      READ (5,20) ETA0
      WRITE (5,18)
 18   FORMAT( ' GIVE THE STARTING POINT ')
      READ (5,20) ETA1
      WRITE (5,19)
 19   FORMAT( ' GIVE THE INTERVAL STEP ')
      READ (5,20) DETA
      PI=3.141592654
 20   FORMAT(2F)
```

```
C     ------------------------------------------------------------------
      ALF=ALFA*PI/180.0
      EPS=EPSILO*PI/180.0
      SEP1=SEPAR1*PI/180.0
      SEP2=(180.0-SEPAR2)*PI/180.0
      DET=DETA*PI/180.0
      ET1=ETA1*PI/180.0
C     ------------------------------------------------------------------
C     APPROXIMATION OF SC IN THE NEIGHBORHOOD OF
C     THE STAGNATION POINT
C     ------------------------------------------------------------------
      ETA=ETA0
 22   ETAN=ETA+DETA
      ETN=ETAN*PI/180.0
      ET=ETA*PI/180.0
      IF (DETA.GT.0.0) GO TO 23
      IF (ETA.LT.ETA1) GO TO 25
      GO TO 24
 23   IF (ETA.GT.ETA1) GO TO 25
 24   E=1.0
      IF (NBL.EQ.0) SC=1.0/6.0
      IF (NBL.EQ.1) SC=1.0/5.0
      E0=E
      SC0=SC
      GO TO 26
C     ------------------------------------------------------------------
C     CALCULATE THE INTEGRAL FUNCTION : E
C     ------------------------------------------------------------------
 25   SC1=SC0
      CALL ROME (ALF,EPS,SEP1,SEP2,S1,S2,ET1,ET,EIN)
      IF (NBL.EQ.0) RC=6
      IF (NBL.EQ.1) RC=4.25
      E=EXP(RC*EPS*EIN)
C     ------------------------------------------------------------------
C     EVALUATE THE DERIVATIVE : dV/d(eta)
C     ------------------------------------------------------------------
      CALL VEL(ALF,EPS,SEP1,SEP2,S1,S2,ET,V,CP)
      CALL VEL(ALF,EPS,SEP1,SEP2,S1,S2,ETN,V1,CP1)
      DVETA=(V1-V)/ABS(DET)
C     ------------------------------------------------------------------
C     EVALUATE THE DERIVATIVE : dCp/d(eta)
C     ------------------------------------------------------------------
      DCPETA=(CP1-CP)/ABS(DET)
C     ------------------------------------------------------------------
C     COMPUTE THE SEPARATION CRITERION
C     ------------------------------------------------------------------
      CALL ROMSC(ALF,EPS,SEP1,SEP2,S1,S2,ET1,ET,SCIN,NBL)
      IF (NBL.EQ.0) M=6
      IF (NBL.EQ.1) M=5
      SC2=(DVETA+EPS)*SCIN/(E*V**M)
      SC=SC1+SC2
 26   CALL VEL(ALF,EPS,SEP1,SEP2,S1,S2,ET,V,CP)
C     ------------------------------------------------------------------
      PARAM=21.526*V**2/((1+ALF**2)*DCPETA)
C     ------------------------------------------------------------------
      WRITE (5,30) ETA,SC,CP,PARAM
 30   FORMAT (4F15.3)
```

```
      ETA=ETAN
      IF (DETA.GT.0.0) GO TO 35
      IF (ET.GT.SEP1) GO TO 22
      GO TO 38
35    IF (ET.LT.SEP1) GO TO 22
38    WRITE (5,40)
40    FORMAT(/,' DO YOU WANT TO CONTINUE ? (1 FOR YES-0 FOR NO)>',$)
      READ (6,*) ILOG
      IF (ILOG.EQ.1) GO TO 1
      STOP
      END


      SUBROUTINE ROME(ALF,EPS,SEP1,SEP2,S1,S2,ET1,ET,RES)
C     ------------------------------------------------------------
C     THIS PROGRAM COMPUTES THE INTEGRAL FOR THE FUNCTION "E"
C     BY THE ROMBERG METHOD.
C     THE INPUTS ARE :
C     EI    : THE FUNCTION TO BE INTEGRATED
C     ET1   : THE LOWER LIMIT
C     ET    : THE UPPER LIMIT
C     ERR   : THE DESIRED ACCURACY
C     THE OUTPUT IS :
C     RES   : THE RESULT
C     ------------------------------------------------------------
      COMPLEX S1,S2
      EXTERNAL EI
C     ------------------------------------------------------------
C     "ZR" IS THE ARRAY OF APPROXIMATIONS
C     ------------------------------------------------------------
      DIMENSION ZR(10,10)
C     ------------------------------------------------------------
C     INITIALIZE THE INDEX AND COMPUTE THE FIRST APPROXIMATION
C     ------------------------------------------------------------
      I=1
      DEL=ET-ET1
      EI1=EI(ALF,EPS,SEP1,SEP2,S1,S2,ET1)
      EI2=EI(ALF,EPS,SEP1,SEP2,S1,S2,ET)
      ZR(1,1)=0.5*DEL*(EI1+EI2)
C     ------------------------------------------------------------
C     THE MAIN LOOP.
C     THE FIRST PART COMPUTES THE INTEGRAL USING A 2J+1 POINT
C     TRAPEZOID RULE. THE METHOD MAKES MAXIMAL USE OF THE
C     VALUES ALREADY COMPUTED.
C     ------------------------------------------------------------
101   J=2**(I-1)
      DEL=DEL/2
      I=I+1
      ZR(I,1)=0.5*ZR(I-1,1)
      DO 103 K=1,J
      XR=ET1+(2*K-1)*DEL
      EI3=EI(ALF,EPS,SEP1,SEP2,S1,S2,XR)
      ZR(I,1)=ZR(I,1)+DEL*EI3
103   CONTINUE
C     ------------------------------------------------------------
C     DO THE RICHARDSON EXTRAPOLATION
C     ------------------------------------------------------------
```

```
      DO 105 K=2,I
      ZR(I,K)=(4**(K-1)*ZR(I,K-1)-ZR(I-1,K-1))/(4**(K-1)-1)
105   CONTINUE
C     ---------------------------------------------------------------
C     ERROR CONTROL
C     ---------------------------------------------------------------
      ERR=0.001
      DIFF=ABS(ZR(I,I)-ZR(I,I-1))
      IF (DIFF.LT.ERR) GO TO 115
C     ---------------------------------------------------------------
C     THE MAXIMUM NUMBER OF ITERATIONS ALLOWED IS 10
C     ---------------------------------------------------------------
      IF (I.LT.10) GO TO 101
      WRITE (5,110)
110   FORMAT(' MORE THAN 10 ITERATIONS REQUIRED, CHECK PARAMETERS')
      STOP
115   RES=ABS(ZR(I,I))
      RETURN
      END


      SUBROUTINE VEL(ALF,EPS,SEP1,SEP2,S1,S2,ET,V,CP)
C     ---------------------------------------------------------------
C     THIS PROGRAM EVALUATES THE CROSS-FLOW VELOCITY COMPONENTS
C     ON THE CROSS-SECTION OF THE BODY.
C     ---------------------------------------------------------------
      COMPLEX A1,A2,B1,B2,C1,C2
      COMPLEX CS1,CS2,CSP1,CSP2,D1,D2,D3,D4,D5
      COMPLEX DWA,DWS,DWS1,DWS2,DWS3,K1,K2,S,S1,S2,SP1,SP2
      COMPLEX WA,WA1,WA2,WA3,WK1,WK2,WS1,WS2,WCS1,WCS2
C     ---------------------------------------------------------------
      A=1.0
      PI=3.14159
      SP1=A*CMPLX(COS(SEP1),SIN(SEP1))
      SP2=A*CMPLX(COS(SEP2),SIN(SEP2))
      CS1=CONJG(S1)
      CS2=CONJG(S2)
      CSP1=CONJG(SP1)
      CSP2=CONJG(SP2)
      Y=A*COS(ET)
      Z=A*SIN(ET)
      S=CMPLX(Y,Z)
      A1=1+A**2/SP1**2
      A2=1+A**2/SP2**2
      B1=1/(SP1-S1)-CS1/(CS1*SP1-A**2)
      B2=1/(SP2-S1)-CS1/(CS1*SP2-A**2)
      C1=1/(SP1-S2)-CS2/(CS2*SP1-A**2)
      C2=1/(SP2-S2)-CS2/(CS2*SP2-A**2)
      K1=ALF*(A1*C2-A2*C1)/(B2*C1-B1*C2)
      K2=ALF*(A1*B2-A2*B1)/(B2*C1-B1*C2)
      WA1=+2*(0,1)*ALF*(A/S)
      WA2=-2*(0,1)*K1*A/(S*CS1-A**2)
      WA3=+2*(0,1)*K2*A/(S*CS2-A**2)
      WS1=+K1*(0,1)/(S-S1)
      WS2=-K2*(0,1)/(S-S2)
      WCS1=+(0,1)*K1*A**2/(CS1*(S*CS1-A**2))
      WCS2=-(0,1)*K2*A**2/(CS2*(S*CS2-A**2))
```

```
C     -----------------------------------------------------------------
      D1=CLOG(S)
C     -----------------------------------------------------------------
      D2=CLOG(S-S2)
      D2R=REAL(D2)
      D2I=AIMAG(D2)
      IF (ET.GE.SEP2) D2I=D2I+2*PI
      D2=CMPLX(D2R,D2I)
C     -----------------------------------------------------------------
      D3=CLOG(S-S1)
      D3R=REAL(D3)
      D3I=AIMAG(D3)
      IF (ET.GE.SEP1) D3I=D3I+2*PI
      D3=CMPLX(D3R,D3I)
C     -----------------------------------------------------------------
      D4=CLOG(S-A**2/CS2)
      D4R=REAL(D4)
      D4I=AIMAG(D4)
      DD4I=ABS(D4I-D4IO)
      IF (DD4I.GT.4.0) D4I=D4I+2*PI
      D4=CMPLX(D4R,D4I)
      D4IO=AIMAG(D4)
C     -----------------------------------------------------------------
      D5=CLOG(S-A**2/CS1)
      D5R=REAL(D5)
      D5I=AIMAG(D5)
      DD5I=ABS(D5I-D5IO)
      IF (DD5I.GT.4.0) D5I=D5I+2*PI
      D5=CMPLX(D5R,D5I)
      D5IO=AIMAG(D5)
C     -----------------------------------------------------------------
      WK1=-(0,1)*(D3-D5)
      WK2=+(0,1)*(D2-D4)
      DWS1=-ALF*(0,1)*(1+A**2/S**2)
      DWS2=-(0,1)*K1*(1/(S-S1)-CS1/(S*CS1-A**2))
      DWS3=+(0,1)*K2*(1/(S-S2)-CS2/(S*CS2-A**2))
      WA=WA1+WA2+WA3+EPS*D1
      DWA=WA+WS1*S1+WS2*S2+WCS1*CS1+WCS2*CS2+WK1*K1+WK2*K2
      DWS=DWS1+DWS2+DWS3+EPS*(A/S)
      VX=EPS*REAL(DWA)
      VY=+REAL(DWS)
      VZ=-AIMAG(DWS)
      V=SQRT(VY**2+VZ**2)
      CP=ALF**2-2*VX-VY**2-VZ**2
      RETURN
      END

      FUNCTION EI(ALF,EPS,SEP1,SEP2,S1,S2,ET)
C     -----------------------------------------------------------------
C     THIS PROGRAM CALCULATES THE INTEGRAND FUNCTION FOR "E"
C     -----------------------------------------------------------------
      COMPLEX S1,S2
      CALL VEL(ALF,EPS,SEP1,SEP2,S1,S2,ET,V,CP)
      EI=1.0/V
      RETURN
      END
```

```
      SUBROUTINE ROMSC(ALF,EPS,SEP1,SEP2,S1,S2,ET1,ET,RES,NBL)
C     -------------------------------------------------------------
C     THIS PROGRAM COMPUTES THE INTEGRAL FOR THE SEPARATION
C     CRITERION BY THE ROMBERG METHOD.
C     THE INPUTS ARE :
C     SCI   : THE FUNCTION TO BE INTEGRATED
C     ET1   : THE LOWER LIMIT
C     ET    : THE UPPER LIMIT
C     EPS   : THE CONE SEMIAPEX ANGLE (IN RADIANS)
C     ERR   : THE DESIRED ACCURACY
C     THE OUTPUT IS :
C     RES   : THE RESULT
C     -------------------------------------------------------------
      COMPLEX S1,S2
      EXTERNAL EI,SCI
C     -------------------------------------------------------------
C     "ZR" IS THE ARRAY OF APPROXIMATIONS
C     -------------------------------------------------------------
      DIMENSION ZR(10,10)
C     -------------------------------------------------------------
C     INITIALIZE THE INDEX AND COMPUTE THE FIRST APPROXIMATION
C     -------------------------------------------------------------
      I=1
      DEL=ET-ET1
      SCI1=SCI(ALF,EPS,SEP1,SEP2,S1,S2,ET1,ET1,NBL)
      SCI2=SCI(ALF,EPS,SEP1,SEP2,S1,S2,ET1,ET,NBL)
      ZR(1,1)=0.5*DEL*(SCI1+SCI2)
C     -------------------------------------------------------------
C     THE MAIN LOOP.
C     THE FIRST PART COMPUTES THE INTEGRAL USING A 2J+1 POINT
C     TRAPEZOID RULE. THE METHOD MAKES MAXIMAL USE OF THE
C     VALUES ALREADY COMPUTED.
C     -------------------------------------------------------------
401   J=2**(I-1)
      DEL=DEL/2
      I=I+1
      ZR(I,1)=0.5*ZR(I-1,1)
      DO 403 K=1,J
      XR=ET1+(2*K-1)*DEL
      SCI3=SCI(ALF,EPS,SEP1,SEP2,S1,S2,ET1,XR,NBL)
      ZR(I,1)=ZR(I,1)+DEL*SCI3
403   CONTINUE
C     -------------------------------------------------------------
C     DO THE RICHARDSON EXTRAPOLATION
C     -------------------------------------------------------------
      DO 405 K=2,I
      ZR(I,K)=(4**(K-1)*ZR(I,K-1)-ZR(I-1,K-1))/(4**(K-1)-1)
405   CONTINUE
C     -------------------------------------------------------------
C     ERROR CONTROL
C     -------------------------------------------------------------
      ERR=0.001
      DIFF=ABS(ZR(I,I)-ZR(I,I-1))
      IF (DIFF.LT.ERR) GO TO 415
```

```
C      ----------------------------------------------------------------
C      THE MAXIMUM NUMBER OF ITERATIONS ALLOWED IS 10.
C      ----------------------------------------------------------------
       IF (I.LT.10) GO TO 401
       WRITE (5,410)
410    FORMAT(' MORE THAN 10 ITERATIONS REQUIRED, CHECK PARAMETERS')
       STOP
415    RES=ABS(ZR(I,I))
       RETURN
       END

       FUNCTION SCI(ALF,EPS,SEP1,SEP2,S1,S2,ET1,ET,NBL)
C      ----------------------------------------------------------------
C      THIS PROGRAM COMPUTES THE INTEGRAND FUNCTION
C      FOR THE SEPARATION CRITERION.
C      ----------------------------------------------------------------
       COMPLEX S1,S2
       EXTERNAL EI
       CALL VEL(ALF,EPS,SEP1,SEP2,S1,S2,ET,V,CP)
       CALL ROME(ALF,EPS,SEP1,SEP2,S1,S2,ET1,ET,EIN)
       IF (NBL.EQ.0) RC=6
       IF (NBL.EQ.1) RC=4.25
       E=EXP(RC*EPS*EIN)
       IF (NBL.EQ.0) M=5
       IF (NBL.EQ.1) M=4
       SCI=E*V**M
       RETURN
       END
```

END

DATE

NOV. 2, 1987